R. & M. No. 3758

PROCUREMENT EXECUTIVE, MINISTRY OF DEFENCE

AERONAUTICAL RESEARCH COUNCIL

REPORTS AND MEMORANDA

On the Application of Subsonic Linearised Wing Theory to Second-Order Forces and Moments

Part I   General Principles and Mathematical Models

By G. J. HANCOCK
Queen Mary College, University of London

Part II   Edge Forces and Roll-Rate Derivatives

By H. C. GARNER
Aerodynamics Dept., R.A.E., Farnborough

LONDON: HER MAJESTY'S STATIONERY OFFICE

1975

PRICE £3·50 NET

On the Application of Subsonic Linearised Wing Theory to Second-Order Forces and Moments

By G. J. HANCOCK

Queen Mary College, University of London—Part I

By H. C. GARNER†

Aerodynamics Dept., R.A.E., Farnborough—Part II

Reports and Memoranda No. 3758*
March, 1973

Summary

The report comprises two contrasting and complementary approaches to the evaluation of the second-order aerodynamic side force and yawing moment on lifting wings when leading-edge and side-edge forces play an important rôle.

In Part I the usual lifting-surface model, in which the vorticity is placed on a planar surface, is shown to lead to inconsistent results; consistent results are obtained when the vorticity is placed on the camber surface while the standard lifting-surface integral equation takes its usual form. In a further supplementary momentum analysis involving the Trefftz plane, the side force and yawing moment are derived from approximate expressions which avoid calculation of any edge forces.

In Part II the analysis of linearised subsonic lifting-surface theory is extended to provide expressions for the leading-edge and side-edge forces. The side force and yawing moment under conditions of asymmetric spanwise loading are obtained as the sum of three contributions, from normal pressures, leading-edge suction and tip suction. These quantities are used to treat lifting wings in roll, and from a few numerical examples some general trends in the theoretical derivatives are observed. The related evidence from experiment and from semi-empirical methods is discussed, and one such method is transcribed for use in conjunction with the theoretical computations. Much of the non-linear experimental behaviour of the side force and yawing moment due to rate of roll can be accounted for by the removal of an increasing proportion of the theoretical edge forces as the lift increases.

LIST OF CONTENTS

2

Preface

The relative importance of stability derivatives changes from one generation of aircraft to another. Because of trends in aircraft geometry and mass distribution, particular derivatives may assume increased significance in the determination of lateral stability. For example, the characteristics of the dutch-roll oscillation of highly swept or slender aircraft at moderate or high lift coefficient depend to a greater extent than hitherto on derivatives such as the yawing moment due to rate of roll and less on the direct damping in sideslip and yaw. It is therefore desirable to analyse the principles underlying the theoretical estimation of forces on a lifting wing in roll, and to study the nature of the contributory edge forces against a background of limited experimental data.

The aerodynamic wing loading associated with lateral aircraft motions at subsonic speeds is usually treated more crudely than that relating to longitudinal flight. Until recent years rigorous treatment by lifting-surface theory has been discouraged by the amount of computation that would be necessary, and perhaps also by the lack of conviction as regards the validity of the edge forces. With the increased capability of lifting-surface methods of the present decade it is opportune to consider such problems afresh.

Some contributions to lateral stability derivatives are of first order in wing motion and attitude, while others are of second order. The rolling moment on the wing due to rate of roll is of first order and correspondingly easy to calculate. On the other hand, the yawing moment due to rate of roll includes a second-order contribution from the wing surface, which becomes increasingly important at high lift notwithstanding a first-order contribution from the fin. The wing contribution arises from an interaction between symmetric and antisymmetric parts of the spanwise loading and poses considerable theoretical problems.

Estimation of these second-order derivatives raises, once again, the fundamental question of the validity of determining second-order quantities from a first-order or linearised theory. It is well-known that lift-dependent drag, or vortex drag, which is a second-order quantity compared with wing lift, can be estimated directly and unambiguously from linearised wing theory either by integration of the cross-flow kinetic energy in the downstream Trefftz plane or by direct calculation of the components of normal surface pressures and the leading-edge suction force. But the basis for the calculation of the side force and yawing moment has not been so thoroughly assessed.

In Part I of this report an attempt is made to clarify some of the fundamental aspects; emphasis is primarily on the understanding of the implications of various mathematical models rather than on the development of a rigorous mathematical model or on the production of numerical results. It is shown in Part I that the usual lifting-surface model in which all the vorticity is placed on a planar surface leads to inconsistent results, especially for compressible flow; it is argued that singularity distributions should be located on the camber surface so that the local loading is normal to the camber surface. With this interpretation the standard lifting-surface integral equation continues to take its usual form. In a further analysis involving consideration of overall linear and angular momentum the side force and yawing moment are derived from approximate expressions which involve integrals in the downstream Trefftz plane and which avoid any explicit calculation of edge forces.

In Part II of this report, with the correct interpretation of the standard lifting-surface integral equation, existing computer programs have been applied to calculate the normal pressure distribution and hence the leading-edge and tip suction forces. This approach has the advantage that empirical corrections to the edge forces can be incorporated. The total forces on a rolling wing are calculated and then compared with related evidence from experiment and from semi-empirical methods, and it is concluded that a useful approximation to the non-linear experimental behaviour of the side force and yawing moment due to the rate of roll can be introduced quite simply in terms of the measured drag over the practical range of lift coefficient.

Part I

General Principles and Mathematical Models

1. Introduction

As a real fluid flows past and over a finite wing, vorticity, which is created in the boundary layers, is shed from the trailing edge and then convected downstream, forming the wake. Although a small proportion of the trailing vorticity is diffused and dissipated the remainder rolls up into two discrete vortices which remain intact and stable for long distances behind the wing. If the flow does not break away from the surface of the wing it may be assumed that at high Reynolds numbers the effects of viscosity are confined to the thin boundary layers and to the downstream vortex wake. Thus to a first approximation viscosity may be neglected so long as a system of trailing vorticity downstream of the wing is retained in the analysis.

Assuming therefore an inviscid flow, linearisation reduces the overall problem to two separate problems: the first is the lifting problem associated with wing camber and incidence in which all the vorticity, namely the vorticity on the wing and the trailing vorticity, is placed on a surface in the vicinity of the wing and the wake: the second problem is the non-lifting problem associated with wing thickness. Only the lifting problem is considered in this report.

Conventional linearised theory is based on a mathematical model in which all the vorticity is distributed on a plane surface, the wing vorticity is distributed over a planar surface parallel to the free stream direction in the neighbourhood of the wing while the trailing vorticity is distributed over the extension of the (wing) planar surface from the trailing edge region to infinity downstream. This model is referred to as the planar model.

It is shown in this report that the side force and yawing moment determined from this planar model are not necessarily the actual (inviscid) side force and yawing moment experienced by the wing itself. The reason is shown to be the fact that a significant side force and yawing moment are required to sustain and maintain the planar model itself in the vicinity of the wing; a side force and yawing moment are required to maintain the planar trailing sheet but these are shown to be small and negligible.

However it is further shown that this anomaly can be reconciled by a reinterpretation of the basic mathematical model but retaining the main linearisation features. No ambiguity arises if a non-planar model is used in which the wing vorticity is placed on the wing camber surface itself and the trailing vorticity on a surface extending from the wing trailing edge to infinity downstream.

When compressibility effects are included it is shown that the planar model is not a valid model for the estimation of any second-order quantities, including induced drag; the only permitted model is a non-planar one. The reason is associated with the discontinuity in density across the lifting surface.

The actual theoretical values of all the second-order forces and moments (i.e. vortex drag, side force and yawing moment) depend on the magnitude of the edge forces associated with singular behaviour of the vorticity at the leading edge and wing tips. These edge forces are difficult to evaluate numerically; care is required to ensure that values are sufficiently accurate. The evaluation of the various edge forces is described in Part II together with a discussion of their practical significance.

In the case of the vortex drag the difficult calculation of the leading-edge thrust force can be bypassed by consideration of the conservation of linear momentum across the downstream Trefftz plane. In this report similar Trefftz plane analyses are investigated for the side force and yawing moment; both the planar and non-planar models are shown to give consistent results; the effects of compressibility are also considered. Although it is not possible to derive exact formulae in the Trefftz plane for the side force and yawing moment, approximate formulae are proposed. Numerical examples show that these approximate formulae give reasonable results.

2. Planar Wing Theory at Low Speeds

In this section the conventional mathematical formulation of linearised finite wing theory in low speed (incompressible) steady flow is introduced and discussed. The usual mathematical model comprises a discontinuity in velocity potential across a plane surface (parallel to the free stream) in the vicinity of the wing and wake; this model is referred to as the planar model. For the lifting characteristics the discontinuity in velocity potential is determined from the inversion of the standard lifting-surface integral equation when the camber surface is specified. Once the discontinuity in velocity potential is known the overall forces of lift, drag, side force, and the overall moments in roll, pitch and yaw can be found; the edge forces associated with the singular behaviour of the velocity potential at the leading edge and wing tips are significant contributions to the drag, side force and yawing moment. Alternative expressions for the forces and moments can be obtained by

5

consideration of the linear and angular momenta flux out of a large control surface surrounding the wing, resulting in the so-called Trefftz plane results.

Although most of the present section is standard text book knowledge it is included here as a basis and reference for the later developments.

2.1. Formulation of Planar Mathematical Model

To define the wing geometry, cartesian axes are chosen as shown in Fig. 1 with the origin at the centre point of the leading edge; the $0x$ axis is taken parallel to the free stream, the $0y$ axis is to starboard and the $0z$ axis completes a right-handed set. The equations of the leading and trailing edges are denoted by $x = x_l(y)$ and $x = x_t(y)$ respectively, while the wing span is taken to be $2s$. The shape of the wing relative to this axis system can be expressed in the form

$$z = Z(x, y) = Z_c(x, y) \pm Z_t(x, y) \tag{1}$$

where the $\pm$ refers to the upper or lower surface respectively; $Z_c(x, y)$ represents the mean camber surface which includes incidence and spanwise twist, while $Z_t(x, y)$ represents the symmetric thickness distribution superimposed on the camber surface.

The problem, as shown in Fig. 1, is to determine the load distribution on the wing, defined by equation (1), in a uniform low-speed stream of velocity U.

If the perturbation velocities introduced into the uniform stream by the wing and trailing vorticity are denoted as (u, v, w) the equation of continuity for a low speed (incompressible) flow is

$$\frac{\partial(U + u)}{\partial x} + \frac{\partial v}{\partial y} + \frac{\partial w}{\partial z} = 0. \tag{2}$$

Since the flow exterior to the wing and trailing vorticity is irrotational, a perturbation velocity potential Φ exists such that

$$u = \frac{\partial \Phi}{\partial x}, \qquad v = \frac{\partial \Phi}{\partial y}, \qquad w = \frac{\partial \Phi}{\partial z}. \tag{3}$$

On substitution of equation (3), equation (2) becomes the standard Laplace equation

$$\nabla^2 \Phi = \frac{\partial^2 \Phi}{\partial x^2} + \frac{\partial^2 \Phi}{\partial y^2} + \frac{\partial^2 \Phi}{\partial z^2} = 0. \tag{4}$$

Equation (4) is to be solved subject to the boundary conditions:
  (a) that Φ vanishes at infinity upstream and laterally, i.e. at

$$x = -\infty, \qquad y = \pm\infty \quad \text{and} \quad z = \pm\infty;$$

  (b) that the flow normal to the wing surface is zero, that is

$$w(x, y, Z(x, y)) = (U + u)\frac{\partial Z}{\partial x} + v\frac{\partial Z}{\partial y}; \tag{5}$$

  (c) that no load is carried by the trailing vorticity.

The usual linearisation approximation assumes that $Z(x, y)/c_R$ (where c_R is the root chord) is small, and that perturbation velocities (u, v, w) are small compared with U; the basic equations and boundary conditions are then satisfied to first order only.

Linearisation does not affect the fundamental equation (4).

The boundary condition (5) is usually expanded in a Taylor series from $z = \pm 0$ and with the neglect of second-order terms the linearised boundary condition becomes

$$\left.\begin{aligned} w(x, y, +0) &= U\left(\frac{\partial Z_c}{\partial x} + \frac{\partial Z_t}{\partial x}\right) \\ w(x, y, -0) &= U\left(\frac{\partial Z_c}{\partial x} - \frac{\partial Z_t}{\partial x}\right) \end{aligned}\right\}. \tag{6}$$

At the same time it is assumed that the trailing vorticity is confined to the plane $z = 0$ where the condition of zero loading is applied.

6

Thus the basic problem reduces to two independent problems.

(i) The determination of a symmetric solution of $\nabla^2 \Phi = 0$ (i.e. symmetric with respect to z) such that

$$\left(\frac{\partial \Phi}{\partial z}\right)_{z=+0} = -\left(\frac{\partial \Phi}{\partial z}\right)_{z=-0} = U\frac{\partial Z_t}{\partial x} \tag{7}$$

on the wing plan form, denoted as S_W; there is no trailing vorticity in this problem.

(ii) The determination of an antisymmetric solution of $\nabla^2 \Phi = 0$ (i.e. antisymmetric with respect to z) such that

$$\left(\frac{\partial \Phi}{\partial z}\right)_{z=+0} = \left(\frac{\partial \Phi}{\partial z}\right)_{z=-0} = U\frac{\partial Z_c}{\partial x} \tag{8}$$

on S_W. The mathematical model now includes a planar trailing sheet which extends from the trailing edge of S_W to infinity downstream in the plane $z = 0$ and across which no load is applied. This planar system is shown in Fig. 2.

Problem (ii) gives rise to the overall forces and moments; to first order, problem (i) only modifies the pressure distributions to account for thickness effects without contributing to the overall forces or moments. Only problem (ii), the antisymmetric lifting problem, is considered further in this report.

The solution of the lifting problem involves a discontinuity in $\Phi(x, y, z)$ across S_W and S_T expressed in the form

$$\Delta\Phi(x, y) = \Phi(x, y, +0) - \Phi(x, y, -0) = 2\Phi(x, y, +0) \tag{9}$$

by virtue of the antisymmetric nature of Φ.

The discontinuity in pressure across S_W and S_T is obtained by application of Bernoulli's equation for incompressible flow; thus

$$p(x, y, -0) - p(x, y, +0) = \tfrac{1}{2}\rho\{[(U + u)^2 + v^2 + w^2]_{z=+0} - [(U + u)^2 + v^2 + w^2]_{z=-0}\}$$

$$= \rho U(u_{+0} - u_{-0})$$

$$= \rho U\frac{\partial \Delta\Phi}{\partial x}, \tag{10}$$

where the subscripts $+0$, -0 refer to the respective surfaces $z = +0$ and $z = -0$. It is noted that equation (10) is exact in the sense that no further linearisation has been invoked.

Across S_T the loading must be zero; thus, according to equation (10) $\Delta\Phi(x, y)$ must be a function of y only; hence

$$\Delta\Phi(y) \quad \text{on} \quad S_T = \Delta\Phi(x_t(y), y) = \Delta\Phi_t(y). \tag{11}$$

It is well known that the antisymmetric problem reduces to an integral equation

$$\frac{\partial Z_c}{\partial z} = -\frac{1}{8\pi}\iint\limits_{S_W} \frac{\rho U \, \partial\Delta\Phi/\partial x}{\tfrac{1}{2}\rho U^2(y - \eta)^2}\left[1 + \frac{x - \xi}{\{(x - \xi)^2 + (y - \eta)^2\}^{\frac{1}{2}}}\right] d\xi \, d\eta \tag{12}$$

with the proviso that the discontinuity in pressure is zero at the trailing edge to satisfy the Kutta condition. It is not the intention to discuss or describe here the numerical solution of equation (12); the methods of Refs. 2 and 3 have been used for the numerical results quoted later. The main purpose of this report is to enquire in further depth about some of the implications of the planar model which has been formulated so far, in particular to discuss the determination of the forces and moments on the wing once $\Delta\Phi(x, y)$ has been calculated from the integral equation (12).

2.2. Load Distribution on Planar Model

The discontinuity in $\Phi(x, y, z)$ across S_W and S_T implies a system of load component distributions in the x, y and z directions.

Consider a small control element $abcda'b'c'd'$, as shown in Fig. 3, which straddles the plane $z = 0$. Its sides are of length δx, δy, δz. In the following analysis δz tends to zero while δx and δy remain finite although small.

First it is noted that there is continuity of mass flow through the control volume; as $\delta z \to 0$ the mass flow $\rho w \, \delta x \, \delta y$ in the direction across $abcd$ equals that across $a'b'c'd'$. This condition is trivial in the present case but not when the effect of compressibility is included (see Section 4).

7

The load exerted by the fluid on the control volume $abcda'b'c'd'$ in the z direction, in the limit as $z \to 0$, is given by the difference between the pressures acting on $a'b'c'd'$ and $abcd$ since the momentum flux in the z direction across these surfaces are equal. Thus

$$\text{load in } z \text{ direction} = \{p(x, y, -0) - p(x, y, +0)\}\, \delta x \, \delta y$$

$$= \rho U \frac{\partial \Delta \Phi}{\partial x} \delta x \, \delta y \tag{13}$$

from equation (10).

The load exerted on the control volume $abcda'b'c'd'$ in the x direction in the limit as $\delta z \to 0$ is given by the difference in momentum flux in the x direction across $a'b'c'd'$ and $abcd$. Thus

$$\text{load in } x \text{ direction} = \{[\rho w(U + u)]_{z = -0} - [\rho w(U + u)]_{z = +0}\}\, \delta x \, \delta y$$

$$= -\rho w \frac{\partial \Delta \Phi}{\partial x} \delta x \, \delta y. \tag{14}$$

By exactly the same argument, the load in the y direction on the control volume $abcda'b'c'd'$ as $z \to 0$ becomes

$$\text{load in } y \text{ direction} = -\rho w \frac{\partial \Delta \Phi}{\partial y} \delta x \, \delta y. \tag{15}$$

Since the loads in the x and y directions are second-order terms it might be argued that these should be ignored in a linear representation of the problem. But the philosophy adopted here is that the model once formulated can be treated as exact. All second-order results then have validity within the framework of that planar mathematical model. The physical significance of such results is another matter which requires further assessment.

Equations (13), (14) and (15) hold not only on the wing planform S_W but also on the trailing sheet S_T. As already stated $\partial \Delta \Phi / \partial x$ is made zero across S_T so the loading on S_T in the x and z directions are zero. But because w and $\partial \Delta \Phi / \partial y$ are both non-zero on S_T a sideways load distribution is inferred. This result violates the boundary condition that no load be carried by a planar trailing vortex sheet. Thus the planar trailing vorticity can only be maintained in its planar form if some external agency provides the necessary side force distribution to hold it there. This point is not new; it has always been recognised that some restraint has to be applied to the trailing vorticity otherwise the planar sheet rolls up. At this stage, however, an element of doubt appears for the question which now arises is whether or not this external agency also provides some of the side force distribution on S_W to maintain the planar form of S_W; and if so, how much sideforce does this external agency provide; and how is the actual side force on the wing itself calculated. These same questions and doubts also apply to the yawing moment. Before these points can be discussed further, it is necessary to discuss the edge forces which arise from the singular behaviour of $\partial \Delta \Phi / \partial x$ and $\partial \Delta \Phi / \partial y$ at the edge of $S_W + S_T$, for these edge forces contribute not only to the drag but also to the side force and yawing moment.

2.3. Edge Forces

The linearised solution $\Delta \Phi(x, y)$ has infinite rates of change at the leading edge, at the wing tips and along edges of the trailing sheet S_T. These infinities give rise to finite edge forces which must be taken into account. A derivation of edge forces in terms of a complex potential is given by Jones and Cohen[4]; a more direct method is described here.

Consider an element of edge of length δs swept locally through an angle Λ and enclosed in a small cylinder ABCD of radius r, as shown in Fig. 4. Let n be the inward normal distance from the element in the plane $z = 0$. Perturbation cartesian velocities (q_n, q_s, w) are shown parallel to the (n, s, z) directions, while the perturbation cylindrical velocities are denoted as (q_r, q_θ, q_s). Near the element q_s is finite and will not be considered further, but the singular contributions to q_r and q_θ must satisfy the two-dimensional equations of continuity and irrotationality for incompressible flow

$$\left. \begin{array}{l} \dfrac{\partial}{\partial r}(r q_r) + \dfrac{\partial q_\theta}{\partial \theta} = 0 \\[2mm] \dfrac{\partial}{\partial r}(r q_\theta) - \dfrac{\partial q_r}{\partial \theta} = 0 \end{array} \right\} . \tag{16}$$

and

Thus the perturbation potential and velocity components in the plane normal to δs are

$$\Phi = 2kr^{\frac{1}{2}} \cos \tfrac{1}{2}\theta + O(r), \left.\begin{array}{l} \\ \\ \\ \end{array}\right\}$$

and

$$q_r = kr^{-\frac{1}{2}} \cos \tfrac{1}{2}\theta + O(1) \qquad (17)$$

$$q_\theta = -kr^{-\frac{1}{2}} \sin \tfrac{1}{2}\theta + O(1)$$

where k is a constant independent of r and θ. Hence

and

$$q_n = q_r \cos \theta - q_\theta \sin \theta = kr^{-\frac{1}{2}} \cos \tfrac{1}{2}\theta + O(1) \left.\begin{array}{l} \\ \\ \end{array}\right\}$$

$$w = q_r \sin \theta + q_\theta \cos \theta = kr^{-\frac{1}{2}} \sin \tfrac{1}{2}\theta + O(1) \qquad (18)$$

Singular terms in the perturbation pressure

$$\tfrac{1}{2}\rho[2kr^{-\frac{1}{2}}U \cos \Lambda \cos \tfrac{1}{2}\theta + k^2 r^{-1}]$$

do not contribute to the force on the control cylinder, but the flux of momentum in direction n from the cylinder is equivalent to an edge force in the direction of the outward normal to the planform, thus

$$\text{edge force} = \left\{ \int_0^{2\pi} \rho q_n q_r r \, d\theta \right\}_{r \to 0} \delta s$$

$$= \pi \rho k^2 \, \delta s = \pi \rho \left\{ \left(\frac{\partial \Phi}{\partial r} \right)^2_{\theta=0} r \right\}_{r \to 0} \delta s$$

$$= \pi \rho \left\{ \left(\frac{\partial \Phi}{\partial n} \right)^2_{z=+0} \delta_n \right\}_{\delta_n \to 0} \delta s, \qquad (19)$$

where δ_n is the normal inward distance from the edge.

Thus the component of edge force in the $-x$ direction, known as the leading-edge thrust, on an element of spanwise extent $\delta y = \delta s \cos \Lambda$ may be written as

$$\delta T_e = \pi \rho \left\{ \left(\frac{\partial \Phi}{\partial x} \sec \Lambda \right)^2_{+0} \delta_x \cos \Lambda \right\}_{\delta_x \to 0} \delta s \cos \Lambda$$

$$= \pi \rho \left\{ \left(\frac{\partial \Phi}{\partial x} \right)^2_{+0} \delta_x \right\}_{\delta_x \to 0} \sec \Lambda \, \partial y, \qquad (20)$$

where δ_x is the distance from the leading edge measured in the x direction. Similarly the component of edge force on the leading edge in the y direction on the element δy, $(\delta Y_e)_l$ is given by

$$(\delta Y_e)_l = \delta T_e \left(\frac{y}{|y|} \right) \tan \Lambda, \qquad (21)$$

so that the resultant of δT_e and δY_e is normal to the leading edge; the factor $(y/|y|)$ is required if in the usual notation the sweepback $\Lambda(y)$ is regarded as symmetric with respect to y. Since equation (19) holds in the limiting case $\Lambda = \pi/2$, the outward side edge force on an element of length δx on the side edge of both S_W and S_T, $(\delta Y_e)_s$ is given by

$$(\delta Y_e)_s = \pi \rho \left\{ \left(\frac{\partial \Phi}{\partial y} \right)^2_{+0} \delta_y \right\}_{\delta_y \to 0} \delta x. \qquad (22)$$

Equation (22) holds for $y = \pm s$, δ_y being the inward distance from the edge in each case.

2.4. Planar Wing Forces and Moments

In Section 2.2 expressions are given for the load distributions over planar areas S_W and S_T while in Section 2.3 expressions are given for the edge forces acting on the boundary of $S_W + S_T$. The total forces and moments are obtained by integration of the load distributions and adding together the various contributions; these forces and moments will be called the 'planar' forces and moments because they are derived from the planar model and will be denoted by the subscript P.

The planar lift L_P on S_W is, from equation (13),

$$L_P = \iint_{S_W} \rho U \frac{\partial \Delta \Phi}{\partial x} \, dx \, dy = \int_{-s}^{+s} \rho U \, \Delta \Phi_t(y) \, dy, \qquad (23)$$

writing $\Delta \Phi_t(y) = \Delta \Phi(x_t(y), y)$. There is no planar lift on S_T since $\partial \Delta \Phi / \partial x$ is zero on S_T.

9

The total planar drag D_P on S_W is, from equations (14) and (20),

$$D_P = -\iint\limits_{S_W} \rho U \frac{\partial Z_c}{\partial x} \frac{\partial \Delta \Phi}{\partial x} dx\, dy - \int_{-s}^{+s} \pi \rho \left\{ \left(\frac{\partial \Phi}{\partial x}\right)^2_{+0} \delta_x \right\}_{\delta_x \to 0} \sec \Lambda\, dy, \tag{24}$$

where $w(x, y)$ is replaced by $U\, \partial Z_c/\partial x$ according to the boundary condition in equation (8) (remember that $\partial Z_c/\partial x < 0$ implies positive incidence). There is no planar drag on S_T since $\partial \Delta \Phi/\partial x$ is zero on S_T while the edge forces on S_T act in the y direction.

The total planar side force Y_P on $(S_W + S_T)$ is written in the form

$$Y_P = (Y_P)_W + (Y_P)_T, \tag{25}$$

where $(Y_P)_W$ is the side force on S_W and $(Y_P)_T$ is the side force on S_T; thus from equations (15), (21) and (22), replacing $w(x, y)$ on S_W by $U\, \partial Z_c/\partial x$

$$(Y_P)_W = -\iint\limits_{S_W} \rho U \frac{\partial Z_c}{\partial x} \frac{\partial \Delta \Phi}{\partial y} dx\, dy + Y_e, \tag{26}$$

where Y_e is the total edge force on S_W given by

$$Y_e = \int_{-s}^{+s} \pi \rho \left\{ \left(\frac{\partial \Phi}{\partial x}\right)^2_{+0} \delta_x \right\}_{\delta_x \to 0} \sec \Lambda \tan \Lambda \frac{y}{|y|} dy +$$

$$+ \int_{x_l(s)}^{x_t(s)} \pi \rho \left[\left\{ \left(\frac{\partial \Phi}{\partial y}\right)^2_{+0} \delta_y \right\}_{\substack{y = +s \\ \delta_y \to 0}} - \left\{ \left(\frac{\partial \Phi}{\partial y}\right)^2_{+0} \delta_y \right\}_{\substack{y = -s \\ \delta_y \to 0}} \right] dx. \tag{27}$$

Similarly,

$$(Y_P)_T = -\iint\limits_{S_T} \rho w \frac{\partial \Delta \Phi}{\partial y} dx\, dy + \int_{x_t(s)}^{\infty} \pi \rho \left[\left\{ \left(\frac{\partial \Phi}{\partial y}\right)^2_{+0} \delta_y \right\}_{\substack{y = +s \\ \delta_y \to 0}} - \left\{ \left(\frac{\partial \Phi}{\partial y}\right)^2_{+0} \delta_y \right\}_{\substack{y = -s \\ \delta_y \to 0}} \right] dx. \tag{28}$$

The double integral in equation (28) for $(Y_P)_T$ cannot be simply reduced further because $w(x, y)$ on S_T is now a double integral over S_W, involving $\partial \Delta \Phi/\partial x$, given by the right-hand side of equation (12) where the reference point (x, y) is on S_T.

The planar aerodynamic moments can also be formulated. The signs of the moments have been made consistent with the usual convention for aircraft stability and control.

The planar rolling moment on S_W, positive in the sense of port wing up, is

$$\mathscr{L}_P = -\iint\limits_{S_W} \rho U y \frac{\partial \Delta \Phi}{\partial x} dx\, dy = -\int_{-s}^{+s} \rho U y\, \Delta \Phi_t(y)\, dy; \tag{29}$$

there is no rolling moment on S_T.

The planar pitching moment on S_W, nose up about the axis $x = x_0$, becomes

$$\mathscr{M}_P = -\iint\limits_{S_W} \rho U (x - x_0) \frac{\partial \Delta \Phi}{\partial x} dx\, dy; \tag{30}$$

there is no pitching moment on S_T.

The planar yawing moment about an axis parallel to $0z$, through $(x_0, 0, 0)$ is taken to be positive in the sense of port wing forward. Thus the total yawing moment on $(S_W + S_T)$ is

$$\mathscr{N}_P = (\mathscr{N}_P)_W + (\mathscr{N}_P)_T, \tag{31}$$

where, on S_W

$$(\mathscr{N}_P)_W = \iint\limits_{S_W} \rho U \frac{\partial Z_c}{\partial x} \left\{ -y \frac{\partial \Delta \Phi}{\partial x} + (x - x_0) \frac{\partial \Delta \Phi}{\partial y} \right\} dx\, dy + N_e, \tag{32}$$

with

$$\mathscr{N}_e = -\int_{-s}^{+s} \pi \rho \left\{ \left(\frac{\partial \Phi}{\partial x}\right)^2_{+0} \delta_x \right\}_{\delta_x \to 0} \left\{ y + (x_l(y) - x_0) \frac{y}{|y|} \tan \Lambda \right\} \sec \Lambda\, dy -$$

$$- \int_{x_l(s)}^{x_t(s)} \pi \rho (x - x_0) \left[\left\{ \left(\frac{\partial \Phi}{\partial y}\right)^2_{+0} \delta_y \right\}_{\substack{y = +s \\ \delta_y \to 0}} - \left\{ \left(\frac{\partial \Phi}{\partial y}\right)^2_{+0} \delta y \right\}_{\substack{y = -s \\ \delta_y \to 0}} \right] \tag{33}$$

10

from the edge forces on S_W; and on S_T

$$(\mathcal{N}_P)_T = \iint_{S_T} \rho w (x - x_0) \frac{\partial \Delta \Phi}{\partial y} dx \, dy - \int_{x_t(s)}^{\infty} \pi \rho (x - x_0) \left[\left\{ \left(\frac{\partial \Phi}{\partial y} \right)_{+0}^2 \delta_y \right\}_{\substack{y=+s \\ \delta_y \to 0}} - \left\{ \left(\frac{\partial \Phi}{\partial y} \right)_{+0}^2 \delta_y \right\}_{\substack{y=-s \\ \delta_y \to 0}} \right] dx. \quad (34)$$

It is noted that in the above expressions for the forces and moments, lift, pitching moment and rolling moment are first order in $\Delta \Phi$ while drag, side force, and yawing moment are of second order in $\Delta \Phi$ and Z_c.

2.5. Integral Relationships; Trefftz Plane Analysis

An alternative approach to the estimation of the total forces and moments on a finite wing is to apply the principles of linear and angular momentum to a large control volume enclosing the wing. Such an approach leads to the standard result for induced, or vortex, drag in terms of a simple single integral relationship in a transverse plane far downstream, known as the Trefftz plane. The usefulness of this simple integral relationship for the drag is that it bypasses the evaluation of the surface integral over S_W and the determination of the leading edge thrust, as expressed in equation (24). The purpose of this section is to show that similar simple relationships exist for side force and yawing moment.

A large control volume $ABCDA'B'C'D'$ is constructed, as shown in Fig. 5, enclosing S_W; the planar trailing sheet S_T cuts the downstream transverse plane $DCC'D'$ in a line of width $2s$.

At the upstream transverse section $ABB'A'$ the normal velocity is U, the free stream velocity, and the static pressure is the free stream static pressure p_∞. It is assumed that the downstream transverse section $DCC'D'$ is sufficiently far downstream for the longitudinal perturbation u to be negligibly small so the normal velocity across $DCC'D'$ is again the freestream velocity U. However perturbation velocities v and w exist in the plane of $DCC'D'$ due to the trailing vortex sheet S_T; because of these perturbation velocities v and w the static pressure p on $DCC'D'$ is less than p_∞. Perturbation velocities and pressures on the four surfaces parallel to the stream direction are small, but their effects are not necessarily negligible.

First the lift on the system is considered by application of the linear momentum principle in the z direction; in the limit as $ABB'A'$ and $DCC'D'$ tend to infinity, the only contribution to the lift arises from the vertical momentum flux crossing the downstream Trefftz plane (i.e. $DCC'D'$); thus the lift, which is identical to the planar lift as defined in equation (23), is given by

$$L_P = - \iint_{DCC'D' \to \infty} \rho U w \, dy \, dz$$

$$= - \iint_{DCC'D' \to \infty} \rho U \frac{\partial \Phi}{\partial z} dy \, dz$$

$$= \left\{ \int_{-s}^{+s} \rho U \, \Delta \Phi \, dy \right\}_{x \to +\infty} \quad (35)$$

after integration with respect to z, remembering the discontinuity in Φ across the slit $|y| \leqslant s$ on $z = 0$ and that Φ tends to zero as $|z| \to \infty$. It is noted that equation (35) is identical to equation (23). It should also be noted that equation (35) can be derived from a large finite control volume $ABCDA'B'C'D'$; it is not necessary for this control volume to tend to infinity to obtain equation (35).

To obtain the drag the linear moment principle is applied in the x direction; in the limit as $ABB'A'$ and $CDD'C'$ tend to infinity, the only contribution arises from the difference between the static pressure on the upstream plane $ABB'A'$ and the static pressure on the downstream plane. Thus the drag, which is identical to the planar drag as defined in equation (24), is given by

$$D_P = \iint_{DCC'D' \to \infty} (p_\infty - p) \, dy \, dz = \iint_{DCC'D' \to \infty} \tfrac{1}{2} \rho (v^2 + w^2) \, dy \, dz$$

$$= \iint_{DCC'D' \to \infty} \tfrac{1}{2} \rho \left[\left(\frac{\partial \Phi}{\partial y} \right)^2 + \left(\frac{\partial \Phi}{\partial z} \right)^2 \right] dy \, dz$$

$$= \iint_{DCC'D' \to \infty} \tfrac{1}{2} \rho \left[\frac{\partial}{\partial y} \left(\Phi \frac{\partial \Phi}{\partial y} \right) + \frac{\partial}{\partial z} \left(\Phi \frac{\partial \Phi}{\partial z} \right) \right] dy \, dz$$

11

(since on $DCC'D'$ $\partial^2\Phi/\partial y^2 + \partial^2\Phi/\partial z^2 = 0$)

$$= -\left\{\int_{-s}^{+s} \tfrac{1}{2}\rho\,\Delta\Phi\frac{\partial\Phi}{\partial z}\,dy\right\}_{x\to+\infty}. \qquad (36)$$

Equation (36) is the standard expression for vortex drag. As described in Ref. 5, the numerical equivalence between equations (24) and (36) for vortex drag is a test of the accuracy of the numerical solution of the lifting surface integral equation (equation (12)). It should be noted that equation (36) is only obtained in the limit as the control volume $ABCDA'B'C'D'$ tends to infinity; if a large finite control volume $ABCDA'B'C'D'$ is taken, the linear momentum principle leads directly to equation (24) and not to equation (36).

The side force relationship follows by application of the linear momentum principle in the y direction, in the same manner as for the lift. Hence the total side force, that is the combined side force on S_W and S_T, from equations (25) to (28), is

$$Y_P = (Y_P)_W + (Y_P)_T = -\iint\limits_{DCC'D'\to\infty} \rho U v\,dy\,dz$$

$$= -\iint\limits_{DCC'D'\to\infty} \rho U\frac{\partial\Phi}{\partial y}\,dy\,dz$$

$$= 0 \qquad (37)$$

after integration with respect to y since Φ tends to zero as $|y|\to\infty$. Thus the total planar side force is zero; the implications of this result are discussed in the following section.

Next the principle of conservation of angular momentum is applied about each axis.

The application of the principle of angular momentum about the $0y$ axis, to give the pitching moment $\mathscr{M}_P$, is not a fruitful exercise. The pitching moment appears as the difference of two large quantities namely, $(x - x_0)L_P$ (where x is the location of the downstream Trefftz plane and L_P is the planar lift) and integrals over the streamwise planes $ABCD$ and $ADD'A'$; this difference can be shown to reduce to the standard integral over S_W as expressed in equation (30).

In the application of the principle of angular momentum about the $0x$ axis, in the limit as the control volume becomes infinitely large, the only terms which remain appear in the Trefftz plane and the rolling moment becomes

$$\mathscr{L}_P = \iint\limits_{DCC'D'\to\infty} \rho U(wy - vz)\,dy\,dz = -\int_{-s}^{+s} \rho U y\,\Delta\Phi_t(y)\,dy, \qquad (38)$$

which tallies with equation (29).

Finally, when the principle of angular momentum is applied about an axis parallel to the $0z$ axis through the point $(x_0, 0, 0)$, since the total side force is zero, in the limit of the control surface tending to infinity again the only contributions appear in the Trefftz plane, and so the total yawing moment becomes

$$\mathscr{N}_P = (\mathscr{N}_P)_W + (\mathscr{N}_P)_T$$

$$= \iint\limits_{DCC'D'\to\infty} (p_\infty - p)y\,dy\,dz$$

$$= -\left\{\int_{-s}^{+s} \tfrac{1}{2}\rho y\,\Delta\Phi\frac{\partial\Phi}{\partial z}\,dy\right\}_{x\to+\infty} \qquad (39)$$

where $(\mathscr{N}_P)_W$ and $(\mathscr{N}_P)_T$ are the planar yawing moments on S_W and S_T respectively, given by equations (31), (32) and (34). The implications of equation (39) are discussed in Section 2.7.

2.6. Discussion of Side Force

Equation (37) states that the overall planar side force Y_P is zero. It is now argued that $(Y_P)_T$, the planar side force on the planar trailing sheet S_T, is negligibly small, implying that $(Y_P)_W$, the planar side force on S_W, is virtually zero.

Consider first the side force $(Y_P)_T$ on S_T aft of a rectangular wing (chord c, span $2s$). Suppose that in Fig. 5 a transverse plane $cdd'c'$ is drawn parallel to the Trefftz plane, but upstream of the Trefftz plane, at the wing

12

trailing edge. Then the side force on S_T, $(Y_P)_T$, is equal to the difference in the sideways momentum flux (in the y direction) across $cdd'c'$ and across $CDD'C'$, thus

$$(Y_P)_T = \iint\limits_{cdd'c' \to \infty} \rho(U + u)v \, dy \, dz - \iint\limits_{CDD'C' \to \infty} \rho U v \, dy \, dz$$

$$= \iint\limits_{cdd'c' \to \infty} \rho u v \, dy \, dz \tag{40}$$

where u, v are the perturbation velocities, since the integral over $CDD'C'$ is zero.

Now in the integrand of equation (40) u is a continuous anti-symmetric function of z and so u vanishes on $z = 0$. Also v is an antisymmetric function of z but v is discontinuous on the slit $|y| \leqslant s$, $z = 0$ and the magnitude of v decreases with increasing $|z|$. Furthermore, for any value of z, $\int_{-\infty}^{+\infty} v \, dy$ is zero. The combination of all of these factors suggests that the second order integral in equation (40) is negligible to the order of approximation of the present analysis.

For a swept wing the above argument suggests that the contribution to $(Y_P)_T$ from the trailing sheet aft of $x_t(s)$ is small; unfortunately the above argument cannot be extended to that part of the trailing sheet between $x_t(y)$ and $x_t(s)$. However it is assumed that for all wings

$$(Y_P)_T \approx 0. \tag{41}$$

Numerical examples, given later, support this assumption.

It should be emphasised that although the total side force $(Y_P)_T$ is taken to be negligibly small the actual distribution of side force on S_T is not everywhere small. For example, the edge force distribution in the y direction on a side edge of S_T (i.e. $y = \pm s$) is virtually the same as the wing tip force on S_W. All that equation (41) states is that the overall side force on S_T is negligible.

Thus the implication of equations (37) and (41) is that the planar side force on S_W is negligibly small, so

$$(Y_P)_W \approx 0. \tag{42}$$

It is necessary now to interpret equation (42).

As an example, consider a twisted rectangular wing whose camber shape is given by

$$Z_c(x, y) = -\alpha x \left(1 + \frac{y}{s} \right). \tag{43}$$

For this wing $Z_c(x, y)$ is zero at the leading edge (i.e. where $x = 0$); $Z_c(x, y)$ is zero at the port wing tip ($y = -s$); the wing incidence increases linearly with y from zero at the port wing tip ($y = -s$) to $Z\alpha$ at the starboard wing tip ($y = +s$). Everywhere on this wing $\partial Z_c / \partial y$ is negative.

When the wing defined in equation (43) is placed in a uniform low speed stream a differential pressure distribution is created which acts normal to the camber surface $Z_c(x, y)$; and tip edge forces are produced. Now the total side force is made up from two contributions

(i) the integrated component of the differential pressure in the y direction;
and
(ii) the resultant of the edge forces.

Now, since $\partial Z_c / \partial y$ is everywhere negative and since the loading distribution is expected to be everywhere positive (i.e. upward), contribution (i) must lead to a positive side force in the y direction. And since the present example is confined to a rectangular wing, only the wing tip edge forces contribute to the side force; the incidence of the port tip ($y = -s$) is zero while the incidence of the starboard tip ($y = +s$) is 2α, so the larger tip force will act on the starboard tip and contribution (ii) above will also be positive.

Thus an example has been given where the actual side force cannot be zero; this result is at variance with equation (42). Denoting the actual (inviscid) side force experienced by the wing as Y, then Y is not identical to the planar side force $(Y_P)_W$, which has been shown to be virtually zero. An approximate relationship between Y and $(Y_P)_W$ is established later in Section 3.

2.7. Discussion of Yawing Moment

Similar lines of reasoning to those presented for the side force in the preceding section can be applied to the yawing moment. The planar yawing moment on S_T can be assumed to be negligible since the planar yawing

13

moment on S_T arises from the drag on S_T, which is identically zero, and from the side force on S_T, which has already been assumed to be negligibly small by equation (41), then it is consistent to neglect the planar yawing moment on S_T. Thus

$$(\mathcal{N}_P)_T \approx 0. \tag{44}$$

Again numerical results, which are presented later, support this assumption. On substitution of equation (44) into equation (39) then the planar yawing moment on the wing becomes

$$(\mathcal{N}_P)_W \approx -\left\{ \int_{-s}^{+s} \tfrac{1}{2}\rho y \, \Delta\Phi \frac{\partial \Phi}{\partial z} \, dy \right\}_{x=+\infty}. \tag{45}$$

Since the actual (inviscid) side force Y cannot be identified with the planar side force $(Y_P)_W$ it would be expected that the actual (inviscid) yawing moment $\mathcal{N}$ would differ from the planar yawing moment $(\mathcal{N}_P)_W$. It is not possible to give a simple physical example to illustrate this difference as in the case of side force in the previous section, however approximate relationships for $\mathcal{N}$ and $(\mathcal{N}_P)_W$ are given later in Section 3.

3. Non-Planar Wing Theory at Low Speeds

It is shown in Section 2 that the planar model described there leads to uncertainties in the estimation of side force and yawing moment. In this section it is shown that by the reinterpretation of the results already obtained in the solution of the planar model it is possible to explain and to relate, approximately, the actual (inviscid) side force and yawing moment to their planar values.

A non-planar model is now formulated in which the discontinuity in velocity potential $\Delta\Phi(x, y)$ is situated across the wing camber ($+$ incidence) surface $Z_c(x, y)$ and across a trailing surface which is formed at the trailing edge of the wing $Z_c(x = x_t(y), y)$ with downstream generators parallel to the freestream direction. This model is shown in Fig. 6.

In the formulation of the boundary conditions on the wing, with the assumption that $u \ll U$, the overall problem again divides into two independent problems for (camber and incidence) effects and thickness effects. However, neither of these two problems now is purely symmetric and antisymmetric with respect to z, although the lifting problem is still associated with camber and incidence only. Restricting attention to the lifting problem the appropriate boundary condition is

$$w(x, y, Z_c(x, y)) = U \frac{\partial Z_c}{\partial x}. \tag{46}$$

If it is further assumed that,
   (i) $Z_c(x, y)/c_R$ is small (where c_R is the root chord)
and
   (ii) that on the trailing surface

$$\Delta\Phi = \Delta\Phi(x_t(y), y) = \Delta\Phi_t(y), \tag{47}$$

then the integral equation relating $w(x, y, Z_c)$ and $(\partial \Delta\Phi/\partial x)$ can be taken to be the same equation as in the planar model, as given by equation (12). Thus any standard numerical solution of the lifting surface integral equation, namely equation (12), can be regarded as the solution of the non-planar model subject to the two assumptions (i) and (ii) as above.

The pressure difference across the wing camber surface and across the downstream trailing sheet can be determined, as before, by the application of Bernoulli's equation. In this case

$$p_l - p_u = \rho \left\{ U \frac{\partial \Delta\Phi}{\partial x} + v_m \frac{\partial \Delta\Phi}{\partial y} \right\} \tag{48}$$

where the subscripts l and u refer to the lower and upper surfaces respectively and where v_m is the mean side velocity across the sheet discontinuity, i.e.

$$v_m = \frac{1}{2} \left\{ \left(\frac{\partial \Phi}{\partial y} \right)_l + \left(\frac{\partial \Phi}{\partial y} \right)_u \right\}.$$

For the planar model v_m is identically zero but for the non-planar model v_m is not zero. Hence the pressure loading $(p_l - p_u)$ consists of a first order term, depending on $\partial \Delta\Phi/\partial x$ and a second order term, depending on v_m and $\partial \Delta\Phi/\partial y$.

14

It has been assumed in equation (47) that $\partial\Delta\Phi/\partial x$ is zero on the trailing surface, thus from equation (48) $(p_l - p_u)$ is not zero on the trailing surface to second order. In particular, the Kutta trailing edge condition is not satisfied to second order. It can be argued however that the solution of the standard lifting-surface equation (i.e. equation (12)) will give a solution for $\Delta\Phi$ correct to first order for both the planar and non-planar models.

Once $\Delta\Phi$ has been determined the overall forces and moments on the wing can then be calculated. For the non-planar model, by virtue of the boundary condition, the resultant velocity on the wing camber surface is parallel to that surface, there is therefore no flow across $Z_c(x, y)$; all the load distributions derive directly from the resolution of the pressure loading. Thus

$$\text{Lift} = L = \iint_{\text{wing}} (p_l - p_u)\, dx\, dy; \tag{49}$$

$$\text{Drag} = D = \iint_{\text{wing}} (p_l - p_u)\left(-\frac{\partial Z_c}{\partial x}\right) dx\, dy - T_e, \tag{50}$$

where T_e is the leading edge thrust given by the integration of equation (20);

$$\text{Side Force} = Y = \iint_{\text{wing}} (p_l - p_u)\left(-\frac{\partial Z_c}{\partial y}\right) dx\, dy + Y_e \tag{51}$$

where Y_e is the sum of the edge forces in the y direction as given by equation (27);

$$\text{Rolling Moment} = \mathscr{L} = \iint_{\text{wing}} (p_l - p_u)(-y)\, dx\, dy; \tag{52}$$

$$\text{Pitching Moment} = \mathscr{M} = \iint_{\text{wing}} (p_l - p_u)(x_0 - x)\, dx\, dy; \tag{53}$$

$$\text{Yawing Moment} = \mathscr{N} = \iint_{\text{wing}} (p_l - p_u)\left\{\left(-\frac{\partial Z_c}{\partial x}\right)y - \left(-\frac{\partial Z_c}{\partial y}\right)(x - x_0)\right\} dx\, dy + \mathscr{N}_e, \tag{54}$$

where $\mathscr{N}_e$ is the sum of all the yawing moments due to edge forces given by equation (33).

In the above expressions the lift L, the pitching moment $\mathscr{M}$, and the rolling moment $\mathscr{L}$ are correct to first order; the drag D, the side force Y and the yawing moment $\mathscr{N}$ are correct to second order.

Since to first order $(p_l - p_u)$ is equal to $\rho U\, \partial\Delta\Phi/\partial x$, it is seen that the lift L, drag D, rolling moment $\mathscr{L}$ and pitching moment $\mathscr{M}$ given by equations (49), (50), (52) and (53) on the basis of the non-planar model are identical to the planar expressions L_P, D_P, $\mathscr{L}_P$, and $\mathscr{M}_P$ as given by equations (23), (24), (29) and (30). But the expressions for side force Y and yawing moment $\mathscr{N}$ given by equations (51) and (54) on the basis of the non-planar model are not identical to the planar expressions $(Y_P)_W$ and $(\mathscr{N}_P)_W$ as given by equations (26) and (32); these differences are discussed in the following sections.

3.1. Side Force

The side force on a wing, according to the non-planar model, is given by equation (51); to a first order

$$Y = \iint_{\text{wing}} \left(\rho U\frac{\partial\Delta\Phi}{\partial x}\right)\left(-\frac{\partial Z_c}{\partial y}\right) dx\, dy + Y_e, \tag{55}$$

where Y_e is the total edge force contribution in the y direction (given by equation (27)). On the other hand, the planar side force condition is from equations (26) and (42)

$$(Y_P)_W = \iint_{S_W} \left(\rho U\frac{\partial\Delta\Phi}{\partial y}\right)\left(-\frac{\partial Z_c}{\partial x}\right) dx\, dy + Y_e \approx 0, \tag{56}$$

where Y_e, the side edge force, is the same in both equations (55) and (56).

A physical explanation of why the two models should give different expressions for the side force is given later, at this stage the algebraic relationship is developed.

Integration of equation (55) once by parts with respect to x gives

$$Y = \int_{-s}^{+s} \left[\rho U \, \Delta\Phi \left(-\frac{\partial Z_c}{\partial y} \right) \right]_{x=x_t(y)} dy - \iint_{\text{wing}} \rho U \, \Delta\Phi \left(-\frac{\partial^2 Z_c}{\partial x \, \partial y} \right) dx \, dy + Y_e,$$

and with a second integration by parts with respect to y,

$$Y = \int_{-s}^{+s} \left[\rho U \, \Delta\Phi \left(-\frac{\partial Z_c}{\partial y} \right) \right]_{x=x_t(y)} dy + \int_{x_t(0)}^{x_t(s)} \left[\rho U \, \Delta\Phi \left(-\frac{\partial Z_c}{\partial x} \right) \right]_{y=-y_t(x)}^{y=+y_t(x)} dx + \iint_{S_W} \rho U \frac{\partial \Delta\Phi}{\partial y} \left(-\frac{\partial Z_c}{\partial x} \right) dx \, dy + Y_e.$$

(57)

The sign of the second line integral is plus assuming that the trailing edge is swept back; a swept forward trailing edge requires a negative sign. Comparing equations (56) and (57) it is seen that

$$Y = \int_{-s}^{+s} [\rho U \, \Delta\Phi]_{x=x_t(y)} \left[-\frac{dZ_c(x_t(y), y)}{dy} \right] dy + (Y_P)_W$$

$$\approx \int_{-s}^{+s} [\rho U \, \Delta\Phi_t(y)] \left[-\frac{dZ_c(x_t(y), y)}{dy} \right] dy,$$

(58)

since $(Y_P)_W$ is taken to be negligibly small according to equation (56). Equation (58) is valid whether or not the trailing edge is swept forward or backward.

Thus the side force is given purely in terms of conditions at the wing trailing edge, assuming that the side force on the trailing sheet can be neglected. When $Z_c(x_t(y), y)$ is independent of y then the side force Y is zero; in such a case the side force contribution from the integration of the pressure distribution over the wing surface cancels the side force due to the edge forces. When $dZ_c(x_t(y), y)/dy$ is uniform, as in the example expressed by equation (43), then

$$Y \approx (\text{Lift}) \left(-\frac{dZ_c(x_t(y), y)}{dy} \right).$$

(59)

In Part II Garner has evaluated the lifting surface characteristics (i.e. pressure distribution and edge forces) of a number of wings with asymmetric twist. Results for a series of rectangular wings of aspect ratio 2 at low speed with different camber surfaces, all of which have Z_c zero along the trailing edge, are shown in Table 1. These results are presented in terms of side force coefficients: the total side force coefficient C_Y is made up from the side force coefficient due to the integration of the normal pressure distribution (C_{Y1}) and the side force coefficient due to the wing-tip edge forces (C_{Y3}, for consistency with Garner's notation). Equation (58) suggests that the total side force in all of these cases is virtually zero (i.e. $C_Y = C_{Y1} + C_{Y3} = 0$) since $Z_c(x_t(y), y)$ at the trailing edge is identically zero. It is seen that the numerical values shown in Table 1 confirm this conclusion with remarkable accuracy.

Results obtained when the effects of compressibility are considered are discussed in Section 4.4.

3.2. Yawing Moment

A similar process can be followed for the yawing moment as that presented in the previous section for the side force.

The yawing moment on a wing, according to the non-planar model, is given by equation (54) namely

$$\mathcal{N} = \iint_{\text{wing}} \left(\rho U \frac{\partial \Delta\Phi}{\partial x} \right) \left\{ \left(-\frac{\partial Z_c}{\partial x} \right) y - \left(-\frac{\partial Z_c}{\partial y} \right)(x - x_0) \right\} dx \, dy + \mathcal{N}_e$$

(60)

where $\mathcal{N}_e$ is the yawing moment due to the edge forces (given by equation (33)). The planar yawing moment on the wing, according to the planar model, is, from equations (32) and (45),

$$(\mathcal{N}_P)_W = \iint_{S_W} \rho U \left\{ -y \frac{\partial \Phi}{\partial x} + (x - x_0) \frac{\partial \Delta\Phi}{\partial y} \right\} \frac{\partial Z_c}{\partial x} dx \, dy + \mathcal{N}_e$$

$$\approx \left\{ -\int_{-s}^{+s} \frac{1}{2} \rho y \, \Delta\Phi \frac{\partial \Phi}{\partial z} dy \right\}_{x \to +\infty}$$

(61)

where $\mathcal{N}_e$ the yawing moment due to the edge forces is the same in both equations (60) and (61).

16

On integration of the second term in equation (60) by parts and by rearrangement it follows that

$$\mathcal{N} \approx \left\{ -\int_{-s}^{+s} \tfrac{1}{2}\rho y \, \Delta\Phi \frac{\partial\Phi}{\partial z} \, dy \right\}_{x \to +\infty} + \int_{-s}^{+s} [\rho U \, \Delta\Phi_t(y)](x_t(y) - x_0)\left[\frac{dZ_c(x_t(y), y)}{dy}\right] dy - \iint_{S_W} \rho U \, \Delta\Phi \frac{\partial Z_c}{\partial y} \, dx \, dy.$$

(62)

It is noted from equation (62) that when $Z_c(x_t(y), y)$ is zero or constant the yawing moment is virtually independent of yawing axis position x_0.

Garner has also calculated the various terms which make up both sides of equation (62) for the same rectangular wings of aspect ratio 2 with the various camber surfaces as specified in Table 1 where the results for the side force are presented. In non-dimensional terms the yawing moment C_n is made up from

C_{n1} = yawing moment coefficient due to the integration of the pressure loading over S_W,

C_{n2} = yawing moment coefficient due to leading edge thrust,

C_{n3} = yawing moment coefficient due to wing tip edge forces.

The terms on the right-hand side of equation (62) are denoted:

C_{nI} = yawing moment coefficient due to Trefftz plane integral (first term on right-hand side of equation (62) in non-dimensional form)

C_{nII} = yawing moment coefficient from the line integral along the trailing edge (i.e. second term on right-hand side of equation (62) in non-dimensional form)

C_{nIII} = yawing moment coefficient from surface integral (i.e. third term on right-hand side of equation (62) in non-dimensional form).

The numerical results are listed in Table 2.

It is noted that C_{nII} is zero in all of these examples since $Z_c(x_t(y), y)$ is zero.

The agreement between $(C_{nI} + C_{nIII})$ and $(C_{n1} + C_{n2} + C_{n3})$ is reasonable, the difference being within 6 per cent of the value of either term. It is thought that most of this difference is associated with the neglect of the yawing moment on S_T, while the remainder is due to numerical deficiencies in the calculation of the wing-tip edge forces.

Further results are quoted later when compressibility effects are described.

3.3. Integral Relationships; Trefftz Plane Analysis

In the analysis so far, integral relationships have already been obtained for the side force and yawing moment (i.e. equations (58) and (62)) essentially by equating the actual side force and yawing moment on the non-planar wing model to the Trefftz plane results for the planar model. Now it is axiomatic that the forces and moments estimated from a large control volume analysis should be consistent with the forces and moments estimated at the wing itself assuming the same model, thus equations (58) and (62) should appear from a Trefftz plane analysis of the non-planar model. This analysis is not presented fully here, an outline is given to show how and where the various terms arise.

Consider a large control volume $ABCDA'B'C'D'$ as shown in Fig. 5 enclosing the non-planar model. The trailing sheet now cuts the down-stream Trefftz plane (surface $CDD'C'$) in a curved line

$$z(y) = Z_c(x_t(y), y)$$

(63)

as shown in Fig. 6 across which the discontinuity $\Delta\Phi_t(y)$ acts.

The same arguments as those presented in Section 2.5 are followed through.

First for the lift

$$L = \iint_{CDD'C' \to \infty} \rho U(-w) \, dy \, dz = -\iint_{CDD'C' \to \infty} \rho U \frac{\partial\Delta\Phi}{\partial z} \, dy \, dz$$

$$= \int_{-s}^{+s} \rho U \, \Delta\Phi_t(y) \, dy$$

(64)

assuming that $\partial Z_c/\partial y$ is small; this relationship is the standard formula for the lift.

For the drag

$$D = \iint_{CDD'C' \to \infty} (p_\infty - p)\,dy\,dz = -\int_{-s}^{+s} \left\{ \tfrac{1}{2}\rho\, \Delta\Phi \frac{\partial\Phi}{\partial z} \right\}_{\substack{z = Z_c(x_t(y),y) \\ x \to +\infty}} dy \tag{65}$$

which, assuming Z_c small, is the standard form.

The expression for side force becomes, neglecting the side force required to maintain the trailing surface,

$$Y = \iint_{CDD'C' \to \infty} \rho U(-v)\,dy\,dz$$

$$= -\iint_{CDD'C' \to \infty} \rho U \frac{\partial\Phi}{\partial y}\,dy\,dz$$

$$= \int_{Z_c(-s)}^{Z_c(+s)} \rho U(-\Delta\Phi_t)\,dz$$

$$= \int_{-s}^{+s} \rho U\, \Delta\Phi_t(y)\left(-\frac{dZ_c(x_t(y),y)}{dy} \right)dy \tag{66}$$

which is now identical to equation (58) as anticipated.

By the principle of conservation of angular momentum, the rolling moment and pitching moment analyses follow similar lines to those described for the purely planar model.

The yawing moment derivation is far more complicated; a complete analysis is not attempted here, only a rough outline is presented. The contribution to the yawing moment from the Trefftz plane is

$$\iint_{CDD'C' \to \infty} (p_\infty - p)y\,dy\,dz + (x - x_0)\iint_{CDD'C' \to \infty} \rho U(-v)\,dy\,dz.$$

There are now additional contributions from the streamwise surfaces $ADD'A'$ and $BCC'B'$ (*see* Fig. 5) due to the yawing moment from the momentum flux ρUv. One term will combine with the second term in the above equation to give the overall side force contribution to the yawing moment, namely

$$-\int_{-s}^{+s} \rho U(x_t(y) - x_0)\,\Delta\Phi_t \frac{dZ_c(x_t(y),y)}{dy}\,dy.$$

(This step is analogous to an equivalent step in the pitching moment analysis.) Another term arises on surfaces $ADD'A'$ and $BCC'B'$ due to the fact that the trailing vorticity $\partial\Delta\Phi/\partial y$ on the wing and trailing sheet is skew, since $\partial Z_c(x,y)/\partial y$ is non-zero, thus the velocity in the far field is no longer antisymmetric with respect to z. It is conjectured that integration of this effect leads to the term

$$\iint_{S_W} \rho U\, \Delta\Phi \frac{\partial Z_c}{\partial y}(x,y)\,dx\,dy$$

which must arise to preserve conformity with the results already obtained from the alternative planar model, as given by equation (62).

It is now possible to explain why the planar side force $(Y_P)_W$ is not identical to the actual side force Y. According to equation (66) the side force Y can be regarded as the inclination of the lift distribution vector through the angle $-\{dZ_c(x_t(y),y)/dy\}$ in the non-planar model; thus if a planar model is postulated, a side force $\{Y - (Y_P)_W\}$ is required to set and maintain the trailing vorticity at the wing trailing edge in the plane $z = 0$. When the trailing sheet in the non-planar model emanates from the trailing edge in the plane $z = 0$ (i.e. when $Z_c(x_t(y),y) = 0$) no additional side force is required to set and maintain the planar trailing sheet in the plane $z = 0$, thus $Y = (Y_P)_W \approx 0$. However, even when $Z_c(x_t(y),y)$ is zero, the actual yawing moment $\mathcal{N}$ is not equal to the planar yawing moment $(\mathcal{N}_P)_W$; the double surface integral over S_W in equation (62) still remains. This implies that a distribution of side force is required over S_W to maintain the planar form of S_W in the planar model; and this explains why the distributions, leading to Y and $(Y_P)_W$ in equations (55) and (56) differ. The side force to maintain the planar wake on S_T aft of the trailing edge, namely $(Y_P)_T$, has been shown to be negligibly small; similarly the yawing moment $(\mathcal{N}_P)_T$ required to maintain the non-planar wake aft of the trailing edge has also been neglected. The difference in side force distribution between the actual and planar systems is to maintain the planar wing model, not to maintain any shape of trailing vorticity.

18

4. Linearised Wing Theory in Subsonic Compressible Flow

4.1. Basic Equations

To complete the present investigation it is necessary to ensure that the results derived so far for the low speed (incompressible) flow problem can be extended to the higher subsonic Mach number regime. The derivation of linearised wing theory incorporating compressibility effects is presented in many textbooks as a routine piece of work which is fully wrapped up. Such an attitude is reasonable if linearised wing theory is regarded purely as a first-order theory. But there is a need to clarify the second-order quantities such as induced drag, side force and yawing moment when compressibility effects become important. In the consideration of these second-order quantities further insight is gained into the implications of linearised subsonic wing theory. The following analysis is not fully rigorous, but it is hoped that the main points are adequately discussed.

Again a lifting surface theory is proposed of the uniform flow past an infinitesimal thin wing, $Z_c(x, y)$, (with either the planar or non-planar representation at this stage) behind which extends a system of trailing vorticity. Axes are chosen as before (Fig. 1).

The uniform free stream is denoted by U; the perturbation velocities are u, v, w; the static pressure of the free stream is p_∞, the density of the freestream is ρ_∞, the speed of sound in the free stream is a_∞.

Assuming an inviscid, isentropic flow the standard equations for the variation of speed of sound, pressure and density are

$$a^2 = a_\infty^2 \left\{ \frac{1 + \frac{1}{2}(\gamma - 1)M_\infty^2}{1 + \frac{1}{2}(\gamma - 1)M^2} \right\} \tag{67}$$

$$p = p_\infty \left\{ \frac{1 + \frac{1}{2}(\gamma - 1)M_\infty^2}{1 + \frac{1}{2}(\gamma - 1)M^2} \right\}^{\gamma/(\gamma - 1)}, \tag{68}$$

$$\rho = \rho_\infty \left\{ \frac{1 + \frac{1}{2}(\gamma - 1)M_\infty^2}{1 + \frac{1}{2}(\gamma - 1)M^2} \right\}^{1/(\gamma - 1)}, \tag{69}$$

where γ is the ratio of specific heats and

$$M^2 = \frac{(U + u)^2 + v^2 + w^2}{a^2}. \tag{70}$$

Division of equation (68) by equation (69) is equivalent to equation (67).

The equation of continuity is

$$\frac{\partial}{\partial x}(\rho[U + u]) + \frac{\partial}{\partial y}(\rho v) + \frac{\partial}{\partial z}(\rho w) = 0. \tag{71}$$

Expanding equations (67 to 71) in terms of the perturbation velocities

$$a^2 = a_\infty^2 - (\gamma - 1)Uu - \frac{(\gamma - 1)}{2}(u^2 + v^2 + w^2), \tag{72}$$

$$p = p_\infty - \rho_\infty Uu - \frac{\rho_\infty}{2}(\beta^2 u^2 + v^2 + w^2) + O(u, v, w)^3, \tag{73}$$

$$\rho = \rho_\infty \left[1 - M_\infty^2 \frac{u}{U} - \frac{M_\infty^2}{2}(1 - (2 - \gamma)M_\infty^2)\left(\frac{u}{U}\right)^2 + \frac{(v^2 + w^2)}{2a_\infty^2} + O(u, v, w)^3 \right] \tag{74}$$

and

$$\left[\beta^2 - \frac{u}{U}M_\infty^2(3 - (2 - \gamma)M_\infty^2) \right]\frac{\partial u}{\partial x} + \frac{\partial v}{\partial y} + \frac{\partial w}{\partial z} + O(uv, uw, u^3) = 0 \tag{75}$$

where

$$\beta^2 = 1 - M_\infty^2.$$

Since the flow is irrotational outside of the wing and trailing vorticity a velocity potential Φ exists such that

$$u = \frac{\partial \Phi}{\partial x}, \qquad v = \frac{\partial \Phi}{\partial y} \quad \text{and} \quad w = \frac{\partial \Phi}{\partial z}. \tag{76}$$

19

Away from the transonic region the basic linearised flow equation takes the standard form

$$\beta^2 \frac{\partial^2 \Phi}{\partial x^2} + \frac{\partial^2 \Phi}{\partial y^2} + \frac{\partial^2 \Phi}{\partial z^2} = 0. \tag{77}$$

It can be seen, by reference to equation (75), that the basic equation (77) is based on the assumption that

$$M_\infty^2 \frac{u}{U} \ll \frac{\beta^2}{3 - 2(1 - \gamma)M_\infty^2}.$$

To the same order of approximation it would appear from equation (74) that it would be consistent to take $\rho = \rho_\infty$. But although the change in density is small, it has the same order of magnitude as the change in pressure. Since first-order changes of pressure are retained in the analysis, the first-order changes in density should also be retained. Thus in addition to a first-order discontinuity in pressure across any lifting surface there is an associated first-order discontinuity in density.

It is said in the literature that an appropriate co-ordinate transformation can reduce the linearised problem in compressible flow to one in incompressible flow. This statement is not altogether true, for the discontinuity in density is invariant with respect to the co-ordinate transformation so the 'incompressible' problem retains a first-order discontinuity in density.

The linearised boundary condition, as before, for the planar model, is

$$\left.\frac{\partial \Phi}{\partial z}\right|_{z=0} = U \frac{\partial Z_c}{\partial x}, \tag{78}$$

while for the non-planar model

$$\left.\frac{\partial \Phi}{\partial z}\right|_{z=Z_c} = U \frac{\partial Z_c}{\partial x}. \tag{79}$$

To first order, the pressure loading becomes, from equation (73),

$$p_l - p_u = \rho_\infty U \frac{\partial \Delta\Phi}{\partial x}. \tag{80}$$

Equations (77 to 80) constitute the standard subsonic linearised wing theory problem. It is not disputed that a solution is valid within first-order theory as far as lift, rolling moment and pitching moment are concerned. But for the calculation of induced drag, side force and yawing moment it is necessary to ensure that second-order terms are adequately covered.

4.2. Formulation of Mathematical Model

As already stated there is a density discontinuity across the wing where for a planar model

$$\rho(z = +0) = \rho_\infty \left[1 - \frac{M_\infty^2}{U} \frac{\partial \Phi}{\partial x}\right]_{z=+0}, \qquad \rho(z = -0) = \rho_\infty \left[1 - \frac{M_\infty^2}{U} \frac{\partial \Phi}{\partial x}\right]_{z=-0}. \tag{81}$$

Suppose a planar model is considered as shown in Fig. 2; S_W is the wing planform; S_T is the planar trailing sheet; $\Delta\Phi(x, y)$ exists across S_W and S_T; equation (78) holds on S_W while $\partial\Delta\Phi/\partial x$ is zero across S_T.

To calculate the load distributions in the (x, y, z) directions on this planar model, the small control volume $abcda'b'c'd'$ of Fig. 3 is set up, as in Section 2. The load distributions are to be determined on the element $\delta x\,\delta y$ as δz tends to zero.

First, however, it is necessary to check that continuity is preserved. As $\delta z \to 0$ it is necessary for the mass flow across $abcd$ to equal the mass flow across $a'b'c'd'$; now

$$\text{mass flow across } abcd = \rho w\,\delta x\,\delta y = \rho_\infty \left[1 - M_\infty^2 \frac{u}{U}\right] w\,\delta x\,\delta y,$$

and

$$\text{mass flow across } a'b'c'd' = \rho w\,\delta x\,\delta y = \rho_\infty \left[1 - M_\infty^2 \frac{u}{U}\right]_{z=-0} w\,\delta x\,\delta y. \tag{82}$$

While w is continuous across $z = 0$ by virtue of the boundary condition, u is discontinuous. So continuity is only satisfied to first order, there is a second-order term which remains, equal to

$$\rho_\infty M_\infty^2 \frac{w}{U} \frac{\partial\Delta\Phi}{\partial x}\,\delta x\,\delta y;$$

this term is of the same order as the local streamwise force and so it cannot be dismissed lightly.

20

Without proceeding further the conclusion at this stage must be that the planar model is inadequate as a basis for estimating second-order terms in subsonic compressible flow.

The next step therefore is to consider the non-planar model which can be defined in exactly the same manner as the model in Section 3 and shown in Fig. 6. The discontinuity $\Delta\Phi$ is situated on the camber surface $Z_c(x, y)$ on the wing, while the trailing surface is generated by the streamwise extension of the trailing edge $Z_c(x_t(y), y)$ downstream to $x = +\infty$.

In this case, since on the wing the camber surface is identified with the streamline, continuity of mass is automatically conserved.

The only force distributions on the wing surface are due to normal pressure distribution; thus neglecting third and higher-order terms

$$
\left.
\begin{aligned}
\text{element of force in } z \text{ direction} &= (p_l - p_u)\,\delta x\,\delta y = \rho_\infty U \frac{\partial \Delta\Phi}{\partial x}\,\delta x\,\delta y, \\[2mm]
\text{element of force in } x \text{ direction} &= (p_l - p_u)\left(-\frac{\partial Z_c}{\partial x}\right)\delta x\,\delta y, \\[2mm]
&= \rho_\infty U \frac{\partial \Delta\Phi}{\partial x}\left(-\frac{\partial Z_c}{\partial x}\right)\delta x\,\delta y, \\[2mm]
\text{element of force in } y \text{ direction} &= (p_l - p_u)\left(-\frac{\partial Z_c}{\partial y}\right)\delta x\,\delta y \\[2mm]
&= \rho_\infty U \frac{\partial \Delta\Phi}{\partial x}\left(-\frac{\partial Z_c}{\partial y}\right)\delta x\,\delta y.
\end{aligned}
\right\}
\tag{83}
$$

In addition to these distributions of loads over the surface there are also the edge forces. Ideally it would be satisfying to formulate the edge force distribution directly in a similar manner to the treatment for incompressible flow as presented in Section 2.3. Unfortunately such a procedure introduces considerable difficulties which are all associated with the variations in density in the edge regions. However an indirect method is possible; by using the fact that an infinite swept aerofoil has zero overall drag an estimation of the local leading edge force can be made. Garner presents this approach in Section 2.2 of Part II in full.

Thus subsonic linearised lifting surface theory is applicable when equations (83) are used for the load distributions together with the appropriate edge forces, with the minor reservation that a strictly non-planar model is implied.

4.3. Integral Relationships; Trefftz Plane Analysis

Since the main theme of the earlier sections is the compatibility between forces and moments on the wing and conditions on a large control surface, it is necessary to confirm that compressibility does not affect the Trefftz plane formulae. As far as is known even the formula for vortex drag has always been taken for granted without proof.

Consider the large control volume $ABCDA'B'C'D'$ as shown in Fig. 5 surrounding the non-planar model. On the Trefftz plane, plane $CDD'C'$, there are transverse velocity components v and w induced by the trailing vorticity situated on the non-planar trailing sheet (i.e. on $z = Z_c(x_t(y), y)$). Now these transverse velocities v and w induce a change in density, for according to equation (74)

$$
\rho = \rho_\infty \left[1 - M_\infty^2 \frac{u}{U} - \frac{v^2 + w^2}{2a_\infty^2} + \cdots \right].
\tag{84}
$$

It is now argued that since induced drag depends on the integration of $(v^2 + w^2)$ over the Trefftz plane then terms like $(v^2 + w^2)$ must be retained in all the parameters, thus the small change in density implicit in equation (84) must be retained. And if the density varies over the Trefftz plane then from continuity

$$
\iint_{CDD'C' \to \infty} \{ \rho(U + u) - \rho_\infty U \}\,dy\,dz = 0,
\tag{85}
$$

which gives

$$
\iint_{CDD'C' \to \infty} \rho_\infty \left(\beta^2 \frac{u}{U} - \frac{v^2 + w^2}{2a_\infty^2} \right) dy\,dz = 0.
\tag{86}
$$

21

Equation (86) implies that a small longitudinal perturbation velocity u must exist in the Trefftz plane. The velocity u/U must be symmetric with respect to z, even for the lifting problem, and its order of magnitude is $\{(v^2 + w^2)/U^2\} M_\infty^2/\beta^2$.

It is of interest to note that even retaining the second-order term u/U in the Trefftz plane the basic differential equation again becomes

$$\frac{\partial^2 \Phi}{\partial y^2} + \frac{\partial^2 \Phi}{\partial z^2} = 0, \tag{87}$$

to a first order.

The overall forces and moments can be obtained by applying the arguments presented in Section 3. Neglecting third-order terms, the lift on the wing is

$$L = \iint_{CDD'C' \to \infty} \rho(U + u)(-w)\,dy\,dz = \int_{-s}^{+s} \rho_\infty U \, \Delta\Phi_t(y)\,dy, \tag{88}$$

and the side force on the wing is

$$Y \approx \iint_{CDD'C' \to \infty} \rho(U + u)(-v)\,dy\,dz = \int_{-s}^{+s} \rho_\infty U \, \Delta\Phi_t(y)\left(-\frac{dZ_c}{dy}(x_t(y), y)\right) dy. \tag{89}$$

Neglecting the side force on the non-planar trailing sheet, it follows that the side force on the wing is given by the same approximate formula as in the incompressible case (i.e. equation (58)).

The drag force on the wing is

$$
\begin{aligned}
D &= \iint_{CDD'C' \to \infty} \{(p_\infty - p) - \rho(U + u)^2 + \rho_\infty U^2\}\,dy\,dz \\
&= \iint_{CDD'C' \to \infty} \left\{\left[\rho_\infty U u + \frac{\rho_\infty}{2}(\beta^2 u^2 + v^2 + w^2)\right] - \right.\\
&\quad \left. - \left[\rho_\infty U u + \rho_\infty \beta^2 u U + \rho_\infty(1 - 2M_\infty^2)u^2 - \rho_\infty \frac{M_\infty^2}{2}(v^2 + w^2)\right]\right\}dy\,dz
\end{aligned}
$$

on substitution of equations (73) and (74). Hence with the aid of equation (86),

$$
\begin{aligned}
D &= \iint_{CDD'C' \to \infty} \frac{\rho_\infty}{2}(v^2 + w^2)\,dy\,dz + O(u^2)_{x=+\infty} \\
&= \int_{-s}^{+s} \left\{\rho_\infty U \, \Delta\Phi \frac{\partial\Phi}{\partial z}\right\}_{x=+\infty} dy + O(u^2)_{x=+\infty}
\end{aligned} \tag{90}
$$

using equation (87). Thus the standard formula for the vortex drag can be derived, even when the density variations in the Trefftz plane are taken into account.

Since the yawing moment $\mathcal{N}$ is a combination of the above side force and drag terms, it is conjectured that the formula for $\mathcal{N}$ is the same for both the incompressible and compressible cases, as given by equation (62); the numerical results presented in the following section support this assumption.

4.4. Numerical Example

Part II includes a numerical solution for a tapered swept wing of aspect ratio 2 at $M_\infty = 0\cdot7806$; the camber surface is

$$Z_c(x, y) = -\frac{(1 + y/s)(x - x_t(y))}{c}$$

such that $Z_c(x_t(y), y)$ is zero.

22

The side force contributions are:

$$C_{Y1} = \text{side force coefficient due to integration of normal pressures}$$

$$= -2.778,$$

$$C_{Y2} = \text{side force coefficient from leading edge}$$

$$= 1.759,$$

$$C_{Y3} = \text{side force coefficient from wing tips}$$

$$= 0.974.$$

Thus

$$C_Y = C_{Y1} + C_{Y2} + C_{Y3} = -0.045. \tag{91}$$

The inference from equation (89) that C_Y is negligibly small when $Z_c(x_t(y), y)$ is zero is supported by the numerical result given by equation (91).

For the yawing moment about an axis through the leading apex of the wing, the contributions are:

$$C_{n1} = \text{yawing moment coefficient due to integration of normal pressures}$$

$$= 1.920,$$

$$C_{n2} = \text{yawing moment coefficient from leading edge}$$

$$= -1.467,$$

$$C_{n3} = \text{yawing moment coefficient from wing tips}$$

$$= -0.941.$$

Thus

$$C_n = C_{n1} + C_{n2} + C_{n3} = -0.488. \tag{92}$$

Now from equation (62) C_n is also approximately equal to $(C_{nI} + C_{nII} + C_{nIII})$ where, by reference to equation (62),

$$C_{nI} = \text{yawing moment coefficient from Trefftz plane}$$

$$= 0.236,$$

$$C_{nII} = \text{yawing moment coefficient from line integral}$$

$$= 0,$$

$$C_{nIII} = \text{yawing moment coefficient from surface integral}$$

$$= -0.710.$$

Thus

$$C_{nI} + C_{nII} + C_{nIII} = -0.474. \tag{93}$$

Again the agreement between equations (92) and (93) is reasonable.

5. Conclusions

(1) It is shown that linearised theory can be used to predict second-order quantities such as drag, side force and yawing moment as long as the mathematical model is a non-planar model; the forces should be calculated from the resolution of the pressure loading distribution, which acts normal to the wing surface, together with the edge forces.

(2) Approximate alternative expressions are derived for the side force and yawing moment which do not involve the edge forces.

LIST OF SYMBOLS

a_∞	Speed of sound in free stream
C_{Y1}, C_{Y2}, C_{Y3}	Side force coefficients due to normal pressure distribution, and leading edge suction force, and wing tips suction forces respectively
C_{n1}, C_{n2}, C_{n3}	Yawing moment coefficients due to normal pressure distribution, leading edge suction force, and wing tips suction forces respectively
$C_{nI}, C_{nII}, C_{nIII}$	Yawing moment coefficient terms defined by the three terms in equation (62)
D	Drag on wing
D_P	Drag on planar surface S_W
L	Lift on wing
L_P	Lift on planar surface S_W
$\mathscr{L}$	Rolling moment on wing
$\mathscr{L}_P$	Rolling moment on planar surface S_W
$\mathscr{M}$	Pitching moment on wing
$\mathscr{M}_P$	Pitching moment on planar surface S_W
M, M_∞	Mach number of local flow and free stream respectively
$\mathscr{N}$	Yawing moment on wing
$\mathscr{N}_P$	Yawing moment on planar surface $S_W + S_T$
$\mathscr{N}_{P_W}$	Yawing moment on planar surface S_W
$\mathscr{N}_{P_T}$	Yawing moment on planar surface S_T
$\mathscr{N}_e$	Yawing moment due to edge forces from leading edge and wing tips
p	Static pressure
$p_l - p_u$	(Pressure on lower surface of wing) − (pressure on upper surface of wing)
q_r, q_θ	Perturbation velocity components in cylindrical co-ordinates on an edge
q_n, q_s	Perturbation velocity components normal and parallel to edge in vicinity of an edge
r	Cylindrical radial co-ordinate
S_W	Wing planform on plane $z = 0$
S_T	Trailing sheet on plane $z = 0$
U	Free stream velocity
u, v, w	Cartesian velocity components
x, y, z	Cartesian axis system with origin at wing apex, $0x$ in free stream direction, $0y$ to starboard
x_0	Position of either pitching axis or yawing axis
$x_l(y)$	Equation of leading edge of S_W
$x_t(y)$	Equation of trailing edge of S_W
$Z_c(x, y)$	Wing camber surface
$Z_t(x, y)$	Wing thickness distribution
α	Incidence
β	$(1 - M_\infty^2)^{\frac{1}{2}}$

24

$\delta_n, \delta_x, \delta_y$	Distances away from nearby edge, normal to edge, in x direction, in y direction respectively
γ	Ratio of specific heats
Λ	Local angle of wing sweep
ρ, ρ_∞	Local density and density of free stream
Φ	Velocity potential
$\Delta\Phi$	Discontinuity in velocity potential
$\Delta\Phi_t(y)$	$= \Delta\Phi(x_t(y), y)$

REFERENCES

No.	Author(s)	Title, etc.
1	B. Thwaites	*Incompressible Aerodynamics.* Oxford University Press 1960.
2	H. C. Garner and D. A. Fox ..	Algol 60 programme for Multhopp's low frequency subsonic lifting surface theory. A.R.C. R. & M. 3517 (1966).
3	D. E. Lehrian and H. C. Garner ..	Theoretical calculation of generalised forces and load distribution on wings oscillating at general frequency in a subsonic stream. A.R.C. R. & M. 3710 (1971).
4	R. T. Jones and D. Cohen	*High Speed Wing Theory.* Princeton University Press 1960.
5	H. C. Garner	Some remarks on vortex drag and its spanwise distribution in incompressible flow. *Aero. J. (R.Ae.S.)* Vol. 72, pp. 623–625 (1968).

26

TABLE 1

Side Forces on Rectangular Wing of Aspect Ratio 2

Case	Camber surface $Z_c(x, y)$	$\alpha(x, y)$	Side force due to normal pressures C_{Y1}	Side force due to wingtip edge forces C_{Y3}
(a)	$\left(1 + \dfrac{y}{s}\right)\left(1 - \dfrac{x}{c}\right)$	$1 + \dfrac{y}{s}$	$-1\cdot9673$	$+1\cdot9454$
(b)	$\dfrac{y}{s}\left(1 + \dfrac{y}{s}\right)\left(1 - \dfrac{x}{c}\right)$	$\dfrac{y}{s}\left(1 + \dfrac{y}{s}\right)$	$-1\cdot1500$	$+1\cdot1448$
(c)	$\left(\dfrac{y}{s}\right)^2\left(1 + \dfrac{x}{c} + \dfrac{y}{s}\right)\left(1 - \dfrac{x}{c}\right)$	$\left(\dfrac{y}{s}\right)^2\left(\dfrac{2x}{c} + \dfrac{y}{s}\right)$	$-1\cdot0186$	$+1\cdot0162$

TABLE 2

Yawing Moment Contributions

Case	$Z_c(x, y)$	C_{n1}	C_{n2}	C_{n3}
(a)	$\left(1 + \dfrac{y}{s}\right)\left(1 - \dfrac{x}{c}\right)$	$0\cdot6426 - 0\cdot9781\dfrac{x_0}{c}$	$-0\cdot2575$	$-0\cdot5637 + 0\cdot9727\dfrac{x_0}{c}$
(b)	$\dfrac{y}{s}\left(1 + \dfrac{y}{s}\right)\left(1 - \dfrac{x}{c}\right)$	$0\cdot2754 - 0\cdot5750\dfrac{x_0}{c}$	$-0\cdot1009$	$-0\cdot3237 + 0\cdot5724\dfrac{x_0}{c}$
(c)	$\left(\dfrac{y}{s}\right)^2\left(1 + \dfrac{y}{s} + \dfrac{x}{c}\right)\left(1 - \dfrac{x}{c}\right)$	$0\cdot2354 - 0\cdot5093\dfrac{x_0}{c}$	$-0\cdot0220$	$-0\cdot3349 + 0\cdot5081\dfrac{x_0}{c}$

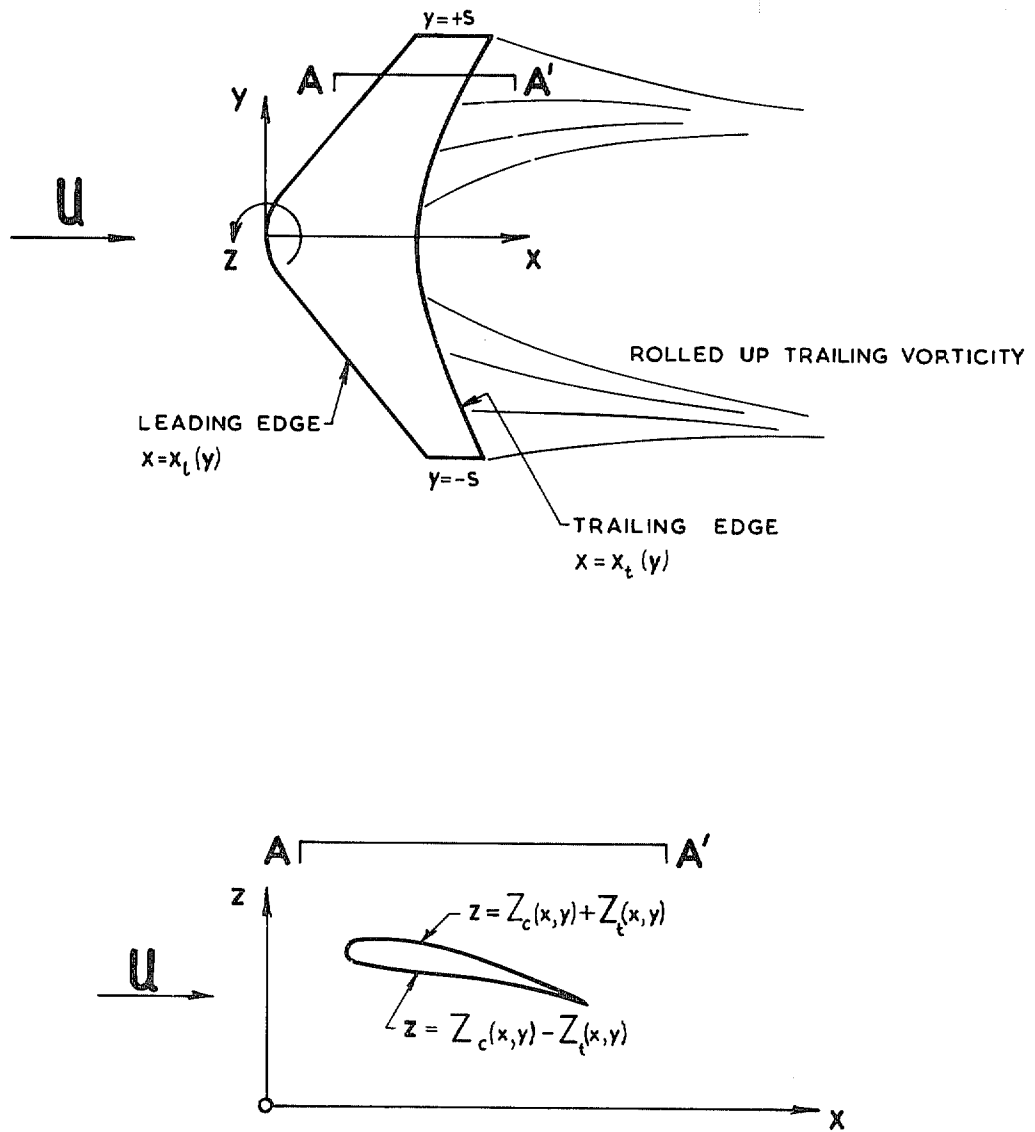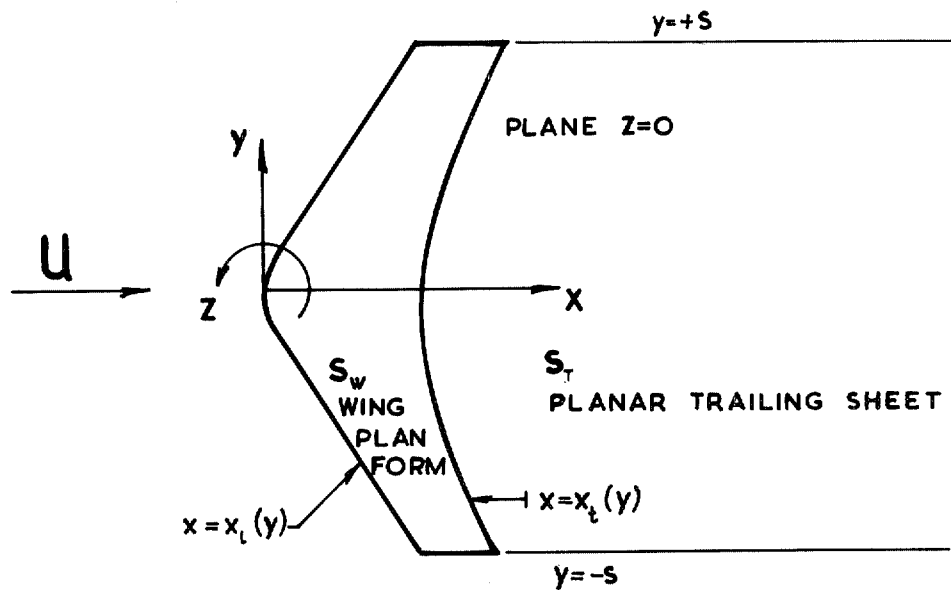| Case	C_{nI}	C_{nIII}	$C_{nI} + C_{nIII}$	$C_{n1} + C_{n2} + C_{n3}$
(a)	$0\cdot2297$	$-0\cdot4195$	$-0\cdot1898$	$-0\cdot1785 - 0\cdot0054\,x_0/c$
(b)	$0\cdot0977$	$-0\cdot2534$	$-0\cdot1557$	$-0\cdot1492 - 0\cdot0026\,x_0/c$
(c)	$0\cdot0973$	$-0\cdot2210$	$-0\cdot1237$	$-0\cdot1214 - 0\cdot0012\,x_0/c$

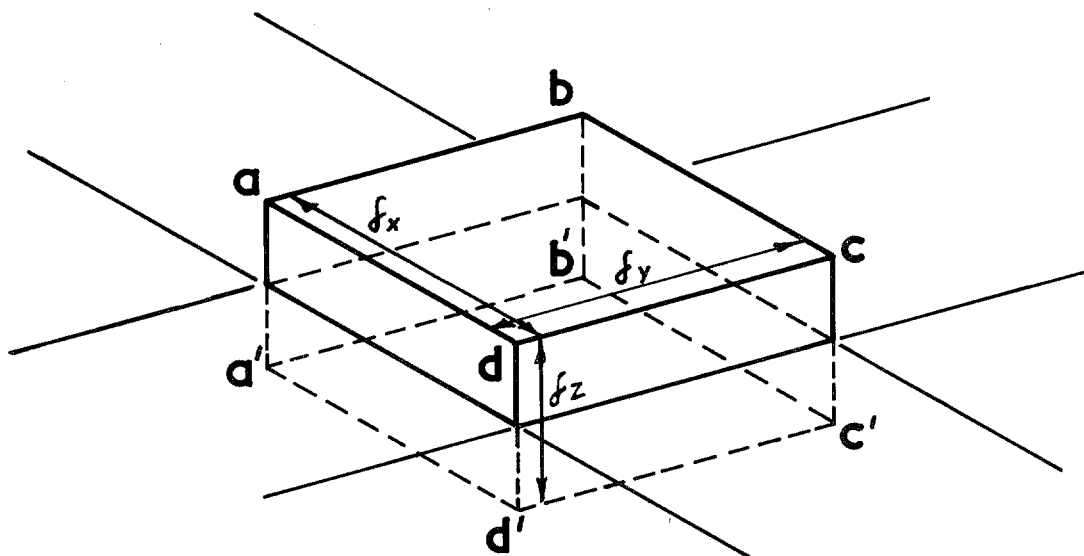FIG. 1.   Basic problem.

28

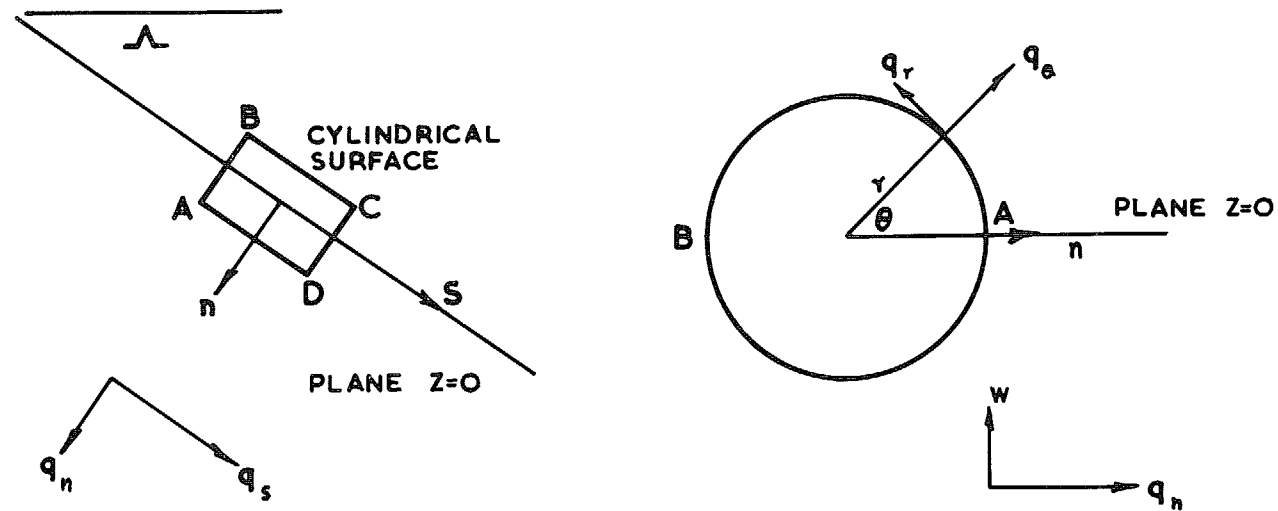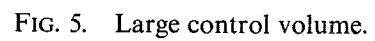FIG. 2.   Planar mathematical model.

FIG. 3.   Small control volume.

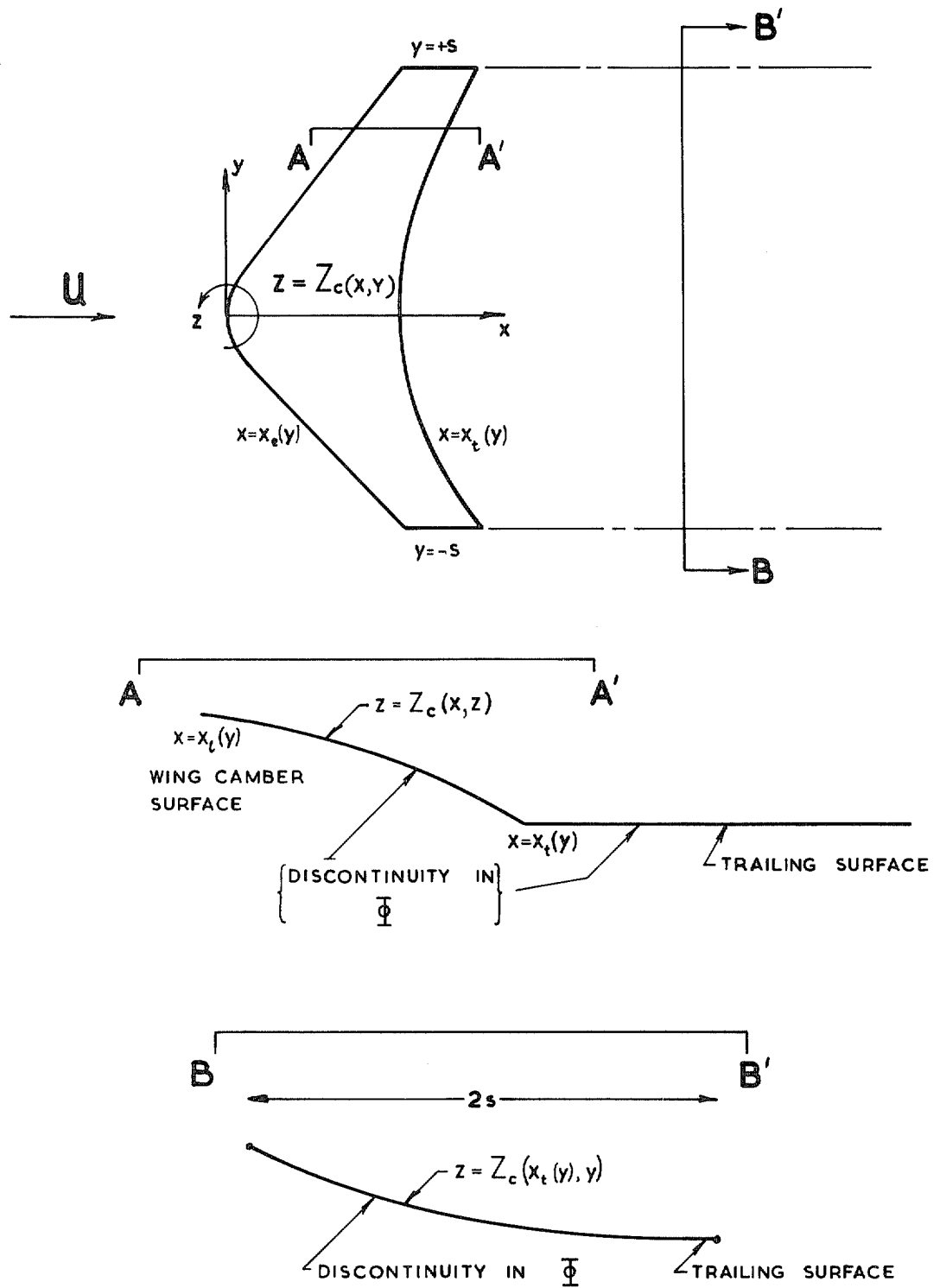Fig. 4.   Notation for edge considerations.

FIG. 5. Large control volume.

FIG. 6.   Non-planar model.

Part II

Edge Forces and Roll-Rate Derivatives

1. Introduction

As stated in the Preface, lifting-surface theory has not been extensively applied to the calculation of various lateral stability derivatives; approximate and simple expressions have played a major part in their estimation during the past two decades. For example, Toll and Queijo[1] used the concept of a sheared unswept wing to found the basis of rapid estimation of these lateral derivatives for swept wings in incompressible flow. Goodman and Fisher[2] have used experimental evidence on rolling stability derivatives at low speeds for untapered wings of varying aspect ratio and sweepback to devise a semi-empirical method, which incorporates tip suction and non-linear characteristics associated with drag at high lift. The effect of Mach number for a range of sweepback is considered experimentally and semi-empirically by Wiggins[3] and more recently by Queijo[4] in terms of simple theoretical formulae akin to those in Ref. 1, which only apply to linear conditions.

As established in Part I, the standard lifting-surface integral equation can be applied to the calculation of side force and yawing moment with the correct interpretation of the pressure distribution. Here the approach, based on an extension to lifting-surface theory,[5,6] is to sum the separate contributions from the loading normal to the camber surface and from the leading-edge and side-edge suction forces. In reconciling two different concepts of lift-dependent drag from kinetic energy in the wake and from integrated forces at the wing, the author has stated in Ref. 7 that the accuracy of leading-edge suction is perhaps the severest requirement of a lifting-surface solution. However, it is quite as difficult to ascertain the distribution of tip suction, and hence its contribution to the side force and yawing moment under asymmetric spanwise conditions. In this respect the demands on lifting-surface theory are alleviated by the margin of error that can be accepted in the estimation of lateral stability derivatives.

From the theoretical standpoint it is necessary to make the distinction between sideslip and yawing motion, which involve asymmetry of wing planform relative to the mainstream, and aileron deflection and rolling motion where the asymmetry is confined to the boundary conditions. The present investigation is restricted to problems of the latter type, including the lateral forces and moments on wings with asymmetric twist and camber.

The purpose of the present report is threefold. Analytical and numerical studies of local and integrated edge forces are undertaken, in order to investigate their theoretical behaviour and importance. The contributions to the roll-rate derivatives of side force and yawing moment are deduced for two rectangular wings and one tapered swept wing, to establish some general trends in these theoretical derivatives and to make comparison with the appropriate formulae and charts from the simplified methods of Refs. 1 and 4. The related experimental evidence from Ref. 2 and the semi-empirical methods of Refs. 2 and 3 are used to provide some assessment of the validity of the present calculations; in particular, the rôle of the edge forces in the non-linear experimental behaviour of the yawing moment due to rate of roll can be clarified.

2. Steady Subsonic Wing Theory

Under the usual assumptions in linearised lifting-surface theory the wing is taken to have zero thickness. The origin of co-ordinates is chosen where the centre line of the wing planform intersects the leading edge; Fig. 1a shows the right-handed system of stream axes with $0x$ in the direction of the stream depicted as horizontal, $0y$ to starboard and $0z$ drawn vertically upwards. The stream of uniform velocity U, subsonic Mach number M and density ρ is supposed to be inviscid and irrotational and therefore subject to a perturbation velocity potential Φ.

The planform occupies the region

$$x_l(\eta) \leqslant x \leqslant x_t(\eta) = x_l(\eta) + c(\eta) \qquad (-1 \leqslant \eta \leqslant 1) \tag{1}$$

where $\eta = y/s$ and s denotes wing semi-span. In terms of the geometric mean chord $\bar{c}$, the planform area is $S = 2s\bar{c}$ and its aspect ratio is $A = 2s/\bar{c}$. The camber surface of the wing

$$z = -\bar{c}Z(x/\bar{c}, \eta) \tag{2}$$

is so slightly displaced from the plane $z = 0$ that the boundary condition

$$\frac{1}{U}\frac{\partial \Phi}{\partial z} = -\frac{\partial Z}{\partial(x/\bar{c})} = -\alpha(x, y) \tag{3}$$

may be satisfied on $z = 0$.

33

In the usual mathematical model of the flow the potential Φ is antisymmetric in z with discontinuity $\Delta\Phi(x, y)$ in crossing from below to above the plane $z = 0$ in the region (1) and also in the wake

$$x_t(\eta) \leqslant x \qquad (-1 \leqslant \eta \leqslant 1). \tag{4}$$

From Bernoulli's equation for compressible flow of a perfect gas the lift per unit area is obtained to first order as

$$\Delta p = \tfrac{1}{2}\rho U^2 l(x, y) = \rho U \frac{\partial}{\partial x}(\Delta\Phi). \tag{5}$$

The vortex sheet in the wake does not sustain lift, and it follows from equation (5) that

$$\Delta\Phi(x, y) = \Delta\Phi(x_t, y) \qquad (x \geqslant x_t). \tag{6}$$

It is well established[8] from the mathematical model that equation (3) leads to an integral equation

$$\frac{\partial Z}{\partial(x/\bar{c})} = \alpha(x, y) = -\frac{1}{8\pi} \int_{-s}^{s} \int_{x_l}^{x_t} \frac{l(x', y')}{(y - y')^2} \left[1 + \frac{x - x'}{\{(x - x')^2 + \beta^2(y - y')^2\}^{\frac{1}{2}}} \right] dx'\, dy' \tag{7}$$

where $\beta^2 = 1 - M^2$. Subject to the Kutta condition that $l = 0$ along the trailing edge, equation (7) is sufficient to determine $l(x, y)$ when $Z(x/\bar{c}, \eta)$ is given.

However, for the purpose of satisfying equation (3) to first order, there is no need to assume a planar vortex sheet. The discontinuity $\Delta\Phi(x, y)$ should be regarded as occupying the camber surface (2). Likewise it should be recognised that in the wake the vortex sheet is a stream surface which is convected away from the plane $z = 0$; although the local vertical displacements tend to grow indefinitely with increasing x, their upstream influence at the wing can reasonably be ignored. As far as the flow at the wing is concerned, the rolling-up of the trailing vorticity is also of secondary importance.

The pressure loading Δp of equation (5) acts normal to the camber surface (2) with components of force per unit area

$$\left. \begin{array}{ll} \tfrac{1}{2}\rho U^2 l(x, y)\dfrac{\partial Z}{\partial(x/\bar{c})} & \text{in direction } 0x \\[3mm] \tfrac{1}{2}\rho U^2 l(x, y)\dfrac{\bar{c}}{s}\dfrac{\partial Z}{\partial\eta} & \text{in direction } 0y \end{array} \right\}. \tag{8}$$

Although both these components are of second order, it is clear that no further contributions of this order would result from higher-order terms in $l(x, y)$. In other words, there is no inconsistency in the derivation of the second-order quantities for drag, side force and yawing moment from linearised subsonic wing theory.

The mathematical procedures for obtaining solutions $l(x, y)$ to the integral equation (7) are legion, and no attempt is made to review them. Most of the present calculations are based on the method of Ref. 6 with zero frequency. It is sufficient in Section 2.1 to define the various steady-flow solutions and to give the necessary equations for the subsequent analysis of local edge forces and total side force and yawing moment in Sections 2.2 and 2.3.

2.1. Lifting-Surface Method

For a given planform, camber shape $Z(x/\bar{c}, \eta)$ and subsonic Mach number, solutions for the wing loading by the method of Ref. 6 involve the choice of a trio of integers (N, m, a). The first two determine the location of points (x_{pv}, y_v) on the planform where equation (7) is satisfied,

$$\left. \begin{array}{ll} x_{pv} = x_l(\eta_v) + \tfrac{1}{2}c(\eta_v)(1 - \cos\phi_p), & \\[2mm] \phi_p = 2\pi p/(2N + 1), & p = 1(1)N \\[2mm] y_v = s\eta_v = -s\cos\left(\dfrac{v\pi}{m + 1}\right), & v = 1(1)m \end{array} \right\}. \tag{9}$$

The third one, a, controls the accuracy of the spanwise integration involved in equation (7). The integers N and m also determine the number of coefficients in the expression for the non-dimensional wing loading. Thus

$$l(x, y) = \frac{8s}{\pi c(\eta)} \sum_{q=1}^{N} \Gamma_q(\eta) \frac{\cos(q - 1)\phi + \cos q\phi}{\sin\phi}, \tag{10}$$

where the angular chordwise parameter ϕ is given by

$$x = x_l(\eta) + \tfrac{1}{2}c(\eta)(1 - \cos\phi); \tag{11}$$

the spanwise loading functions are defined by the double series

$$\Gamma_q(\eta) = \frac{2}{m+1} \sum_{r=1}^{m} \left[\Gamma_{qr} \sum_{\mu=1}^{m} \sin\mu\theta \sin\mu\theta_r \right] \tag{12}$$

with $\eta = -\cos\theta$ and $\Gamma_{qr} = \Gamma_q(\eta_r)$, where

$$\eta_r = -\cos\theta_r = -\cos\left(\frac{r\pi}{m+1}\right), \qquad r = 1(1)m. \tag{13}$$

The solutions are the sets of mN coefficients Γ_{qr} that determine $l(x, y)$.

It is convenient to define generalised force coefficients for certain standard modes

$$Z_i(\xi, \eta) \quad \text{or} \quad Z_j(\xi, \eta) = \xi^\sigma \eta^\tau, \tag{14}$$

where $\xi = x/\bar{c}$ and the indices σ and τ relate to i (or j). The camber surface is taken in the form

$$Z(\xi, \eta) = \sum_{j=1}^{J} b_j Z_j(\xi, \eta) \tag{15}$$

to produce the wing loading

$$l(x, y) = \sum_{j=1}^{J} b_j l_j(x, y). \tag{16}$$

The corresponding force coefficient is defined by

$$Q_i = \frac{1}{2S} \iint_S Z_i(\xi, \eta) l(x, y)\, dx\, dy$$

$$= \sum_{j=1}^{J} b_j Q_{ij}, \tag{17}$$

where

$$Q_{ij} = \frac{1}{2S} \iint_S Z_i(\xi, \eta) l_j(x, y)\, dx\, dy. \tag{18}$$

The modes with spanwise symmetry are treated independently of the antisymmetric ones, and equation (18) is replaced by

$$\left.\begin{array}{l} (Q_{ij})_{\text{sym}} = \dfrac{1}{2S} \displaystyle\iint_S (Z_i)_{\text{sym}}(l_j)_{\text{sym}}\, dx\, dy \\[2em] (Q_{ij})_{\text{anti}} = \dfrac{1}{2S} \displaystyle\iint_S (Z_i)_{\text{anti}}(l_j)_{\text{anti}}\, dx\, dy \end{array}\right\}. \tag{19}$$

For the present purposes it is sufficient to take the first ten symmetric modes and the first six antisymmetric modes from Table B1 of Ref. 6 and to numerate equation (14) as follows.

i (or j)		1	2	3	4	5	6	7	8	9	10
$(Z_i)_{\text{sym}}$	σ	0	1	2	3	4	1	1	2	3	0
	τ	0	0	0	0	0	2	2	2	2	4
$(Z_i)_{\text{anti}}$	σ	0	1	2	3	0	1	–	–	–	–
	τ	1	1	1	1	3	3	–	–	–	–

35

While Ref. 6 has been used in the present applications to rectangular wings, the calculations for a tapered swept wing are by the lifting-surface method of Ref. 5 with a similar trio of integers (m, N, q) including the quantity q analogous to a in Ref. 6. Although the solutions are transcribed to the present notation, there are certain complications on account of the sweepback. Additional force modes

$$\left.\begin{array}{l} (Z_I)_{sym} = |\eta| \\ (Z_{II})_{sym} = \xi|\eta| \\ (Z_I)_{anti} = \eta/|\eta| \\ (Z_{II})_{anti} = \xi\eta/|\eta| \end{array}\right\} \tag{20}$$

arise in the evaluation of yawing moment. The planform is rounded so that the true leading edge and chord in the region $|\eta| < \eta_{iR}$ are replaced by

$$\left.\begin{array}{l} x_l(\eta) = x_{lR} + f(\lambda)[x_l(\eta_{iR}) - x_{lR}] \\ c(\eta) = c_R + f(\lambda)[c(\eta_{iR}) - c_R] \end{array}\right\}, \tag{21}$$

where $x_{lR}(= 0)$ and c_R denote the root leading edge and chord, and

$$\left.\begin{array}{ll} f(\lambda) = \tfrac{1}{3} + \lambda^2 - \tfrac{1}{3}\lambda^3, & 0 \leqslant \lambda \leqslant 1 \\ \lambda = |\eta|/\eta_{iR}, & \eta_{iR} = s\sin\left(\dfrac{\pi}{m+1}\right) \end{array}\right\}. \tag{22}$$

2.2. Evaluation of Edge Forces

The velocity potential difference $\Delta\Phi(x, y)$ is easily obtained from the non-dimensional wing loading by equations (5), (10) and (11), whence

$$\Delta\Phi(x, y) = \tfrac{1}{2}U\int_{x_l}^{x} l(x', y)\,dx' = \tfrac{1}{4}Uc(\eta)\int_0^{\phi} l(x, y)\sin\phi\,d\phi$$

$$= \frac{2sU}{\pi}\left[\Gamma_1(\eta)(\phi + \sin\phi) + \sum_{q=2}^{N}\Gamma_q(\eta)\left\{\frac{\sin(q-1)\phi}{q-1} + \frac{\sin q\phi}{q}\right\}\right]. \tag{23}$$

With regard to edge forces the three-dimensionality of the problem is fully taken into account in the behaviour of $\Delta\Phi$. The local edge forces, acting normal to the edge and in the plane of the wing, arise from the infinite gradients of $\Delta\Phi$ normal to the leading and side edges, $\phi = 0$ and $\eta = \pm 1$, irrespective of any local variations parallel to the edges. Thus we can use a two-dimensional argument without loss of generality, recognising that the edge force is a necessary approximation to a component that arises naturally from normal surface pressures on a thick wing.

The simplest approach to the formulation of these edge forces in terms of the behaviour of $\Delta\Phi$ on a lifting wing is to consider a two-dimensional thin sheared wing at uniform incidence α and to use the condition that its drag is zero. Let c and Λ denote the wing chord and the angle of sweepback. Then the load distribution is that of an unswept two-dimensional wing of chord $c\cos\Lambda$ at uniform incidence $\alpha\sec\Lambda$ in a stream of velocity $U\cos\Lambda$ and Mach number $M\cos\Lambda$. Thus

$$\Delta p = \tfrac{1}{2}\rho U^2\cos^2\Lambda(1 - M^2\cos^2\Lambda)^{-\frac{1}{2}}4\alpha\sec\Lambda\cot\tfrac{1}{2}\phi$$

$$= 2\rho U^2\alpha(\beta^2 + \tan^2\Lambda)^{-\frac{1}{2}}\cot\tfrac{1}{2}\phi. \tag{24}$$

Denote the distance normal to the leading edge by

$$n = \tfrac{1}{2}c\cos\Lambda(1 - \cos\phi). \tag{25}$$

Then the discontinuity in velocity potential is

$$\Delta\Phi = \int_0^n \frac{\Delta p}{\rho U\cos\Lambda}\,dn = \int_0^{\phi}\frac{\Delta p}{\rho U}\tfrac{1}{2}c\sin\phi\,d\phi$$

$$= Uc\alpha(\beta^2 + \tan^2\Lambda)^{-\frac{1}{2}}(\phi + \sin\phi). \tag{26}$$

The lift force per unit length of leading edge is

$$\rho U\cos\Lambda(\Delta\Phi)_{\phi=\pi} = \pi\rho U^2 c\alpha\cos\Lambda(\beta^2 + \tan^2\Lambda)^{-\frac{1}{2}}.$$

36

Since the pressure loading acts at the angle $\alpha \sec \Lambda$ to the axis $0z$ the streamwise component of force must be balanced by the leading-edge suction force per unit length

$$E_l = \pi \rho U^2 c \alpha^2 (\beta^2 + \tan^2 \Lambda)^{-\frac{1}{2}}. \tag{27}$$

It remains to relate E_l to the behaviour of $\Delta \Phi$ near the edge

$$\left.\begin{aligned} \Delta \Phi &= 2U c \alpha \phi (\beta^2 + \tan^2 \Lambda)^{-\frac{1}{2}} \\ \phi^2 &= 4(n/c) \sec \Lambda \end{aligned}\right\}. \tag{28}$$

By equations (27) and (28)

$$E_l = \tfrac{1}{16} \pi \rho \cos \Lambda (\beta^2 + \tan^2 \Lambda)^{\frac{1}{2}} [(\Delta \Phi)^2/n]_{n \to 0}. \tag{29}$$

The tip is treated as the limiting case when Λ tends to $90°$. Thus equation (29) gives the outward side-edge force per unit length

$$E_s = \tfrac{1}{16} \pi \rho [(\Delta \Phi)^2/n]_{n \to 0} \tag{30}$$

where now $n/s = 1 - |\eta|$.

It may be observed that equation (29) also reduces to equation (30) in the limiting case of incompressible flow. An alternative derivation of this special result is given by Hancock in Part I. While the expression for tip suction is unaffected by compressibility, the leading-edge suction shows explicit dependence on Mach number. Moreover, just as Ref. 7 reconciles the lift-dependent drag from the Trefftz plane ($x = \infty$) with components acting at the wing in incompressible flow, so with the aid of equation (29) the same equivalence can be demonstrated in subsonic compressible flow in accord with the Prandtl-Glauert similarity rule.

The local edge forces can be deduced from equations (23), (29) and (30). Near the leading edge equation (23) becomes

$$\Delta \Phi = (4/\pi) s U \Theta \phi + O(\phi^3) \tag{31}$$

where

$$\Theta = \sum_{q=1}^{N} \Gamma_q(\eta). \tag{32}$$

If $\Lambda_l(\eta)$ denotes the local leading-edge sweepback, it follows from equation (11) that

$$n = \tfrac{1}{4} c \phi^2 \cos \Lambda_l = O(\phi^4). \tag{33}$$

By equations (29), (31) and (33)

$$E_l = \frac{4 \rho U^2 s^2 \Theta^2}{\pi c(\eta)} (\beta^2 + \tan^2 \Lambda_l)^{\frac{1}{2}}. \tag{34}$$

To evaluate E_s, it is convenient to let

$$\bar{\Gamma}_q = [(1 - \eta^2)^{-\frac{1}{2}} \Gamma_q(\eta)]_{\eta \to 1}. \tag{35}$$

A general expression for $\bar{\Gamma}_q$ is obtained from equations (12), (13) and (35) in the limit as $\theta \to \pi$. It is found that

$$\Gamma_q(\eta) = (\pi - \theta) \sum_{r=1}^{m} (-1)^{r-1} \Gamma_{qr} \tan\left(\frac{\frac{1}{2} \pi r}{m + 1}\right) + O(\pi - \theta)^3,$$

whence

$$\bar{\Gamma}_q = \sum_{r=1}^{m} (-1)^{r-1} \Gamma_{qr} \tan\left(\frac{\frac{1}{2} \pi r}{m + 1}\right). \tag{36}$$

According as Γ_{qr} is symmetric or antisymmetric in η_r, the summation in equation (36) can be shortened to give

$$\begin{aligned} (\bar{\Gamma}_q)_{\text{sym}} &= 2 \sum_{r=1}^{\frac{1}{2}(m-1)} (-1)^{r-1} \Gamma_{qr} \operatorname{cosec}\left(\frac{\pi r}{m + 1}\right) - \Gamma_{q,\frac{1}{2}(m+1)} \\ &= 2 \sum_{r=1}^{\frac{1}{2}(m-1)} (-1)^{r-1} \Gamma_q(\eta_r)(1 - \eta_r^2)^{-\frac{1}{2}} - \Gamma_q(0) \end{aligned} \tag{37}$$

37

or

$$(\bar{\Gamma}_q)_{\text{anti}} = 2 \sum_{r=1}^{\frac{1}{2}(m-1)} (-1)^r \Gamma_{qr} \cot\left(\frac{\pi r}{m+1}\right)$$

$$= 2 \sum_{r=1}^{\frac{1}{2}(m-1)} (-1)^{r-1} \Gamma_q(\eta_r)\eta_r(1-\eta_r^2)^{-\frac{1}{2}}. \tag{38}$$

It follows from equations (23), (30) and (35) that

$$E_s = \frac{\rho U^2 s \Psi^2}{2\pi} \tag{39}$$

where

$$\Psi = \bar{\Gamma}_1(\phi + \sin\phi) + \sum_{q=2}^{N} \bar{\Gamma}_q \left\{\frac{\sin(q-1)\phi}{q-1} + \frac{\sin q\phi}{q}\right\}. \tag{40}$$

Individual expressions for the outward edge forces per unit length acting at the two tips are then formulated as

$$E_s = \frac{\rho U^2 s}{2\pi}(\Psi_{\text{sym}} \pm \Psi_{\text{anti}})^2 \quad \text{for } \eta = \pm 1, \tag{41}$$

where Ψ_{sym} and Ψ_{anti} are defined by equation (40) in conjunction with $\bar{\Gamma}_q$ from equations (37) and (38) respectively.

2.3. Side Force and Yawing Moment

With the usual sign convention, illustrated in Fig. 1b, the side force is positive to starboard and yawing moment is positive anticlockwise about the axis $0z$. The yawing moment coefficient will be split into three parts

$$C_n = \mathcal{N}/(\rho U^2 Ss) = C_{n1} + C_{n2} + C_{n3}, \tag{42}$$

where C_{n1} is the contribution from normal pressures, C_{n2} and C_{n3} are derived respectively from the leading-edge and side-edge forces. There is no need to consider the side-force coefficient C_Y separately, because C_n is obtained as a linear function of the axis position x_0; thus

$$C_Y = Y/(\tfrac{1}{2}\rho U^2 S) = \partial C_n/\partial(x_0/2s)$$

$$= A\,\partial C_n/\partial\xi_0 \quad \text{with } \xi_0 = x_0/\bar{c}. \tag{43}$$

The first term C_{n1} is derived from the components of local force in (8); with yawing axis through $(x, y) = (x_0, 0)$ they contribute

$$C_{n1} = \frac{1}{2Ss}\int_{-s}^{s}\int_{x_l}^{x_t} l(x,y)\left[\frac{\partial Z}{\partial \xi}y - \frac{\partial Z}{\partial \eta}\frac{\bar{c}}{s}(x-x_0)\right]dx\,dy$$

$$= \int_{-1}^{1}\int_{\xi_l}^{\xi_t} l(x,y)\left[\frac{\eta}{4}\frac{\partial Z}{\partial \xi} - \frac{\xi-\xi_0}{A^2}\frac{\partial Z}{\partial \eta}\right]d\xi\,d\eta \tag{44}$$

where $\xi_l = x_l/\bar{c}$ and $\xi_t = x_t/\bar{c}$. It can be seen from equation (44) that C_{n1} can only be non-zero if the camber shape $Z(\xi, \eta)$ and consequently the loading $l(x, y)$ are asymmetric in η. We write

$$\left.\begin{aligned} Z &= (Z_j)_{\text{sym}} + (Z_j)_{\text{anti}} \\ l &= (l_j)_{\text{sym}} + (l_j)_{\text{anti}} \end{aligned}\right\}, \tag{45}$$

and take the force mode

$$Z = (Z_i)_{\text{sym}} + (Z_i)_{\text{anti}}$$

with

$$\left.\begin{aligned} (Z_i)_{\text{sym}} &= \eta\frac{\partial(Z_j)_{\text{anti}}}{\partial \xi} - \frac{4(\xi-\xi_0)}{A^2}\frac{\partial(Z_j)_{\text{anti}}}{\partial \eta} \\ (Z_i)_{\text{anti}} &= \eta\frac{\partial(Z_j)_{\text{sym}}}{\partial \xi} - \frac{4(\xi-\xi_0)}{A^2}\frac{\partial(Z_j)_{\text{sym}}}{\partial \eta} \end{aligned}\right\}. \tag{46}$$

38

Then in the notation of equations (19)

$$C_{n1} = (Q_{ij})_{\text{sym}} + (Q_{ij})_{\text{anti}}, \tag{47}$$

where the modes i will be linear combinations of those defined below equations (19) or in equations (20).
The leading-edge suction per unit length in equation (34) contributes

$$C_{n2} = -\frac{1}{\rho U^2 Ss} \int_{-s}^{s} E_l \left\{ y + (x_l - x_0)\frac{y}{|y|} \tan \Lambda_l \right\} dy$$

$$= -\frac{A}{\pi} \int_{-1}^{1} \frac{\Theta^2 (\beta^2 + \tan^2 \Lambda_l)^{\frac{1}{2}}}{c(\eta)/\bar{c}} \left\{ \tfrac{1}{2} A\eta + (\xi_l - \xi_0)\frac{\eta}{|\eta|} \tan \Lambda_l \right\} d\eta. \tag{48}$$

In the case of a straight sweptback leading edge with

$$\xi_l = \tfrac{1}{2} A|\eta| \tan \Lambda_l,$$

equation (48) reduces to

$$C_{n2} = -\frac{A}{\pi} \int_{-1}^{1} \frac{\Theta^2 (\beta^2 + \tan^2 \Lambda_l)^{\frac{1}{2}}}{c(\eta)/\bar{c}} \left\{ \tfrac{1}{2} A\eta \sec^2 \Lambda_l - \frac{\xi_0 \eta}{|\eta|} \tan \Lambda_l \right\} d\eta, \tag{49}$$

where it remains to substitute from equation (32)

$$\Theta = \Theta_{\text{sym}} + \Theta_{\text{anti}} = \sum_{q=1}^{N} [\Gamma_q(\eta)]_{\text{sym}} + \sum_{q=1}^{N} [\Gamma_q(\eta)]_{\text{anti}}. \tag{50}$$

Hence

$$C_{n2} = -\frac{4A}{\pi} (\beta^2 + \tan^2 \Lambda_l)^{\frac{1}{2}} \left[\tfrac{1}{2} A \sec^2 \Lambda_l \int_{0}^{1} \frac{\Theta_{\text{sym}} \Theta_{\text{anti}}}{c/\bar{c}} \eta \, d\eta - \xi_0 \tan \Lambda_l \int_{0}^{1} \frac{\Theta_{\text{sym}} \Theta_{\text{anti}}}{c/\bar{c}} d\eta \right]. \tag{51}$$

Like C_{n1}, this contribution vanishes if the spanwise loading is symmetric or antisymmetric.
The side-edge forces per unit length in equation (41) combine to give

$$C_{n3} = -\frac{2}{\pi S} \int_{x_l(1)}^{x_t(1)} \Psi_{\text{sym}} \Psi_{\text{anti}}(x - x_0) \, dx. \tag{52}$$

If we substitute the functions Ψ from equation (40) and put

$$x = \bar{c}\xi_{lT} + \tfrac{1}{2}c_T(1 - \cos \phi) \tag{53}$$

along the tip chord, equation (52) becomes

$$C_{n3} = -\frac{1}{\pi A} \int_{0}^{\pi} \left[\Gamma_1(\phi + \sin \phi) + \sum_{q=2}^{N} \Gamma_q \left\{ \frac{\sin(q-1)\phi}{q-1} + \frac{\sin q\phi}{q} \right\} \right]_{\text{sym}} \times \left[\Gamma_1(\phi + \sin \phi) + \right.$$

$$\left. + \sum_{q=2}^{N} \Gamma_q \left\{ \frac{\sin(q-1)\phi}{q-1} + \frac{\sin q\phi}{q} \right\} \right]_{\text{anti}} \times \left\{ \frac{c_T}{\bar{c}}(\xi_{lT} - \xi_0) + \frac{1}{2}\left(\frac{c_T}{\bar{c}}\right)^2 (1 - \cos \phi) \right\} \sin \phi \, d\phi$$

$$= -\frac{1}{\pi A} \left[\frac{c_T}{\bar{c}}(\xi_{lT} - \xi_0) \sum_{q,a=1}^{N} I_{qa} \Gamma_q \Gamma_a + \left(\frac{c_T}{\bar{c}}\right)^2 \sum_{q,a=1}^{N} \tfrac{1}{2}(I_{qa} - J_{qa})\Gamma_q \Gamma_a \right]. \tag{54}$$

Here the subscripts q and a are used to denote symmetry and antisymmetry, so that the summations are taken over the N^2 combinations of

$$\left. \begin{aligned} \Gamma_q &= (\Gamma_q)_{\text{sym}} \quad \text{from equation (37)} \\ \Gamma_a &= (\Gamma_q)_{\text{anti}} \quad \text{from equation (38)} \end{aligned} \right\}, \tag{55}$$

39

and the integrals $I_{qa} = I_{aq}$ and $J_{qa} = J_{aq}$ are defined below.

$$
\left.
\begin{aligned}
&I_{11} = \int_0^\pi (\phi + \sin\phi)^2 \sin\phi\, d\phi = \tfrac{3}{2}\pi^2 - \tfrac{8}{3} \\[6pt]
&I_{12} = \int_0^\pi (\phi + \sin\phi)(\sin\phi + \tfrac{1}{2}\sin 2\phi)\sin\phi\, d\phi = \tfrac{1}{4}\pi^2 + \tfrac{8}{9} \\[6pt]
&\left\{\begin{aligned}
I_{1a} &= \int_0^\pi (\phi + \sin\phi)\left\{\frac{\sin(a-1)\phi}{a-1} + \frac{\sin a\phi}{a}\right\}\sin\phi\, d\phi \\[6pt]
I_{qa} &= \int_0^\pi \left\{\frac{\sin(q-1)\phi}{q-1} + \frac{\sin q\phi}{q}\right\}\left\{\frac{\sin(a-1)\phi}{a-1} + \frac{\sin a\phi}{a}\right\}\sin\phi\, d\phi
\end{aligned}\right. \\[6pt]
&\qquad = -\frac{8}{(q+a-3)(q+a+1)(q-a-1)(q-a+1)} \quad \begin{bmatrix} q+a \geqslant 4 \\ \text{and even} \end{bmatrix} \\[6pt]
&\qquad = -\frac{8}{(q+a-2)(q+a)(q-a-2)(q-a+2)} \quad \begin{bmatrix} q+a \geqslant 5 \\ \text{and odd} \end{bmatrix}
\end{aligned}
\right\} \quad (56)
$$

The integrands of J_{qa} include the extra factor $\cos\phi$ in each case and give

$$
\left.
\begin{aligned}
&J_{11} = -\tfrac{1}{4}\pi^2 - \tfrac{8}{9} \\[4pt]
&J_{12} = \tfrac{1}{16}\pi^2 - \tfrac{8}{45} \\[4pt]
&J_{13} = \tfrac{1}{16}\pi^2 + \tfrac{8}{75} \\[10pt]
&J_{qa} = -\frac{8\{(q-a)^2 - 3\}}{\{(q+a-1)^2 - 4\}\{(q-a)^2 - 1\}\{(q-a)^2 - 9\}} \quad \begin{bmatrix} q = a = 2\ \text{or} \\ q+a \geqslant 6 \\ \text{and even} \end{bmatrix} \\[10pt]
&\qquad = -\frac{8\{(q+a-1)^2 - 3\}}{\{(q-a)^2 - 4\}\{(q+a-1)^2 - 1\}\{(q+a-1)^2 - 9\}} \quad \begin{bmatrix} q+a \geqslant 5 \\ \text{and odd} \end{bmatrix}
\end{aligned}
\right\} \quad (57)
$$

For an arbitrary camber shape $Z(\xi, \eta)$ indicated in equation (45), the yawing moment coefficient may be calculated as the sum of equations (44) or (47), (48) or (51) if Λ_l is independent of η, and (54). Given the values of Γ_q at the positions η_r in equation (13) and the necessary generalised force coefficients of equation (19), the computations are straightforward with the aid of equations (37), (38), (46), (50), (56) and (57).

3. Asymmetrically Twisted Wings

The side force and yawing moment in linearised potential flow arise from interactions between the symmetric and antisymmetric parts of the spanwise load distribution. Practical situations in which the two components are present occur on a lifting wing with ailerons deflected or in rolling flight, and the latter will be discussed in Section 4. In the case of ailerons it is questionable whether lifting-surface methods can yet provide reliable edge forces. The artificial problem of a thin wing, whose camber shape $Z(\xi, \eta)$ and local incidence $\partial Z/\partial \xi$ are asymmetric in η, provides a convenient medium for numerical studies relating to the preceding analysis. The results are presented in Tables 1 to 6, and some of these are relevant to rolling flight.

3.1. Rectangular Wings at Low Speeds

The main examples are for the rectangular wing of aspect ratio $A = 2$ in incompressible flow and with camber shapes

$$
\left.
\begin{aligned}
&\text{(a)} \quad Z(\xi, \eta) = (1 + \eta)(\xi - 1) \\[4pt]
&\text{(b)} \quad Z(\xi, \eta) = \eta(1 + \eta)(\xi - 1) \\[4pt]
&\text{(c)} \quad Z(\xi, \eta) = \eta^2(1 + \xi + \eta)(\xi - 1)
\end{aligned}
\right\} \quad (58)
$$

The loadings correspond to distributions of incidence

$$\alpha = \frac{\partial Z}{\partial \xi} = 1 + \eta, \eta^2 + \eta, 2\xi\eta^2 + \eta^3, \tag{59}$$

and in the notation of equation (16) and the table following equation (19) they are respectively

$$\begin{array}{ll}
\text{(a)} & l(x, y) = (l_2)_{\text{sym}} + (l_2)_{\text{anti}} \\
\text{(b)} & l(x, y) = (l_7)_{\text{sym}} + (l_2)_{\text{anti}} \\
\text{(c)} & l(x, y) = (l_8)_{\text{sym}} + (l_6)_{\text{anti}}
\end{array} \tag{60}$$

Each solution has been obtained to sufficient accuracy by the method of Ref. 6 with $N = 4$ chordwise terms, $m = 15$ spanwise terms and spanwise integration parameter $a = 6$. The symmetric and antisymmetric solutions are presented separately in Tables 1 and 2, each in terms of the coefficients $\Gamma_{qr} = \Gamma_q(\eta_r)(\eta_r \geq 0)$ defined in equations (10) to (13). The necessary generalised forces from equations (19) with the associated table are recorded in Table 5a.

For each of the three camber shapes the yawing moment is calculated in the notation of equation (42). From equations (44) and (54) C_{n1} and C_{n3} are linear functions of the arbitrary axis position ξ_0, but for the unswept leading edge C_{n2} in equation (48) is independent of ξ_0. With the aid of the table below equation (19) the procedure of equations (44) to (47) leads to

$$\begin{array}{ll}
\text{(a)} & C_{n1} = \left[Q_{62} + \frac{4}{A^2}\{Q_{22} - Q_{32} + \xi_0(Q_{22} - Q_{12})\} \right]_{\text{sym}} + [Q_{12}]_{\text{anti}} \\
\\
\text{(b)} & C_{n1} = \left[Q_{67} + \frac{4}{A^2}\{Q_{27} - Q_{37} + \xi_0(Q_{27} - Q_{17})\} \right]_{\text{sym}} + \\
\\
& \quad + \left[Q_{52} + \frac{8}{A^2}\{Q_{22} - Q_{32} + \xi_0(Q_{22} - Q_{12})\} \right]_{\text{anti}} \\
\\
\text{(c)} & C_{n1} = \left[Q_{10,8} + \frac{12}{A^2}\{Q_{78} - Q_{88} + \xi_0(Q_{78} - Q_{68})\} \right]_{\text{sym}} + \\
\\
& \quad + \left[2Q_{66} + \frac{8}{A^2}\{Q_{26} - Q_{46} + \xi_0(Q_{36} - Q_{16})\} \right]_{\text{anti}}
\end{array} \tag{61}$$

in the three cases. The negative contributions to the yawing-moment coefficient from the edge forces, C_{n2} and C_{n3}, are easily evaluated from equations (51) and (54) to (57). The results for arbitrary ξ_0 are given in Table 6a.

It is interesting to note that the total C_n is practically independent of ξ_0, as the linear terms in C_{n1} and C_{n3} are of opposite sign and only differ in magnitude by about $\frac{1}{2}$ per cent. Thus the side force C_Y from equation (43) practically vanishes. In Part I Hancock deduces that C_Y becomes very small whenever

$$\frac{\partial Z}{\partial \eta} \equiv 0 \quad \text{at the trailing edge}, \tag{62}$$

a condition that has been satisfied in equations (58). The addition of some quantity $F(\eta)$ to $Z(\xi, \eta)$ would leave α, $l(x, y)$ and the edge forces unchanged, but it could greatly alter C_Y through the coefficient of ξ_0 in equation (44) for C_{n1}. Hancock argues that equation (62) provides an overall condition for small side force in linear potential flow.

From Table 6a it can be observed that C_{n2} and C_{n3} oppose C_{n1}, so that for small ξ_0 the edge forces cause the yawing moment on the rectangular wing of aspect ratio $A = 2$ to change sign in each of the three cases of asymmetric twist. The reality of these contributions will be discussed in relation to rolling derivatives in Section 4.2, for it certainly matters whether or not the edge forces can be sustained in viscous flow.

The other example at low speeds is a rectangular wing of higher aspect ratio $A = 4$ with camber shape (a) from equation (58). The formulation of each contribution is general in aspect ratio, and equations (51) and (54) suggest that $-C_{n2}$ should increase and $-C_{n3}$ decrease. The results obtained from the solutions in Table 3 and the generalised forces in Table 5b are included as case (ii) in Table 6b. The contributions to C_{n1} and C_{n3} proportional to ξ_0 are both much smaller and cancel each other within 1 per cent to give negligible side force under the condition (62). The total coefficient C_n has changed from negative to positive as a result of the increase in aspect ratio, notwithstanding the large increase in $-C_{n2}$ from the leading-edge suction.

Although the resultant edge forces would be linear in any factors applied to the symmetric or antisymmetric parts of $Z(\xi, \eta)$, this is not true of local edge forces. The local leading-edge force corresponds to equation (34) and is proportional to Θ^2: likewise from equations (39) and (40) the local side-edge force is proportional to Ψ^2 and quadratic in $\bar{\Gamma}_q$. In the case $A = 4$ with the camber shape (a), the distribution of edge force depends only on the distribution of incidence $\alpha = 1 + \eta$ in equation (59). The symmetric distributions of edge force for $\alpha = 1$ and $\alpha = \eta$ and the combined asymmetric distribution are shown to scale in Fig. 2. The local leading-edge and side-edge forces are of the same order of magnitude. When the incidences are superposed to give $\alpha = 1 + \eta$, the resulting local side-edge force from equation (41) is

$$E_s = [(E_s)_{\text{sym}}^{\frac{1}{2}} \pm (E_s)_{\text{anti}}^{\frac{1}{2}}]^2 \quad \text{according as } \eta = \pm 1. \tag{63}$$

The non-linear construction of E_s explains the marked reduction in side force in Fig. 2 at the port tip, where there are opposing contributions, in strong contrast to the starboard tip where $(E_s)_{\text{sym}}$ and $(E_s)_{\text{anti}}$ are reinforcing. The resulting local force from equation (63) can be up to four times the larger of $(E_s)_{\text{sym}}$ and $(E_s)_{\text{anti}}$.

3.2. Tapered Swept Wing in Compressible Flow

The planform of the tapered swept wing is that used in Fig. 1 and is defined by

$$\left.\begin{array}{l} \xi_l(\eta) = x_l/\bar{c} = \sqrt{3}|\eta| \\[4pt] \xi_t(\eta) = x_t/\bar{c} = \tfrac{3}{4} + \tfrac{1}{2}\sqrt{3} + \tfrac{1}{2}|\eta| \\[4pt] s = \tfrac{1}{2}A\bar{c} = \bar{c} \end{array}\right\}. \tag{64}$$

It has been chosen for the present investigation, because both symmetric and antisymmetric solutions for wing loading at $M = 0.7806$ were already available to fair accuracy from the lifting-surface method of Ref. 5 with $(m, N, q) = (15, 4, 6)$. For the purpose of these solutions the central cranks in the leading and trailing edges have been rounded according to equations (21) and (22) with $\eta_{iR} = 0.19509$; thus the leading edge is displaced by $0.113\bar{c}$ and the root chord $c_R = 1.616\bar{c}$ is replaced by $c(0) = 1.536\bar{c}$. The loading coefficients for $\alpha = 1$ and $\alpha = \eta$ are recorded in Table 4 in the notation of equations (10) to (13).

The yawing moment coefficient is again calculated from equation (42) as the sum of three parts, and we first consider C_{n1}. To keep the trailing edge of equation (64) in the plane $z = 0$ and to provide $\alpha = \partial Z/\partial \xi = 1 + \eta$, the camber shape is taken as

$$Z(\xi, \eta) = (1 + \eta)[\xi - \xi_t(\eta)]. \tag{65}$$

Then in the notation of equation (45)

$$\left.\begin{array}{l} (Z_j)_{\text{sym}} = -(\tfrac{3}{4} + \tfrac{1}{2}\sqrt{3}) + \xi - \tfrac{1}{2}|\eta| \\[4pt] (Z_j)_{\text{anti}} = -(\tfrac{3}{4} + \tfrac{1}{2}\sqrt{3})\eta + \xi\eta - \tfrac{1}{2}\eta|\eta| \\[4pt] l = (l_2)_{\text{sym}} + (l_2)_{\text{anti}} \end{array}\right\}. \tag{66}$$

The force modes of equation (46) become

$$\left.\begin{array}{l} (Z_i)_{\text{sym}} = (\tfrac{3}{4} + \tfrac{1}{2}\sqrt{3})\xi - \xi^2 + \eta^2 + \xi|\eta| \\[4pt] \qquad\qquad - \xi_0[(\tfrac{3}{4} + \tfrac{1}{2}\sqrt{3}) - \xi + |\eta|] \\[4pt] (Z_i)_{\text{anti}} = \eta + \tfrac{1}{2}\xi\eta/|\eta| - \xi_0[\tfrac{1}{2}\eta/|\eta|] \end{array}\right\}. \tag{67}$$

Hence by equation (47) and with reference to equations (19) and (20)

$$C_{n1} = [(\tfrac{3}{4} + \tfrac{1}{2}\sqrt{3})Q_{22} - Q_{32} + Q_{62} + Q_{112} - \xi_0\{(\tfrac{3}{4} + \tfrac{1}{2}\sqrt{3})Q_{12} - Q_{22} + Q_{12}\}]_{\text{sym}} +$$
$$+ [Q_{12} + \tfrac{1}{2}Q_{112} - \xi_0\{\tfrac{1}{2}Q_{12}\}]_{\text{anti}}, \tag{68}$$

where the generalised force coefficients are evaluated in Table 5c.

The remainder of C_n comes from the edge forces. Because of the straight sweptback leading edge from equation (64), C_{n2} is given by equation (51) whose linear term in ξ_0 no longer vanishes; in the calculation Θ_{sym} and Θ_{anti} are obtained from equation (50) and Table 4, $\beta = 0.625$ and $\sec \Lambda_l = 2$. The side edges contribute C_{n3} from equations (54) to (57) with $c_T/\bar{c} = \tfrac{5}{4} - \tfrac{1}{2}\sqrt{3}$ and $\xi_{lT} = \sqrt{3}$.

The results for arbitrary ξ_0 appear as case (iv) in Table 6b. The side force coefficient $C_Y = -0.045$ from equation (43) is considerably larger than any of the corresponding values for rectangular wings, but it still amounts to less than 2 per cent of the contribution from normal pressures. In this sense it remains true that

42

equation (62) provides a condition for small side force. The yawing moment is only slightly dependent on axis position, and for small ξ_0 the edge forces are seen to dominate. The negative C_n includes large contributions from the leading-edge and side-edge forces despite the considerable taper.

The distribution of edge force has been calculated from equations (34) and (41) and compared in Fig. 3 with that on the rectangular wing of the same aspect ratio in incompressible flow. The two most prominent features for the tapered swept wing are the loss of suction force near the root leading edge and the maintenance of large values on both the leading and side edges ($\eta > 0$) at quite small distances from the leading tip corner where the suction must vanish. The inverse square root singularity in $l(x, y)$ would be expected to disappear at a leading apex; although this characteristic is removed from the numerical solution as a result of rounding the central crank, the tendency remains apparent. High leading-edge suction is a recognised feature of the outward portion of an uncambered tapered swept wing; coupled with this is a forward movement of the local aerodynamic centre as $\eta \to 1$ and the associated tendency for the side-edge force to be fairly constant along the tip chord. Although for swept wings the lifting-surface method is least accurate near the leading edge at the root and tip, the local edge force must vanish at these positions. The present method seems to treat the difficult numerical problem of edge forces to an acceptable approximation for the purpose of estimating lateral stability derivatives.

4. Roll-Rate Derivatives

It is supposed that the rolling motion is slow enough for the helical wake to be treated as planar. Within the framework of linear theory the stability derivatives may be regarded as arising either from a steady rate of roll or from rolling oscillations of low frequency, as considered in Section 2.6 of Ref. 5. The damping forces in the latter case are identified with those from the steady state.

Wing forces due to rolling motion can be obtained by the straightforward application of quantities that have already appeared in Sections 3.1 and 3.2. This particular field of study has been the subject of earlier theoretical investigations[1,4] and semi-empirical methods[2,3] based on wind-tunnel measurements, as mentioned in Section 1. While the experimental data and the existing comparisons are expressed in terms of aerodynamic body axes, called stability axes in the American literature, it is customary now to use standard 'body axes' in calculations of lateral stability. Both systems of axes are therefore included in the theoretical formulations of Section 4.1, and there are different expressions for the yawing moment due to rolling motion in the two cases. In Section 4.2 this derivative is referred to aerodynamic body axes, when the present calculations are compared with other estimates and related to experimental evidence.

4.1. Theoretical Calculations

The rolling moment $\mathscr{L}$ is defined in Fig. 1b as positive about the forward (negative x) axis and has its co-efficient

$$C_l = \mathscr{L}/(\rho U^2 S s). \tag{69}$$

The surface of an untwisted and uncambered wing at incidence $\bar{\alpha}$ and with angular rate of roll, p, about the same axis is

$$z = \bar{\alpha}(x_0 - x) - pyt \tag{70}$$

at time t. On the boundary the required upward velocity in the fluid is

$$\frac{\partial z}{\partial t} + U\frac{\partial z}{\partial x} = -U\bar{\alpha} - py,$$

which corresponds to an incidence distribution

$$\alpha = \bar{\alpha} + (ps/U)\eta. \tag{71}$$

In the notation of equation (66) the non-dimensional wing loading under these conditions is

$$l(x, y) = \bar{\alpha}(l_2)_{\text{sym}} + (ps/U)(l_2)_{\text{anti}}. \tag{72}$$

The rolling moment coefficient in equation (69) is equivalent to the generalised force coefficient Q_i in equation (17) with the force mode

$$Z_i(\xi, \eta) = -\eta = -(Z_1)_{\text{anti}}. \tag{73}$$

Thus

$$C_l = -(Q_1)_{\text{anti}} = -(ps/U)(Q_{12})_{\text{anti}} \qquad (74)$$

with the loading from equation (72), and hence the damping-in-roll derivative is

$$l_p = \frac{\partial \mathscr{L}/\partial p}{\rho U S s^2} = \frac{\partial C_l}{\partial(ps/U)} = -(Q_{12})_{\text{anti}}. \qquad (75)$$

In accord with current practice the derivatives are first referred to body axes, the co-ordinate system of Fig. 1 being rotated about $0y$ through the angle $\bar{\alpha}$ to keep $0x$ in the plane of the wing. Since there is no contribution from normal pressures, the yawing moment about the negative z body axis only involves the edge forces. Therefore in place of equation (42)

$$C_{nB} = C_{n2} + C_{n3} \qquad (76)$$

for the wing without camber and twist, where C_{n2} and C_{n3} are calculated from equations (51) and (54) with the loading from equation (72). Both contributions are proportional to $\bar{\alpha}$ and (ps/U), and equation (76) may be written as

$$C_{nB} = \bar{\alpha}(ps/U)[C_{n2} + C_{n3}]_{\alpha = 1 + \eta}, \qquad (77)$$

whence the derivative of yawing moment is

$$n_{pB} = \frac{\partial C_{nB}}{\partial(ps/U)} = \bar{\alpha}[C_{n2} + C_{n3}]_{\alpha = 1 + \eta}. \qquad (78)$$

If, however, the axis $0x$ remains parallel to the direction of the stream, the yawing moment about the negative $0z$ axis includes a second-order component of the rolling moment in equation (75), since the normal pressures act about the inclined 'body axis' $0x$. Referred to aerodynamic body axes the yawing moment coefficient is

$$C_n = C_{nB} - \bar{\alpha}C_l, \qquad (79)$$

whence

$$n_p = n_{pB} - \bar{\alpha}l_p + \text{ higher order terms*}$$
$$= \bar{\alpha}\{(Q_{12})_{\text{anti}} + [C_{n2} + C_{n3}]_{\alpha = 1 + \eta}\}. \qquad (80)$$

This derivative is usually related to the lift coefficient. Since the lift curve slope is

$$\partial C_L/\partial \bar{\alpha} = 2(Q_{12})_{\text{sym}}, \qquad (81)$$

equation (80) may be rewritten as

$$\frac{n_p}{C_L} = \frac{(Q_{12})_{\text{anti}} + [C_{n2} + C_{n3}]_{\alpha = 1 + \eta}}{2(Q_{12})_{\text{sym}}}. \qquad (82)$$

From equation (43) the side force due to rolling motion is given by

$$y_p = \frac{\partial C_Y}{\partial(ps/U)} = A\frac{\partial}{\partial \xi_0}\left[\frac{\partial C_n}{\partial(ps/U)}\right] = A\frac{\partial n_p}{\partial \xi_0}, \qquad (83)$$

where n_p may be referred to body or aerodynamic body axes in equation (78) or (82) respectively. Since $(Q_{12})_{\text{sym}}$ and $(Q_{12})_{\text{anti}}$ do not depend on ξ_0, the location of the yawing axis, equation (83) becomes

$$\frac{y_p}{C_L} = \frac{A}{2(Q_{12})_{\text{sym}}} \frac{\partial}{\partial \xi_0}[C_{n2} + C_{n3}]_{\alpha = 1 + \eta} \qquad (84)$$

for either axis system.

---

* In terms of roll-rate derivatives l_p and n_p and yaw-rate derivatives l_r and n_r for aerodynamic body axes, the transformation to body axes gives the relationship

$$n_{pB} = n_p \cos^2 \bar{\alpha} + (l_p - n_r)\sin \bar{\alpha} \cos \bar{\alpha} - l_r \sin^2 \bar{\alpha}$$

$$\approx n_p + \bar{\alpha}l_p$$

for the wing contributions when $\bar{\alpha}$ is small.

44

The derivatives l_p, y_p, n_{pB} and n_p have been calculated from equations (75), (84), (78) and (82) for each of the four cases in Table 6b. The coefficients $(Q_{12})_{\text{sym}}$, $(Q_{12})_{\text{anti}}$, C_{n2} and C_{n3} are taken from Tables 5 and 6b. Case (iii), the rectangular wing of aspect ratio 4 at $M = 0.8660$ ($\beta = \frac{1}{2}$), has identical solutions to those in Tables 1 and 2 for $A = 2$ and $M = 0$, but the coefficients in Table 5a require the factor $\beta^{-1} = 2$; on account of the factor A^{-1} in equation (54), C_{n3} is half that for case (i), while for zero leading-edge sweep the first term of equation (51) gives a value of C_{n2} twice that for case (i). The final results are recorded in Table 7.

A few trends in the rolling derivatives from linearised potential flow can be observed; for example, l_p depends more on aspect ratio than anything else. For the $A = 4$ rectangular wing at a fixed incidence $\bar{\alpha}$, y_p is subject to greater changes with Mach number than l_p or n_p, but in the form y_p/C_L the side-force derivative appears to be the least susceptible to compressibility effect. Moreover, y_p/C_L seems to grow according to the streamwise extent of the leading and side edges, increasing as aspect ratio decreases or as sweepback increases. The following table shows similar trends in the magnitude of the yawing-moment derivatives when the yawing axis passes through the aerodynamic centre.

Wing		M	$\xi_0 = \left(\dfrac{Q_{22}}{Q_{12}}\right)_{\text{sym}}$	$\dfrac{n_{pB}}{C_L}$	$\dfrac{n_p}{C_L}$
Rectangular	$A = 2$	0	0.2094	-0.250	-0.173
Rectangular	$A = 4$	0	0.2319	-0.168	-0.075
Rectangular	$A = 4$	0.8660	0.2094	-0.140	-0.064
Tapered swept	$A = 2$	0.7806	1.0812	-0.365	-0.292

Unlike C_n in Table 6b for wings with asymmetric twist, n_p/C_L remains negative, although its magnitude is appreciably smaller for aerodynamic body axes than for body axes; there is a fairly constant difference between n_{pB}/C_L and n_p/C_L, because l_p is roughly proportional to the lift curve slope.

4.2. Related Experimental Evidence

The wind-tunnel evidence is from two sources. Data for low-speed flow are taken from Ref. 2, for which the rolling-flow equipment of the Langley stability tunnel was used. Qualitative comparisons are made with test data from Ref. 3 obtained in subsonic compressible flow by the forced-roll sting-support system described in that paper. No relevant evidence for non-slender wings in oscillatory rolling motion appears to be available.

Low-speed experimental results for $-l_p$ and $-n_p/C_L$ on rectangular wings of aspect ratios $A = 1.34$, 2.61 and 5.16 are included in Fig. 4. For each derivative the mean values over the range $0.2 < C_L < 0.4$ have been taken, and in each case approximate theoretical curves against A have been reproduced from charts in Figs. 8 and 10 of Ref. 1 and in Figs. 9d and 11d of Ref. 4. The comparisons of rolling moment call for little comment; the present theory is in close agreement with the predictions of both Refs. 1 and 4, and all the experimental data lie convincingly just below the theoretical results.

Before discussing the comparisons of yawing moment in Fig. 4, we consider the evidence of $-n_p$ against C_L for four particular wings in Fig. 19 of Ref. 1 and in Fig. 18 of Ref. 4. The approximate formulae of Ref. 1 are based on the simplified concept of strip theory, in which the forces are related to those on a two-dimensional sheared wing with correction for aspect ratio. It is not surprising, therefore, that Ref. 1 achieves its greatest success for the $A = 5.16$ rectangular wing. Fig. 18a of Ref. 4 for a swept-forward wing also shows Ref. 1 in a more favourable light than Ref. 4, which uses a system of bound and trailing vortices that becomes unrealistic with high forward sweep. For the two remaining untapered sweptback wings of aspect ratios 2.61 and 1.34, the method of Ref. 4 provides a great improvement on the older method. A similar pattern emerges in the lower half of Fig. 4. There are large differences between the methods of Refs. 1 and 4, for which no satisfactory explanation can be offered. Neither predicts the rapid increase in $-n_p/C_L$ as A decreases, which is a common feature of the present theory and experiment. The explanation in the case of the theory is provided by the dominant rôle of the side-edge force through C_{n3} in equation (82), a contribution that has been ignored in Refs. 1 and 4. In this respect it is important to note that the present theory without the side-edge force is in close agreement with Ref. 1.

The side force on rectangular wings without camber or twist arises entirely from suction at the side edges. The upper illustration of Fig. 5 shows the side force on rolling rectangular wings of variable aspect ratio. The empirical result from Ref. 2

$$\frac{y_p}{C_L} = \frac{1}{A} \tag{85}$$

45

is an expression of the reality of about two thirds of the resultant side-edge force from the present calculations. The mean experimental values over the range $0.2 < C_L < 0.4$ give rough confirmation of equation (85).

The lower illustrations of Fig. 5 concern the yawing moment on tapered swept wings in rolling motion under different lift conditions. As there are no experimental data for the present example ($A = 2$, $M = 0.7806$), results for a similar taper ratio and sweepback are taken from Fig. 17c of Ref. 2 ($A = 2.61$, $M = 0$). The satisfactory agreement between the empirical method of Ref. 2 and the experimental variation of n_p with C_L is reproduced in Fig. 5. The added theoretical result from equation (7) and Figs. 5 and 6 of Ref. 4, referred to the aerodynamic centre, is equally satisfactory while $C_L < 0.5$. When the method of Ref. 4 is applied similarly to the present example, the result in Fig. 5 is found to correspond to the present theory with about half the side-edge force omitted. These calculations suggest that, just as the extra lift-dependent drag at high lift is accompanied by a loss of leading-edge suction, it may be worthwhile to examine to what extent the non-linearity in n_p against C_L can be accounted for by means of a progressive removal of edge forces from equation (82) as C_L increases.

Curves of y_p and n_p have been drawn in Fig. 6 for the $A = 2$ rectangular wing with yawing-moment axis $\xi_0 = 0.25$ on the hypothesis that equations (82) and (84) hold for $C_L < 0.1$, above which the edge contribution ($C_{n2} + C_{n3}$) gradually falls to half its theoretical value at $C_L = 0.5$ and then smoothly to zero at $C_L = 0.7$. Low-speed experimental points are taken from Fig. 7 of Ref. 2 for $A = 1.34$ and $A = 2.61$ rectangular wings with leading-edge spoiler. For both side force and yawing moment the two sets of points straddle the modified theoretical curve for intermediate aspect ratio up to $C_L = 0.5$. As the stall is approached the curves of Fig. 6 become less convincing, but the change in the sign of n_p is adequately explained by the persisting contribution $-\bar{\alpha}l_p$ at the higher lift coefficients. Since for rectangular wings the whole of y_p derives from side-edge forces, the occurrence of negative y_p near the stall seems to imply that a positive rate of roll precipitates the stall on the starboard wing and delays it on the port wing, so that the outward force at the port tip dominates the normally larger and positive contribution to y_p from the starboard tip. Such a reversal of the resultant leading-edge and side-edge forces could account for the high measured values of n_p near $C_L = 0.6$, but their subsequent decrease is probably associated with the sharp fall in $-\bar{\alpha}l_p$ at the stall (Ref. 2, Fig. 7). The detailed behaviour of n_p might be expected to defy simple treatment, but the semi-empirical methods of Refs. 2 and 3 achieve a remarkable degree of success.

Both of these methods involve empirical corrections dependent on the measurement of the drag coefficient C_D over the required range of C_L. The method of Ref. 2 is well illustrated in Fig. 5, but there are advantages in considering Ref. 3, which has greater success at high lift and is tested up to high subsonic Mach numbers. In the present notation equation (1) of Ref. 3 may be written as

$$n_p = -\bar{\alpha}l_p - K[-\bar{\alpha}l_p - n_p]_{\text{Ref. 1}} + \bar{\alpha}[C_{n3}]_{\alpha = 1 + \eta} \tag{86}$$

with the empirical factor

$$K = \frac{\partial/\partial\bar{\alpha}(C_L \tan\bar{\alpha}) - \partial/\partial\bar{\alpha}(C_D - C_{D0})}{\partial/\partial\bar{\alpha}(C_L \tan\bar{\alpha}) - \partial/\partial\bar{\alpha}(C_L^2/\pi A)}, \tag{87}$$

where C_{D0} is the drag coefficient at zero lift. The tip-suction term at the end of equation (86) was treated empirically by Wiggins, but he preferred to omit it altogether in most of his applications. We have already seen in Fig. 4 that as regards n_p the theory of Ref. 1 is approximately equivalent to the present theory without the side-edge contribution. Thus, with the omission of the last term, equation (86) becomes

$$[n_p]_{\text{emp}} = -\bar{\alpha}l_p - K\bar{\alpha}[-C_{n2}]_{\alpha = 1 + \eta}, \tag{88}$$

which should be just as successful as the method of Ref. 3 without tip suction. Correspondingly the side-force derivative becomes

$$[y_p]_{\text{emp}} = KA\bar{\alpha}[\partial C_{n2}/\partial\xi_0]_{\alpha = 1 + \eta}. \tag{89}$$

The progressive removal of edge forces to half value at $C_L = 0.5$ and to zero at $C_L = 0.7$ is illustrated in Fig. 7 for the $A = 4$ rectangular wing at $M = 0$ and 0.866. The derivatives y_p, n_p and n_{pB} from the respective equations (84), (80) and (78) are calculated for aerodynamic body axes and body axes through the aerodynamic centres $\xi_0 = 0.232$ at $M = 0$ and $\xi_0 = 0.209$ at $M = 0.866$. The results bear out the theoretical indications of Ref. 4, that these derivatives are not subject to large compressibility effects. As the edge forces are reduced, the non-linear effects are reasonably consistent with the behaviour of the measured low-speed derivatives y_p and n_p for the sweptback wings in Figs. 8 and 11 of Ref. 2. Zero y_p occurs at a somewhat higher C_L than does zero n_p, but these values of C_L decrease with increasing sweepback. The loss of edge forces, artificially aided by leading-edge spoilers in Fig. 6, occurs naturally at lower C_L on wings of higher sweepback. The same patterns of

46

behaviour are found for $A = 4$ and over ranges of sweepback and high subsonic Mach number in Figs. 24 and 22 of Ref. 3, which include semi-empirical curves equivalent to equations (89) and (88). Typically y_p changes sign near $C_L = 0.5$, while for n_p this occurs before $C_L = 0.3$. Thus the loss of edge forces appears to be hastened by compressibility, but the associated non-linear dependence of these second-order roll-rate derivatives on C_L or $\bar{\alpha}$ is qualitatively unchanged.

The semi-empirical method of Ref. 3 without tip suction has notable success beyond the range of C_L for which y_p is positive. The negative experimental values of y_p, which usually occur at high C_L and have been tentatively explained in terms of a reversal of the resultant edge forces, arise from equation (89) on account of negative K. This is the inevitable consequence of relating K in equation (87) to the rates of change of the lift-dependent drag coefficient $(C_D - C_{D0})$ and of its theoretical upper and lower bounds $C_L \tan \bar{\alpha}$ and $C_L^2/\pi A$. As $(C_D - C_{D0})$ begins to approach the upper bound, the numerator of equation (87) becomes negative before it eventually tends to zero. At the same time through equation (88) negative K accounts for values of n_p in excess of $-\bar{\alpha}l_p$. Moreover, the observed maximum in this derivative, which cannot arise simply from progressive removal of edge forces, is obtained in Fig. 22 of Ref. 3 whether the derivative l_p is taken from calculation or experiment.

Nevertheless, the success of the semi-empirical method poses an anomaly as regards side-edge forces. Comparisons of the values of C_{n2} and C_{n3} in Table 6 and the distributions of edge force in Figs. 2 and 3 suggest that leading- and side-edge forces are of similar importance: at very small lift the semi-empirical method for n_p would probably be improved by the inclusion of side-edge forces: furthermore, from the fact that for rectangular wings n_p vanishes while y_p is still positive in Fig. 6, the side-edge forces can be as persistent as the leading-edge forces on unswept wings in incompressible flow. Yet on tapered swept wings at high subsonic speeds the neglect of side-edge forces is insufficient to reduce y_p to the small positive values measured at low C_L (Fig. 24 of Ref. 3). It seems that sweepback and taper, both of which tend to boost the loading near the tip leading edge, also combine to suppress the side-edge force through incipient leading-edge flow separation. The process appears to be hastened by the additional influence of compressibility.

5. Conclusions

Of the following conclusions (1) to (3) are mainly concerned with edge forces in potential flow, (4) and (5) relate to the calculated roll-rate derivatives, (6) and (7) deal with semi-empirical approaches to the estimation of these stability derivatives at moderate or high lift coefficient.

(1) The local edge forces are shown to be quadratic functions of the loading coefficients and to have the same order of magnitude on the leading and side edges. All the integrated contributions to side force and yawing moment involve products of the symmetric and antisymmetric parts of the spanwise loading and are linear with respect to the coefficients in either part.

(2) Unlike drag, the total yawing moment in potential flow and its contribution from normal pressures can have opposite signs. The edge forces become increasingly dominant as aspect ratio decreases or as sweepback increases.

(3) If a thin wing is deformed in camber and twist in such a manner that the trailing edge lies in a streamwise plane, then the resultant lateral force in that plane is found to be small if the theoretical edge forces are included.

(4) The rolling moment due to rate of roll is calculated to be in good agreement with charts based on approximate theoretical methods. The values correlate satisfactorily with experimental data for rectangular wings of varying aspect ratio.

(5) While the rolling-moment derivative depends mainly on aspect ratio, the magnitudes of the theoretical derivatives of side force and yawing moment for a given lift seem to grow according to the streamwise extent of the leading and side edges as a fraction of wing span.

(6) Experimental evidence of the side force and yawing moment due to rate of roll invariably shows a non-linear dependence on lift. It is demonstrated that prior to the stall this non-linearity can be accounted for by removing an increasing proportion of the edge forces as the lift increases.

(7) From the present analysis some simple formulae, equivalent to the semi-empirical method of Wiggins[3] without tip suction, are obtained in equations (88) and (89) for the roll-rate derivatives of yawing moment and side force respectively. These should be reasonably successful in conjunction with subsonic wing theory and measured drag over the whole practical range of lift coefficient.

LIST OF SYMBOLS

a	Factor controlling spanwise integration (Ref. 6)
a	Integer $1(1)N$ used in equations (55) to (57)
A	Aspect ratio of planform; $2s/\bar{c}$
b_j	Coefficient of downwash mode in equation (15) with $j = 1(1)J$
$c(\eta)$	Local chord
$\bar{c}$	Geometric mean chord; $S/2s$
c_R, c_T	Root chord, tip chord
C_D	Drag coefficient; drag/$(\frac{1}{2}\rho U^2 S)$
C_{D0}	Drag coefficient at zero lift
C_l	Rolling moment coefficient; $\mathscr{L}/(\rho U^2 S s)$
C_L	Lift coefficient; lift/$(\frac{1}{2}\rho U^2 S)$
C_n	Yawing moment coefficient; $\mathscr{N}/(\rho U^2 S s)$
C_{n1}	Contribution to C_n from normal pressures in equations (44) to (47)
C_{n2}	Contribution to C_n from leading-edge forces in equation (48)
C_{n3}	Contribution to C_n from side-edge forces in equation (54)
C_Y	Side force coefficient; $Y/(\frac{1}{2}\rho U^2 S)$
E_l	Leading-edge force per unit length in equations (29) and (34)
E_s	Side-edge force per unit length in equations (30) and (39)
i	Integer denoting force mode in equation (14); I or II in equations (20)
I_{qa}	Integrals in equations (56) with $q = 1(1)N$ and $a = 1(1)N$
j	Integer denoting downwash mode; *see* table below equation (19)
J_{qa}	Integrals in equations (57) with $q = 1(1)N$ and $a = 1(1)N$
K	Empirical factor in equation (87)
$l(x, y)$	Non-dimensional wing loading in equations (5) and (10)
l_j	Loading in equation (16) for downwash mode j $(\leqslant J)$
l_p	Damping-in-roll derivative in equation (75)
$\mathscr{L}$	Rolling moment (Fig. 1b)
m	Number of collocation sections
M	Mach number of stream
n	Normal inward distance from edge of planform
n_p	Roll-rate derivative of yawing moment about aerodynamic body axis in equations (79) and (82)
n_{pB}	Roll-rate derivative of yawing moment about body axis in equation (78)
N	Number of chordwise loading functions
$\mathscr{N}$	Yawing moment (Fig. 1b)
p	Angular rate of roll in equation (70)
q	Factor controlling spanwise integration (Ref. 5)
q	Integer $1(1)N$ denoting term in chordwise loading

Q_i	Force$/(\rho U^2 S)$ in mode Z_i in equation (17)
Q_{ij}	Generalised force coefficient in equation (18) (Table 5)
s	Semi-span of wing
S	Area of planform; region of integration
t	Time
U	Velocity of stream
x	Ordinate in streamwise direction (Fig. 1a)
x_0	Location of yawing axis (Fig. 1b)
$x_l(\eta)$	Ordinate of leading edge
x_{pv}	Ordinate of collocation point in equation (9)
$x_t(\eta)$	Ordinate of trailing edge
y	Ordinate in starboard direction (Fig. 1a)
y_p	Roll-rate derivative of side force in equations (83) and (84)
y_v	Ordinate of collocation point in equation (9)
Y	Side force (Fig. 1b)
z	Ordinate in upward direction
$Z(\xi, \eta)$	Camber surface in equations (15) and (58); $-z/\bar{c}$
Z_i	Force mode in equation (14), (20) or (46)
Z_j	Downwash mode in equation (14)
α	Local incidence $\partial Z / \partial \xi$; see also equation (71)
$\bar{\alpha}$	Uniform incidence of rolling wing
β	Compressibility factor; $(1 - M^2)^{\frac{1}{2}}$
$\Gamma_q(\eta)$	Spanwise loading function in equation (12) with $q = 1(1)N$
Γ_{qr}	Local value $\Gamma_q(\eta_r)$
$\bar{\Gamma}_a$	Quantity in equation (55) for antisymmetric spanwise loading
$\bar{\Gamma}_q$	Limit in equations (35) and (36); see also equation (55)
Δp	Lift per unit area
$\Delta \Phi$	Discontinuity in Φ from below to above $z = 0$
η	Non-dimensional spanwise ordinate; y/s
η_{iR}	Extent of central rounding in equations (21) and (22)
η_r	Loading station in equation (13) with $r = 1(1)m$
θ, θ_r	Angular spanwise parameters $\cos^{-1}(-\eta)$, $\cos^{-1}(-\eta_r)$
Θ	Leading-edge force parameter in equation (32)
Λ, Λ_l	Angle of sweepback, value at leading edge
ξ	Non-dimensional streamwise ordinate; $x/\bar{c}$
ξ_0	$x_0/\bar{c}$
ξ_l, ξ_t	$x_l/\bar{c}, x_t/\bar{c}$
ξ_{lT}	$x_l(1)/\bar{c}$
ρ	Density of stream

49

σ, τ	Indices related to i (or j) in table below equation (19)
ϕ	Angular chordwise parameter in equation (11)
Φ	Perturbation velocity potential
Ψ	Side-edge force parameter in equation (40)
anti	Subscript denoting spanwise antisymmetry in α or Z_i
B	Subscript denoting body axes at inclination $\bar{\alpha}$
emp	Subscript denoting empirical formula
sym	Subscript denoting spanwise symmetry in α or Z_i

REFERENCES

No.	Author(s)	Title, etc.
1	T. A. Toll and M. J. Queijo	Approximate relations and charts for low-speed stability derivatives of swept wings. N.A.C.A. Technical Note 1581 (1948).
2	A. Goodman and L. R. Fisher	Investigation at low speeds of the effect of aspect ratio and sweep on rolling stability derivatives of untapered wings. N.A.C.A. Report 968 (1950).
3	J. W. Wiggins	Wind-tunnel investigation of effect of sweep on rolling derivatives at angles of attack up to 13° and at high subsonic Mach numbers, including a semiempirical method of estimating the rolling derivatives. N.A.C.A. Technical Note 4185 (1958).
4	M. J. Queijo	Theory for computing span loads and stability derivatives due to sideslip, yawing, and rolling for wings in subsonic compressible flow. N.A.S.A. Technical Note TN D-4929 (1968).
5	H C. Garner and D. A. Fox	Algol 60 programme for Multhopp's low-frequency subsonic lifting-surface theory. A.R.C. R. & M. 3517 (1966).
6	Doris E. Lehrian and H. C. Garner	Theoretical calculation of generalised forces and load distribution on wings oscillating at general frequency in a subsonic stream. A.R.C. R. & M. 3710 (1971).
7	H. C. Garner	Some remarks on vortex drag and its spanwise distribution in incompressible flow. Aeronaut. J. (R.Ae.S.) Vol. 72, pp. 623–625 (1968).
8	H. Multhopp	Methods for calculating the lift distribution of wings (Subsonic lifting-surface theory). A.R.C. R. & M. 2884 (1950).

TABLE 1

Symmetrical Solutions for Rectangular Wing $A = 2, M = 0$

Calculations by method of Ref. 6 with $(N, m, a) = (4, 15, 6)$

η	$\alpha = 1$ (sym. $j = 2$)			
	Γ_1	Γ_2	Γ_3	Γ_4
0	0·77587	0·09332	0·01150	$-0\cdot00069$
0·19509	0·76275	0·09552	0·01266	$-0\cdot00054$
0·38268	0·72325	0·10148	0·01644	$+0\cdot00011$
0·55557	0·65725	0·10905	0·02345	0·00204
0·70711	0·56522	0·11405	0·03363	0·00641
0·83147	0·44895	0·11019	0·04382	0·01336
0·92388	0·31204	0·09069	0·04583	0·01869
0·98079	0·16002	0·05216	0·03062	0·01461

η	$\alpha = \eta^2$ (sym. $j = 7$)			
	Γ_1	Γ_2	Γ_3	Γ_4
0	0·11441	$-0\cdot01029$	$-0\cdot00759$	$-0\cdot00230$
0·19509	0·12492	$-0\cdot00395$	$-0\cdot00590$	$-0\cdot00216$
0·38268	0·15182	$+0\cdot01387$	$-0\cdot00055$	$-0\cdot00151$
0·55557	0·18271	0·03917	$+0\cdot00894$	$+0\cdot00044$
0·70711	0·20170	0·06470	0·02219	0·00489
0·83147	0·19492	0·08038	0·03555	0·01196
0·92388	0·15555	0·07602	0·04044	0·01751
0·98079	0·08654	0·04688	0·02793	0·01391

η	$\alpha = 2\xi\eta^2$ (sym. $j = 8$)			
	Γ_1	Γ_2	Γ_3	Γ_4
0	0·16700	$-0\cdot05877$	$-0\cdot00409$	0·00280
0·19509	0·18591	$-0\cdot07445$	$-0\cdot00280$	0·00233
0·38268	0·23506	$-0\cdot11645$	$+0\cdot00111$	0·00078
0·55557	0·29388	$-0\cdot17063$	0·00768	$-0\cdot00215$
0·70711	0·33494	$-0\cdot21651$	0·01640	$-0\cdot00662$
0·83147	0·33246	$-0\cdot23200$	0·02503	$-0\cdot01170$
0·92388	0·27121	$-0\cdot20015$	0·02830	$-0\cdot01434$
0·98079	0·15324	$-0\cdot11727$	0·01982	$-0\cdot01047$

52

TABLE 2

Antisymmetrical Solutions for Rectangular Wing A = 2, M = 0

Calculations by method of Ref. 6 with (N, m, a) = (4, 15, 6)

η	$\alpha = \eta$ (anti. $j = 2$)			
	Γ_1	Γ_2	Γ_3	Γ_4
0	0	0	0	0
0·19509	0·09145	0·02768	0·00516	0·00007
0·38268	0·16945	0·05471	0·01147	0·00059
0·55557	0·22227	0·07920	0·01996	0·00233
0·70711	0·24163	0·09712	0·03067	0·00637
0·83147	0·22412	0·10223	0·04065	0·01276
0·92388	0·17204	0·08795	0·04247	0·01756
0·98079	0·09327	0·05165	0·02826	0·01365

η	$\alpha = \eta^3$ (anti. $j = 6$)			
	Γ_1	Γ_2	Γ_3	Γ_4
0	0	0	0	0
0·19509	0·02384	0·00205	$-0·00190$	$-0·00113$
0·38268	0·05381	0·01044	$-0·00108$	$-0·00170$
0·55557	0·08940	0·02790	$+0·00478$	$-0·00072$
0·70711	0·12113	0·05082	0·01638	$+0·00321$
0·83147	0·13439	0·06897	0·03025	0·01034
0·92388	0·11740	0·06935	0·03699	0·01643
0·98079	0·06878	0·04429	0·02643	0·01347

TABLE 3

Solutions for Rectangular Wing A = 4, M = 0

Calculations by method of Ref. 6 with (N, m, a) = (4, 31, 6)

η	$\alpha = 1$ (sym. $j = 2$)			
	Γ_1	Γ_2	Γ_3	Γ_4
0	0·54943	0·01959	0·00137	−0·00013
0·09802	0·54769	0·01993	0·00142	−0·00013
0·19509	0·54244	0·02095	0·00158	−0·00014
0·29028	0·53354	0·02269	0·00186	−0·00017
0·38268	0·52076	0·02519	0·00232	−0·00019
0·47140	0·50382	0·02850	0·00303	−0·00021
0·55557	0·48238	0·03260	0·00411	−0·00019
0·63439	0·45606	0·03740	0·00571	−0·00008
0·70711	0·42456	0·04258	0·00805	+0·00027
0·77301	0·38764	0·04761	0·01130	0·00106
0·83147	0·34523	0·05162	0·01543	0·00256
0·88192	0·29748	0·05348	0·01996	0·00493
0·92388	0·24477	0·05191	0·02366	0·00779
0·95694	0·18772	0·04576	0·02459	0·01001
0·98079	0·12719	0·03447	0·02087	0·00997
0·99518	0·06422	0·01859	0·01207	0·00659

η	$\alpha = \eta$ (anti. $j = 2$)			
	Γ_1	Γ_2	Γ_3	Γ_4
0	0	0	0	0
0·09802	0·03937	0·00403	0·00036	−0·00003
0·19509	0·07749	0·00821	0·00076	−0·00007
0·29028	0·11313	0·01266	0·00123	−0·00011
0·38268	0·14508	0·01751	0·00183	−0·00014
0·47140	0·17216	0·02284	0·00264	−0·00017
0·55557	0·19328	0·02868	0·00376	−0·00016
0·63439	0·20748	0·03493	0·00534	−0·00005
0·70711	0·21397	0·04129	0·00755	+0·00027
0·77301	0·21221	0·04721	0·01053	0·00100
0·83147	0·20200	0·05183	0·01425	0·00237
0·88192	0·18350	0·05402	0·01824	0·00448
0·92388	0·15730	0·05256	0·02141	0·00698
0·95694	0·12438	0·04635	0·02209	0·00882
0·98079	0·08606	0·03489	0·01868	0·00853
0·99518	0·04399	0·01880	0·01080	0·00533

TABLE 4

Solutions for Tapered Swept Wing at $M = 0.7806$

$(A = 2, \Lambda_l = 60°, \Lambda_t = \tan^{-1} 0.5)$
Calculations by method of Ref. 5 with $(m, N, q) = (15, 4, 6)$

η	$\alpha = 1$ (sym. $j = 2$)			
	Γ_1	Γ_2	Γ_3	Γ_4
0	0·78499	−0·40702	−0·01222	−0·00489
0·19509	0·77803	−0·26660	−0·03132	+0·00614
0·38268	0·74456	−0·12828	−0·03287	0·01309
0·55557	0·68231	−0·04052	−0·04149	0·01332
0·70711	0·59093	+0·03786	−0·04836	0·00719
0·83147	0·47156	0·11140	−0·03896	−0·01940
0·92388	0·32861	0·15575	+0·02929	−0·02236
0·98079	0·16860	0·12275	0·07999	+0·03848

η	$\alpha = \eta$ (anti. $j = 2$)			
	Γ_1	Γ_2	Γ_3	Γ_4
0	0	0	0	0
0·19509	0·08554	−0·04352	+0·00323	0·00010
0·38268	0·16148	−0·05059	−0·00325	0·00410
0·55557	0·21528	−0·03250	−0·01503	0·00737
0·70711	0·23711	+0·00427	−0·02692	0·00465
0·83147	0·22167	0·05145	−0·02388	−0·01083
0·92388	0·17108	0·08384	+0·01410	−0·01349
0·98079	0·09291	0·07015	0·04581	+0·02167

TABLE 5

Generalised Forces Q_{ij} for Three Wings

(a) Rectangular wing A = 2, M = 0 (Tables 1 and 2)

Symmetrical force mode		$j = 2$	$j = 7$	$j = 8$
i	Z_i	$\alpha = 1$	$\alpha = \eta^2$	$\alpha = 2\xi\eta^2$
1	1	1·23717	0·31385	0·50367
2	ξ	0·25907	0·06226	0·19791
3	ξ^2	0·12004	0·02840	0·11800
6	η^2	0·31386	0·11204	0·18756
7	$\xi\eta^2$	0·06204	0·01828	0·07785
8	$\xi^2\eta^2$	0·02834	0·00773	0·04741
10	η^4	0·15806	0·06443	0·10955

Antisymmetrical force mode		$j = 2$	$j = 6$
i	Z_i	$\alpha = \eta$	$\alpha = \eta^3$
1	η	0·18971	0·09511
2	$\xi\eta$	0·02799	0·01325
3	$\xi^2\eta$	0·01082	0·00502
4	$\xi^3\eta$	0·00588	0·00271
5	η^3	0·09511	0·05380
6	$\xi\eta^3$	0·01324	0·00674

(b) Rectangular wing A = 4, M = 0 (Table 3)

Symmetrical force mode		$j = 2$
i	Z_i	$\alpha = 1$
1	1	1·80597
2	ξ	0·41888
3	ξ^2	0·20301
6	η^2	0·47205

Antisymmetrical force mode		$j = 2$
i	Z_i	$\alpha = \eta$
1	η	0·33598

(c) Tapered swept wing A = 2, M = 0·7806 (Table 4)

Symmetrical force mode		$j = 2$
i	Z_i	$\alpha = 1$
1	1	1·27598
2	ξ	1·37965
3	ξ^2	1·71838
6	η^2	0·32748
I	$|\eta|$	0·55053
II	$\xi|\eta|$	0·69597

Antisymmetrical force mode		$j = 2$
i	Z_i	$\alpha = \eta$
1	η	0·18540
I	$\eta/|\eta|$	0·31171
II	$\xi\eta/|\eta|$	0·40052

TABLE 6

Calculated Yawing Moment on Wings with Asymmetric Twist

(a) Rectangular wing ($A = 2$, $M = 0$)

Case	Camber surface Z	α	Normal pressures C_{n1}
(a)	$(1 + \eta)(\xi - 1)$	$1 + \eta$	$0.6426 - 0.9781\xi_0$
(b)	$\eta(1 + \eta)(\xi - 1)$	$\eta^2 + \eta$	$0.2754 - 0.5750\xi_0$
(c)	$\eta^2(1 + \xi + \eta)(\xi - 1)$	$2\xi\eta^2 + \eta^3$	$0.2354 - 0.5093\xi_0$

Case	Leading edge C_{n2}	Side edge C_{n3}	$C_{n1} + C_{n2} + C_{n3}$
(a)	-0.2574	$-0.5637 + 0.9727\xi_0$	$-0.1785 - 0.0054\xi_0$
(b)	-0.1009	$-0.3237 + 0.5724\xi_0$	$-0.1492 - 0.0026\xi_0$
(c)	-0.0220	$-0.3349 + 0.5081\xi_0$	$-0.1214 - 0.0012\xi_0$

(b) Four examples with $Z = (1 + \eta)(\xi - \xi_t)$

Case	Wing	M	C_{n1}
(i)	Rectangular $A = 2$	0	$0.6426 - 0.9781\xi_0$
(ii)	Rectangular $A = 4$	0	$0.8620 - 0.3468\xi_0$
(iii)	Rectangular $A = 4$	0.8660	$1.0767 - 0.4891\xi_0$
(iv)	Tapered swept $A = 2$	0.7806	$1.9203 - 1.3888\xi_0$

Case	C_{n2}	C_{n3}	$C_{n1} + C_{n2} + C_{n3}$
(i)	-0.2574	$-0.5637 + 0.9727\xi_0$	$-0.1785 - 0.0054\xi_0$
(ii)	-0.4853	$-0.2027 + 0.3436\xi_0$	$+0.1740 - 0.0032\xi_0$
(iii)	-0.5147	$-0.2819 + 0.4864\xi_0$	$+0.2801 - 0.0027\xi_0$
(iv)	$-1.4668 + 0.8793\xi_0$	$-0.9410 + 0.4872\xi_0$	$-0.4875 - 0.0223\xi_0$

57

TABLE 7

Theoretical Rolling Derivatives of Untwisted Wings

(a) Rolling moment and side force

Wing	M	l_p	$y_p/\bar{\alpha}$	$C_L/\bar{\alpha}$	y_p/C_L
Rectangular $A = 2$	0	-0.1897	1.945	2.474	0.786
Rectangular $A = 4$	0	-0.3360	1.374	3.612	0.380
Rectangular $A = 4$	0.8660	-0.3794	1.945	4.949	0.393
Tapered swept $A = 2$	0.7806	-0.1854	2.733	2.552	1.071

(b) Yawing moment

Wing	M	n_{pB}/C_L	n_p/C_L
Rectangular $A = 2$	0	$-0.332 + 0.393\xi_0$	$-0.255 + 0.393\xi_0$
Rectangular $A = 4$	0	$-0.190 + 0.095\xi_0$	$-0.097 + 0.095\xi_0$
Rectangular $A = 4$	0.8660	$-0.161 + 0.098\xi_0$	$-0.084 + 0.098\xi_0$
Tapered swept $A = 2$	0.7806	$-0.944 + 0.535\xi_0$	$-0.871 + 0.535\xi_0$

58
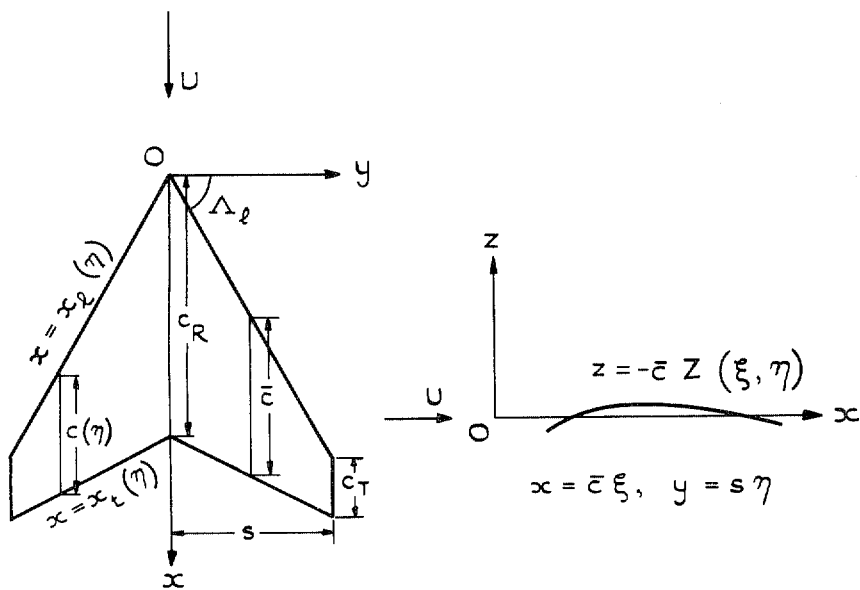
a.   System of co-ordinates
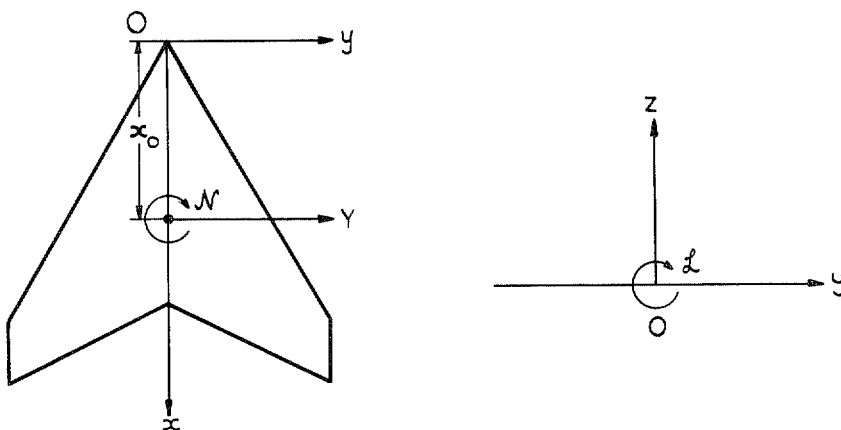
b.   Definition of lateral forces

FIG. 1a and b.   Definition of co-ordinate and lateral-force systems.

59

$\alpha = 1$

$\alpha = \eta$

$\alpha = 1 + \eta$
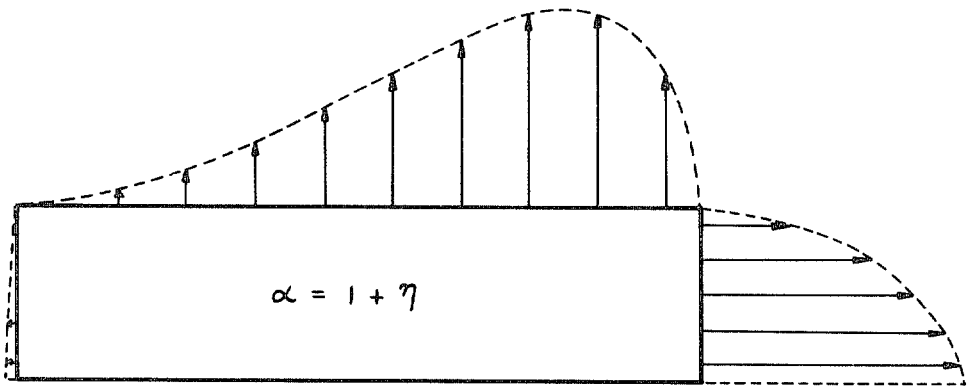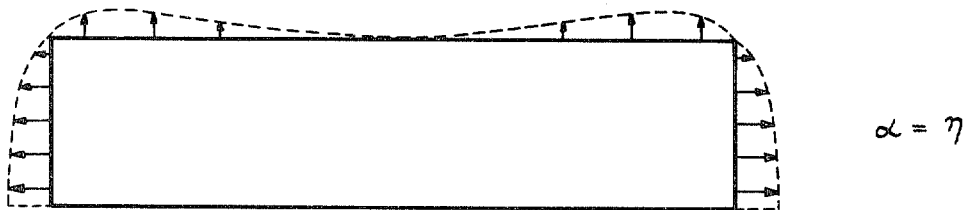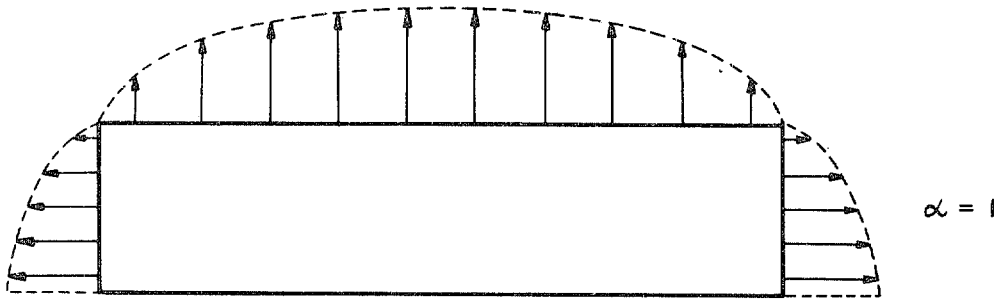
FIG. 2.   Edge forces on a rectangular wing ($A = 4$, $M = 0$).
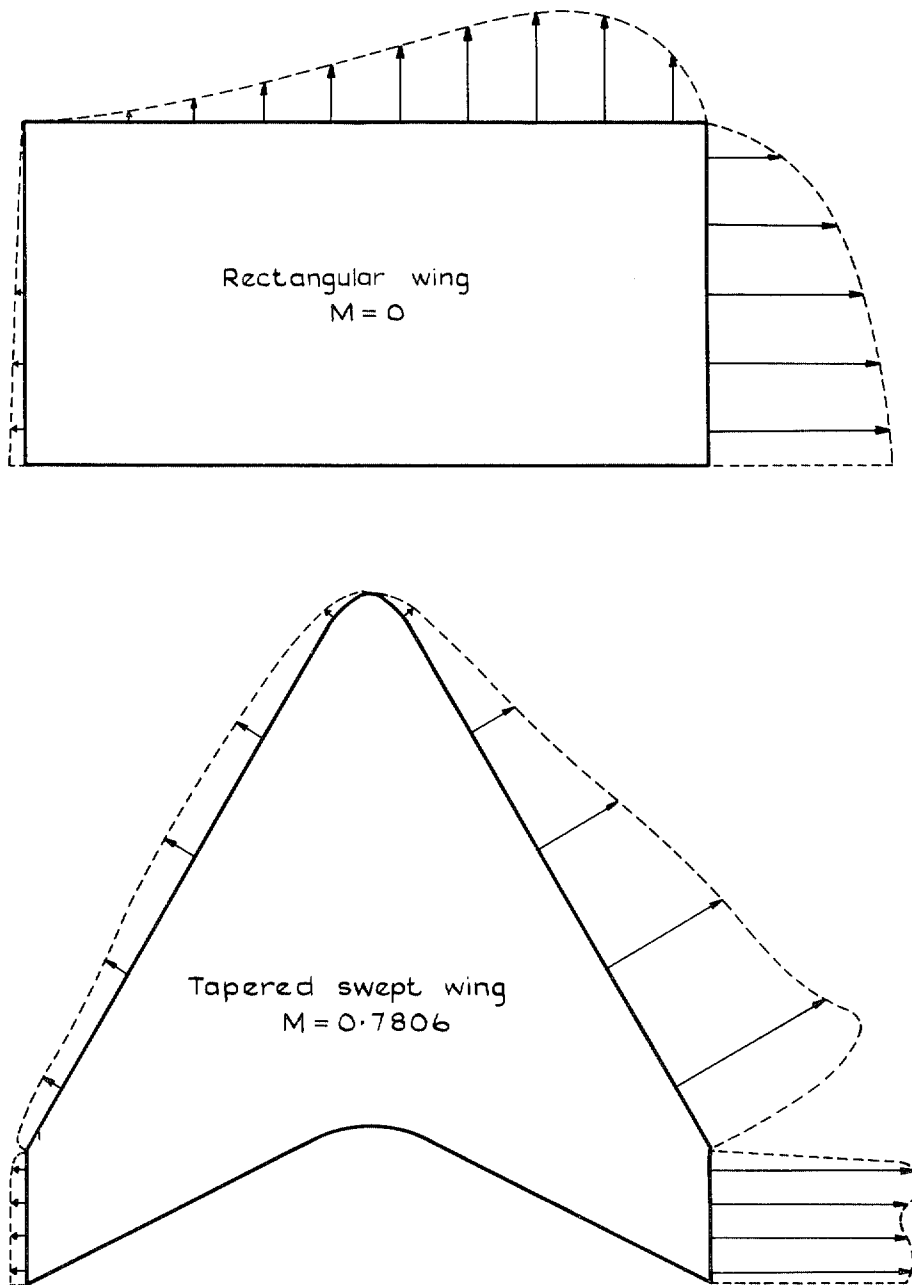
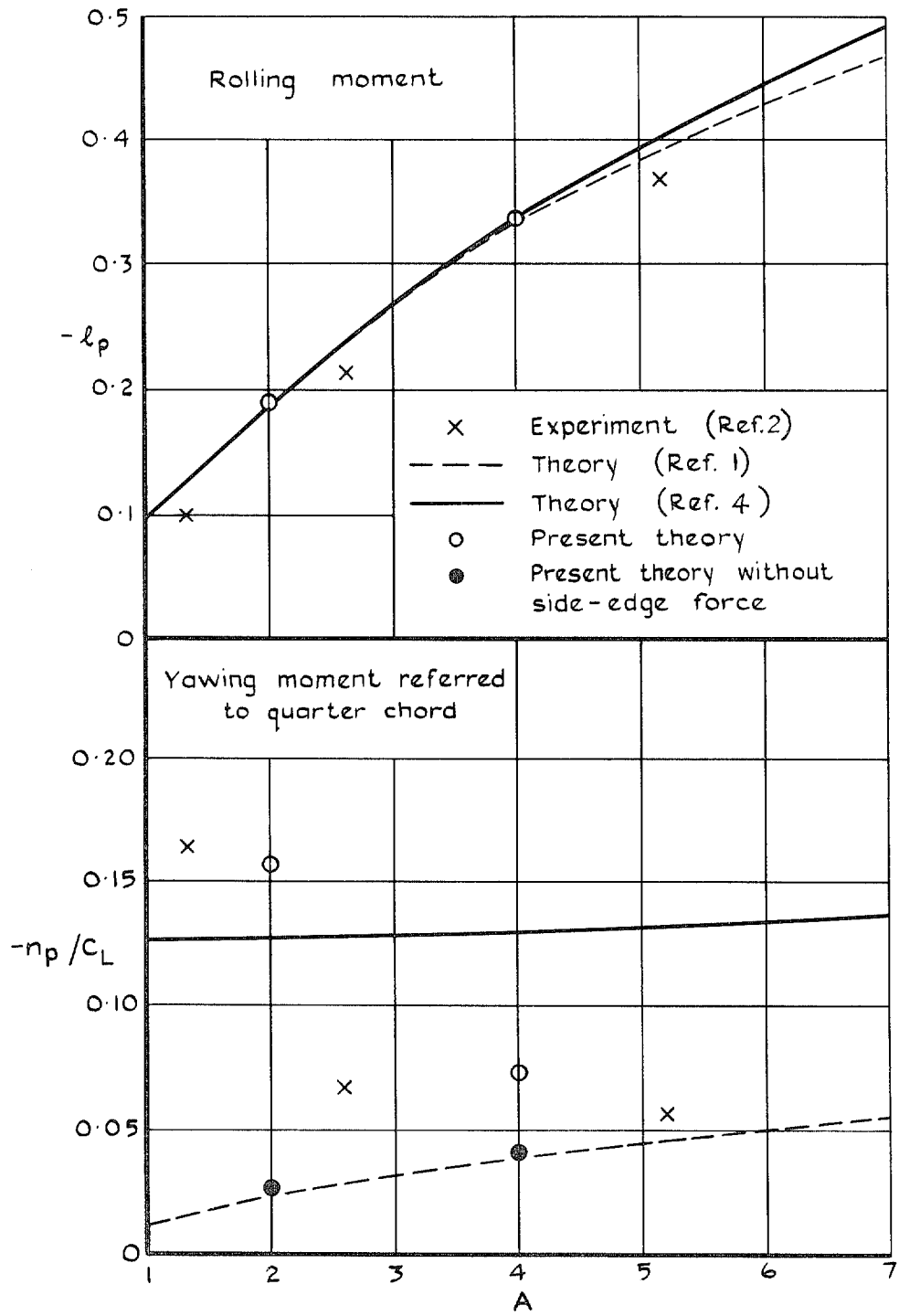FIG 3.   Edge forces on two wings of aspect ratio 2 with $\alpha = 1 + \eta$.

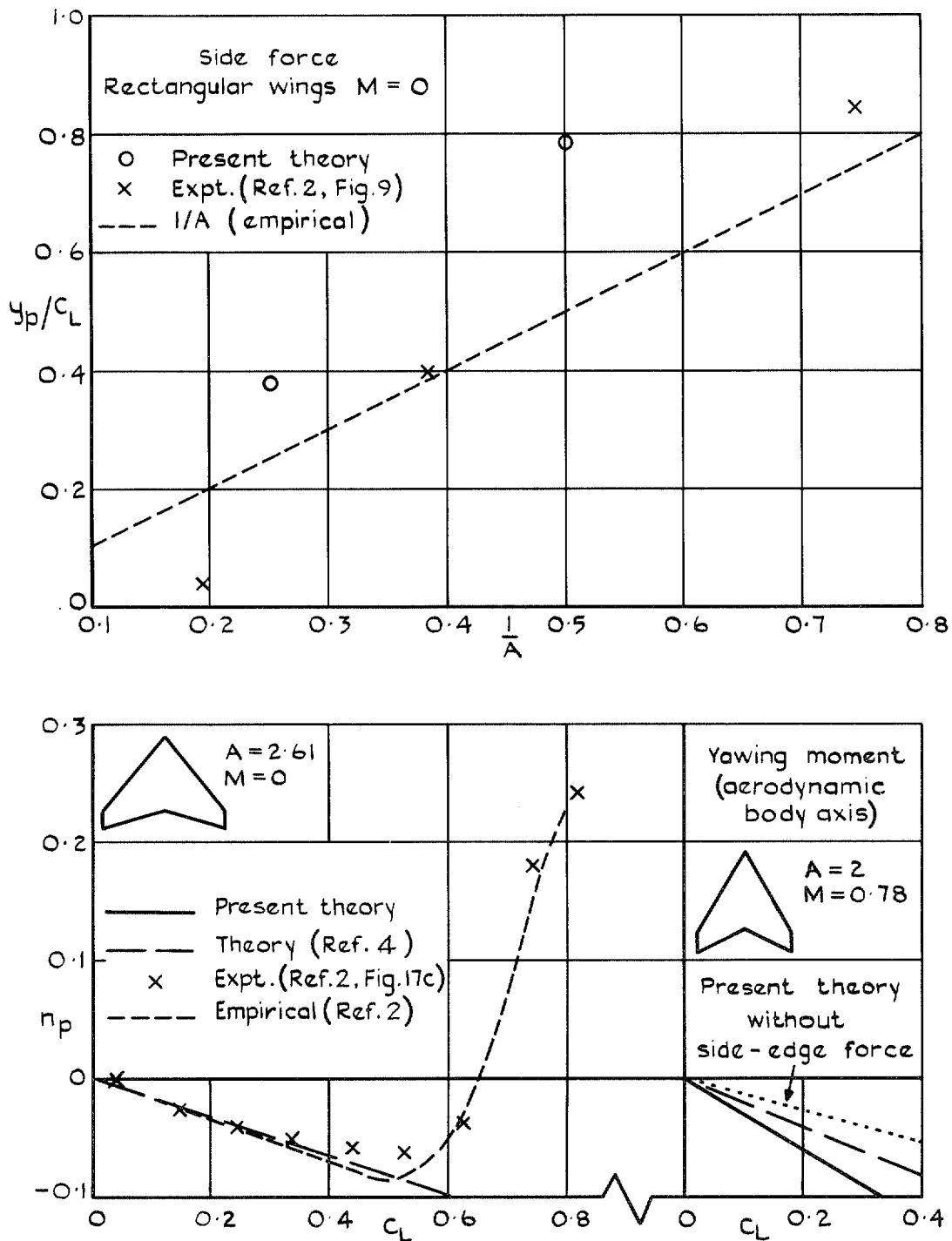FIG. 4.   Roll-rate derivatives for rectangular wings in incompressible flow.

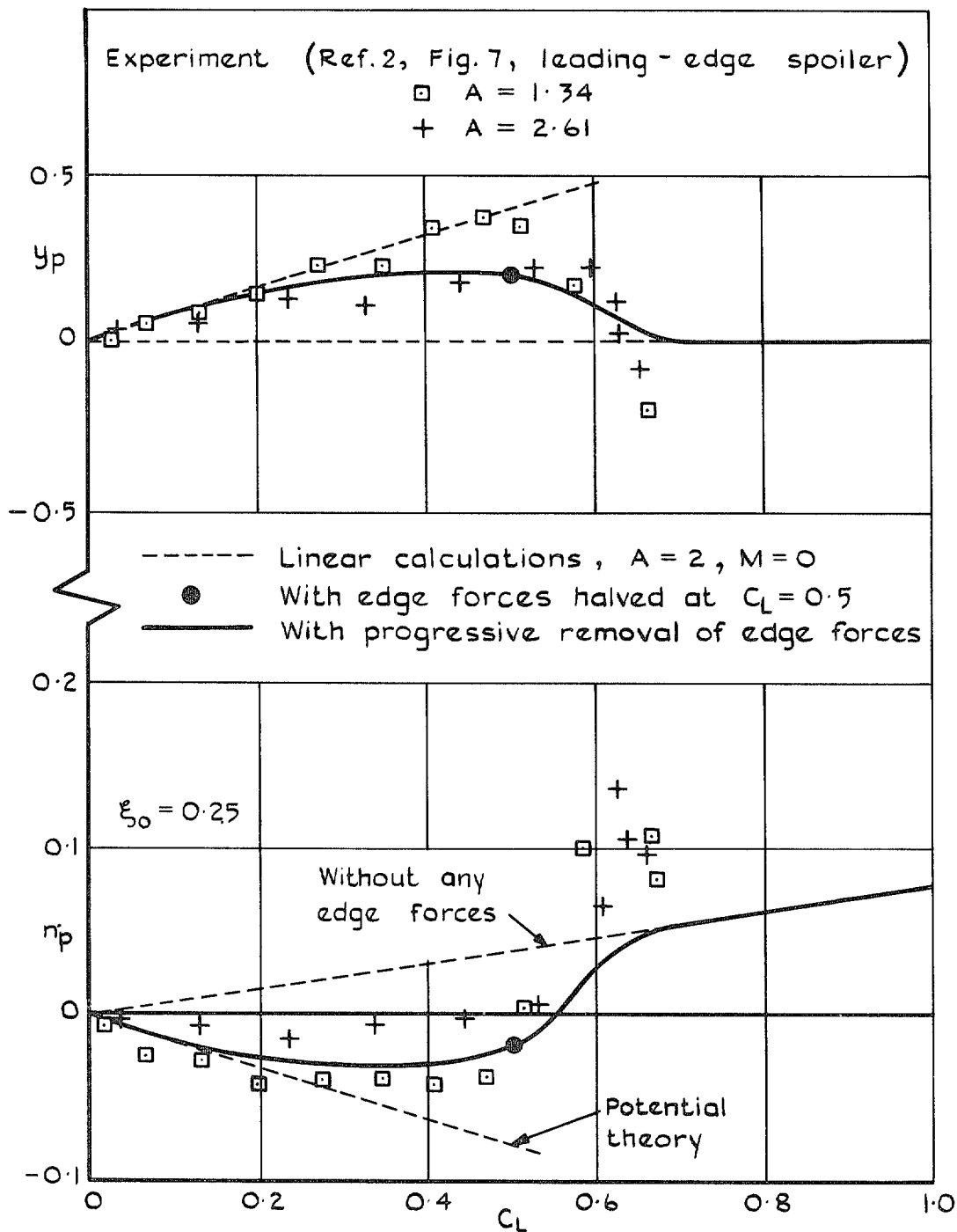FIG 5.   Theoretical, experimental and empirical roll-rate derivatives.

FIG. 6.   Effect of edge forces on rectangular wings in rolling motion.
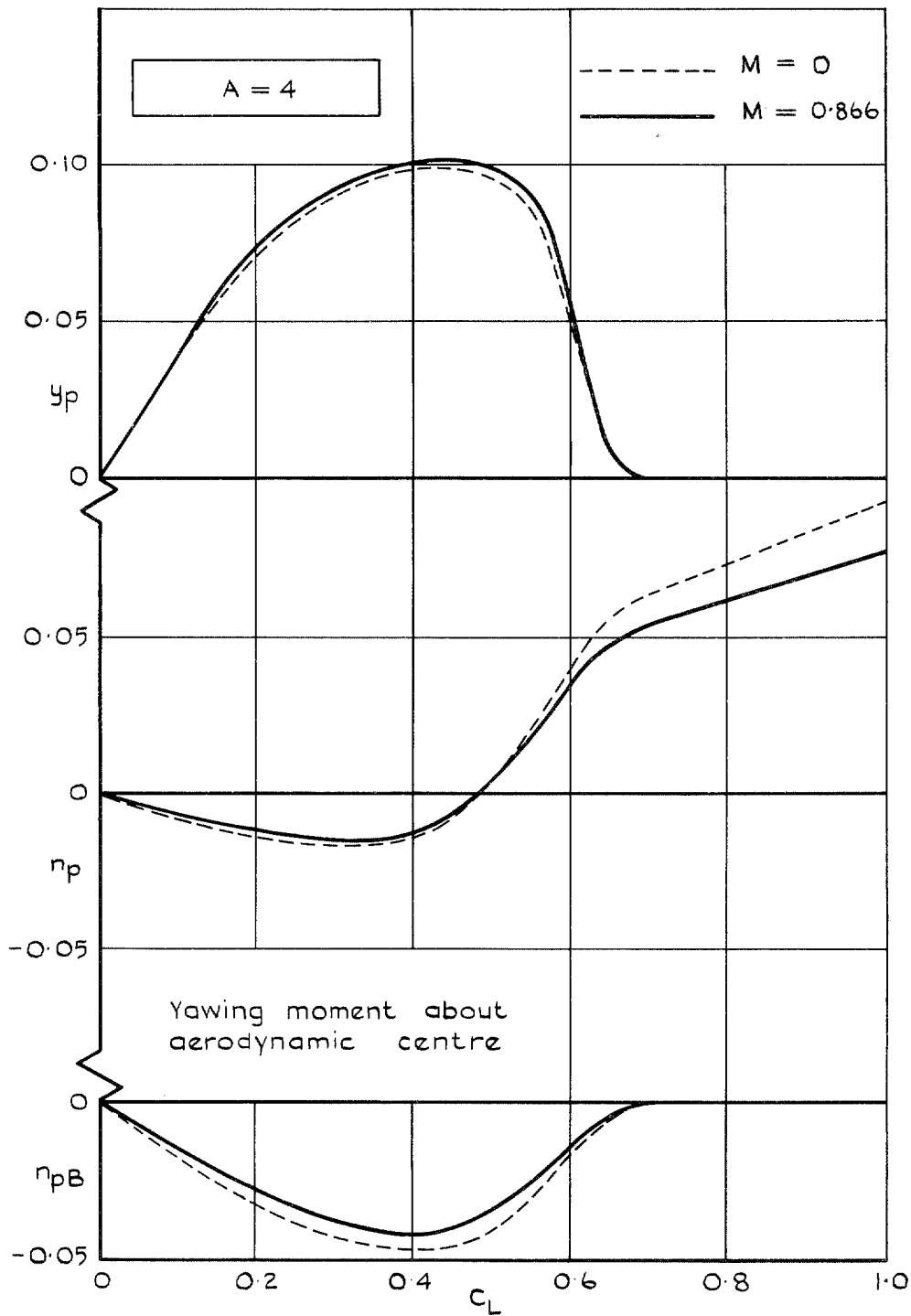
FIG. 7.   Roll-rate derivatives with progressive removal of edge forces.